Degree Project in the Field of Technology Fluid Mechanics and the Main Field of Study Engineering Mechanics

Second cycle, 30 credits

An Experimental Investigation of the Boundary Layer Control System of Volvo's Slotted Wall Automotive Wind Tunnel

Uncovering the Relationship between Boundary Layer Control, Static Pressure, and Drag

DYLAN DE JOURDAY

An Experimental Investigation of the Boundary Layer Control System of Volvo's Slotted Wall Automotive Wind Tunnel

Uncovering the Relationship between Boundary Layer Control, Static Pressure, and Drag

DYLAN DE JOURDAY

Degree Programme in Vehicle Engineering
Date: May 5, 2025

Supervisors: Jens H. M. Fransson, Erik Sällström
Examiner: Jens H. M. Fransson
School of Engineering Sciences
Host company: Volvo Cars
Swedish title: En Undersökning av Inverkan av Gränsskiktkontrollsystem på Aerodynamiska Mätningar i Vindtunnel för Vägfordon
Swedish subtitle: Att Avslöja Sambandet mellan Gränsskiktkontroll, Statiskt Tryck och Luftmotstånd

Abstract

This thesis investigates the impact that boundary layer control systems have on aerodynamic measurements in an automotive wind tunnel with a slotted-wall test section. The study was carried out in the Volvo Cars PVT wind tunnel at the Torslanda site in Gothenburg. Through experimentation a relationship was established between the suction rate of the boundary layer control systems, static pressure, and measured drag.

Reviewing the design and upgrade of the Volvo Cars PVT wind tunnel along with designs of other modern automobile wind tunnels and the relevant literature in the field led to the conclusion that the suction rate of the boundary layer control systems used in the tunnel was too high and excess suction provided little benefit. By reducing the suction rate of these systems by up to $40 - 50\%$ in some cases, a remarkable reduction of five counts in measured drag was observed ($\Delta C_D = -0.005$), with a small increase in displacement thickness. This change is related to the flattening of the axial static pressure curve and is related to the static pressure gradient; however, the large change in C_D cannot be explained by just looking at the change in the centerline axial static pressure in the empty test section. The shape of the boundary layer profiles remained largely unchanged, with negligible influence on the shape factor seen. With further refinement of the parameters of the boundary layer suction systems, the change in C_D could be even greater. This, in combination with the turning off of the tangential blowers and the change of the wind speed determination method from nozzle to plenum led to a large reduction in C_D. The total change with all these changes was twenty counts ($\Delta C_D = -0.020$), with the change in method reducing the measured drag by ten counts ($\Delta C_D = -0.010$) and disabling tangential blowers reducing the measured drag by five counts ($\Delta C_D = -0.005$).

The insights gained in this thesis are valuable both for Volvo Cars and the automobile industry as a whole. Studies related to slotted-wall test sections in automobile wind tunnels are few in number and the effects of boundary layer control systems on the flow in the test section are not as well studied as their $3/4$ open-jet counterpart. This study helps fill that knowledge gap a little more and provides a starting point for further investigation on the topic. The ideas for future investigations are outlined in the conclusion of this thesis.

Keywords

Slotted wall wind tunnel, Automotive wind tunnels, Drag, Static pressure, Boundary layer control, Boundary layer suction, Aerodynamic measurments, Volvo Cars, Ground simulation systems, Automobile aerodynamics, Pressure coefficient, Drag coefficient, Moving ground system, Boundary layer thickness, Displacement thickness

Sammanfattning

Denna uppsats undersöker hur gränsskiktkontrollsystem påverkar aerodynamiska mätningar i en vindtunnel för passagerarfordon med en testsektion med slits-väggar. Studien genomfördes i Volvo Cars vindtunnel PVT vid Torslanda-anläggningen i Göteborg. Genom experiment upptäcktes ett samband mellan sughastigheten hos gränsskiktkontrollsystemen, statiskt tryck och uppmätt luftmotstånd.

En genomgång av designen och uppgraderingen av Volvo Cars vindtunnel PVT, tillsammans med designen av andra moderna fordonsvindtunnlar och relevant litteratur inom området, ledde till slutsatsen att sughastigheten hos de använda gränsskiktkontrollsystemen är för hög och att den förhöjda hastigheten ger liten effeckt. Genom att minska sughastigheten, med i vissa fall upp till 40–50%, observerades en anmärkningsvärd minskning med upp till fem enheter i uppmätt luftmotstånd ($\Delta C_D = -0.005$), tillsammans med en liten ökning av förträngningstjockleken. Denna förändring är relaterad till en tillplattning av den axiella statiska tryckkurvan och är kopplad till den statiska tryckgradienten. Den stora förändringen i C_D kan dock inte förklaras enbart genom att titta på förändringen i det axiella statiska trycket längs mittlinjen i en tom mätsträcka. Gränsskiktsprofilerna förblev i stort sett oförändrade, med en försumbar påverkan på formfaktorn. Vid ytterligare förfining av parametrarna för gränsskiktets sugsystem skulle förändringen av C_D kunna bli ännu större. Detta, i kombination med att de tangentiella blåsarna stängdes av och att metoden för att bestämma vindhastigheten ändrades från munstycke till plenum, ledde till en stor minskning av C_D. Den totala förändringen med alla dessa ändringan var tjugo enheter ($\Delta C_D = -0.020$), där metodbytet minskade det uppmätta C_D-värdet med tio enheter ($\Delta C_D = -0.010$) och avaktiveringen av de tangentiella blåsarna minskade det uppmätta C_D-värdet med fem enheter ($\Delta C_D = -0.005$).

De insikter som erhållits i denna uppsats är värdefulla både för Volvo Cars och för fordonsindustrin i stort. Studier relaterade till testsektioner med slitsade väggar i fordonsvindtunnlar är få till antalet, och effekterna av gränsskiktkontrollsystem på flödet i testsektionen är inte lika väl studerade som för deras 3/4s öppna jet-motsvarighet. Denna studie bidrar till att fylla denna kunskapslucka något och utgör en utgångspunkt för vidare undersökningar inom området. Förslag på framtida undersökningar beskrivs i slutsatsen av denna uppsats.

Nyckelord

Vindtunnel med slitsväggar, Vindtunnel för vägfordon, Luftmotstånd, Statiskt tryck, Gränsskiktkontroll, Gränsskiktsutsug, Aerodynamiska mätningar, Volvo Cars, Marksimuleringssystem, Fordonsaerodynamik, Tryckkoefficient, Luftmotståndskoefficient

Acknowledgments

I want to extend my gratitude to the entire Aerodynamics team at Volvo Cars for their hospitality and for the opportunity to investigate the Volvo PVT wind tunnel. The days spent in their office were always cheerful, and everyone I met was curious about my work and excited to see what I would produce. My sincere thanks go to my supervisor at Volvo Cars, Erik Sällström, for his unwavering support throughout this project, for ensuring I received the necessary data in a user-friendly format, and for his patient guidance when challenges arose. No matter the situation or challenge, his patience and deep understanding of the wind tunnel systems gave me confidence that we would succeed even when I felt like we were hitting a brick wall. I am especially grateful to Erik for welcoming me into his building's guest apartment during the test campaigns. Without his constant support, this thesis would not have reached the same levels of success.

I would like to thank the manager of the aerodynamics team, Johan Sternéus, for his support during the project and for taking the opportunity and believing that I was the right person for the job when I interviewed for the position. I also must acknowledge his contributions to my thesis, as his report on the 2006 upgrade of the Volvo PVT wind tunnel served as a crucial basis for many of the experiments carried out by Erik and I. I also want to thank Volvo Cars for providing some of the figures and images in this report and allowing me to publish some of my own pictures taken during the experiments.

I am deeply appreciative of my supervisor at KTH, Jens Fransson, for his continuous support and for taking a chance on me. I extend my gratitude to everyone in the Fluid Physics Lab for welcoming me into their space, which allowed me to explore and deepen my understanding of fluid mechanics. My experiences in the FPL not only fueled my passion for the subject but also instilled a profound respect for those who pursue science at an academic level. Special thanks are due to Mihai Mihaiescu, whose support as supervisor during my bachelor's thesis encouraged me to dive headfirst into the challenging world of fluid mechanics and ultimately pursue it at the Master's level.

I also cherish the camaraderie and support shared with my friends and colleagues in the Farkostteknik program and within the Fluid Mechanics track. Although our numbers were few, the solidarity and mutual support we exhibited ensured that each of us succeeded, regardless of individual challenges.

Finally, my heartfelt thanks go to my family both here in Sweden and back home in California. I began my academic journey 13 years ago on August 16th, 2012, when I left sunny La Jolla, California for Sweden. With my family's unwavering support, I learned Swedish at an academic level, rebuilt my foundations in mathematics and science, and eventually earned a place at one of the world's leading engineering schools. After overcoming significant challenges with mathematics in my early years and the discouraging experiences with my math teachers in the United States, this achievement is truly beyond my wildest dreams.

Stockholm, May 2025
Dylan De Jourday

You asked me if an ordinary person by studying hard would get to be able to imagine these things like I imagine. Of course! I was an ordinary person who studied hard. There's no miracle people, it just happens they got interested in this thing and they learned all this stuff!

They're just people, there's no talent or special, miracle ability to understand quantum mechanics or a miracle ability to imagine electromagnetic fields that comes without practice and reading and learning and study. So if you say you take an ordinary person who's willing to devote a great deal of time and study and work and thinking and mathematics and ***time****, then he becomes a scientist.*

- Richard Feynman

Contents

List of Figures

List of Tables

List of acronyms and abbreviations

BL1	Boundary layer pre-suction zone one
BL2	Boundary layer pre-suction zone two
BLCS	Boundary Layer Control System
BLRS	Boundary Layer Removal System
CATARC	China Automotive Technology and Research Center
CFD	Computational Fluid Dynamics
GESS	Ground Effect Simulation Systems
ICE	Internal Combustion Engine
MGP	Moving Ground Plane
PIV	Particle Image Velocimetry
TB	Tangential Blower
TGR	Toyota Gazoo Racing
WDU	Wheel Drive Unit

Nomenclature

The following symbols will be later used within the body of the thesis.

δ	Boundary layer height (Also δ^{99})
ΔC_D	Change in drag coefficient
δ^*	Displacement thickness
$\mathbf{g}$	Body force vector
$\mathbf{u}$	Velocity vector
$\mathbf{x}$	Spatial coordinate vector
∇	Gradient operator
∇^2	Laplacian operator
ν	Kinematic viscosity
ρ	Density
θ	Momentum thickness
A	Cross-sectional area
C_D	Drag coefficient
C_p	Pressure coefficient
F_D	Drag force
H	Shape factor
p	Pressure
p_∞	Static free-stream pressure

p_s	Static pressure
q_∞	Dynamic free-stream pressure
t	Time
U	free-stream velocity in x
u	Velocity in x
v	Velocity in y

Chapter 1

Introduction

The aerodynamics of ground vehicles has been an important topic of research in the last century. With a growing need for the reduction of emissions and the increasing popularity of battery electric vehicles, this topic has become even more important in the last 10 years. Motors in electric vehicles are not subject to the same speed-dependent inefficiencies as traditional Internal Combustion Engines (ICE), which means that aerodynamic forces contribute to a higher percentage of the total energy loss of the vehicle [1].

At their inception, the aerodynamics of ground vehicles played a minimal role in their design and performance. These vehicles moved very slowly compared to their modern counterparts and the drag induced by their shape was negligible. These early vehicles rode on dirt tracks and the average speed along those roads was much less than in the modern world [2]. The drag on a body moving through a fluid medium is proportional to the square of its velocity. Thus, at low speeds, these effects are minimal; however, as speed increases, these effects grow rapidly. This drag force is critical in the design of modern ground vehicles; naturally, the question becomes: how to measure this drag force?

Tests and measurements carried out on an open road have too much uncertainty, with variations in wind speed, temperature, and local pressure making it difficult to compare one test to another or one car designed in one region to another. To solve this issue, large wind tunnels are used, designed from the ground up to simulate a ground vehicle moving on an open road. However, these wind tunnels are not perfect and cannot fully simulate the open-air characteristics of an open road. The walls, nozzle, and collector of the tunnel change the streamlines of the flow around the vehicle compared to the open road [2]. These changes influence the pressure measurements around the vehicle in the test section, and thus influence the measured drag when designing a vehicle. To obtain a proper measurement of the forces in the vehicle, special care should be taken when designing a wind tunnel test section.

To simulate the flow in the open road, various systems are put into place to attempt to mimic these conditions, such as moving belts to simulate the ground moving under the car. To recreate the boundary layer profile of a car moving along an open road, suction systems are placed on the floor in front of and sometimes around the car being tested. These systems are important to properly simulate the flow field

near the ground; however, they can negatively influence other parts of the flow field. An example of this is that air suction through Boundary Layer Removal Systems (BLRS) can affect the static pressure gradient along the test section. In an open air environment, there would not be any variation; however, inside a wind tunnel there can be significant variation due to the design of the tunnel and its BLRS.

Today, there are three different types of test sections used in wind tunnels for the aerodynamics of ground vehicles, closed wall, $3/4-$ open jet, and slotted wall. Each of these types of test section provides positive and negative effects when it comes to modeling the conditions of an ideal open road, which will be described further in the next chapter. This paper focuses specifically on a wind tunnel with a slotted wall test section and its ground simulation systems, the Volvo Cars PVT wind tunnel in Gothenburg, Sweden.

1.1 Background

Experimentally simulating open road conditions is not an easy task. The systems involved in these types of simulations are massive in both complexity, construction requirements, and investment. The first wind tunnels were developed for aerospace applications in the first half of the twentieth century and those concepts were adapted for use in the automotive industry. Although it may seem at first glance that one could just place a automobile in a wind tunnel designed for airplanes and get good results, there is a lot more going on ”under the hood” when it comes to accurately simulating the flow conditions for a ground vehicle.

One might think that simply placing a flat plate in a wind tunnel to simulate the ground is enough, and this is what has been done for many years in automotive wind tunnels. However, this does not accurately represent the flow around a vehicle on the open road. One could perhaps make an assumption or design a tunnel such that the walls are far enough away that their influence could be ignored. However, the ground, like gravity, is something one cannot get away from easily. The goal is to simulate a vehicle traveling on an open road without wind, and what one has simulated at this point is a car standing on a flat plate traveling on an open road without wind. One might ask ”Why is this so important? Its just a plate, can it really influence the flow that much?” and the answer is yes! A core concept in fluid mechanics is the idea of a *boundary layer*.

The boundary layer was first hypothesized by Ludwig Prandtl in his 1904 paper *Motions of Fluids with Very Little Friction*. This layer comes from the fact that the fluid particle that is *on* the surface of an object has the velocity of that object. In the case of a flat plate that is not moving, the velocity of the particle is equal to zero. Now, if there is a flow of constant speed moving past this plate, the question becomes what the velocities of the particles *are near* the plate. Are they also zero, or is there a transition from zero to the free-stream velocity? The answer to this is that there is a transition and the transition region is what defines the boundary layer, and its thickness is often defined as the region at which the velocity goes from zero to 99% of the free-stream velocity [3].

Due to the ever-present natural requirement of mass conservation, this boundary layer creates a deficit in the momentum of the flow, which again, due to mass conservation, causes the flow outside of

the boundary layer to compensate. This compensation is the reason why the proposed simulation case is not entirely representative of open-road conditions. In ideal open-road conditions, the air on and above the road is quiescent until influenced by a passing vehicle. This means that there is no boundary layer along the ground as the air remains as the car passes. To counteract the effect that the boundary layer has on the flow field in the wind tunnel, modern wind tunnels use boundary layer control systems to remove the boundary layer and mitigate its effects on the measurements.

In addition to boundary layer control systems, moving belts are positioned underneath the vehicle to simulate the vehicle moving across the ground. This allows the wheels of the vehicle to spin and imposes a ”slip boundary condition” in order to eliminate the boundary layer growing under the vehicle. Imposing suction under the vehicle would give rise to a vertical flow under the car which is not physical. Allowing the wheels to spin also has a significant effect on the flow under and around the vehicle and can lead to non-negligible differences in aerodynamic measurements compared to leaving them stationary [4].

However, both the belts of the moving ground systems and the suction systems of the boundary layer control systems influence the flow, so the goal becomes balancing their influence on the flow with the total amount of the boundary layer that is removed. These systems can have a negative impact on the static pressure gradient within the test section of the tunnel, and it is important to balance this effect with the amount of the boundary layer that is removed. This balance is at the core of the work presented in this thesis, as it aims to investigate this balance within the Volvo Cars PVT wind tunnel.

1.2 Problem

With the information presented in 1.1, the problem is formulated as follows:

- What influence do Boundary Layer Control Systems (BLCS) have on aerodynamic measurements such as static pressure, and measured drag in an automotive slotted wall wind tunnel?
- What is the relationship between static pressure, measured drag, and the characteristics of the boundary layer such as height and displacement thickness?

1.3 Purpose

The purpose of this project is to investigate the Ground Effect Simulation Systems (GESS) used in the Volvo PVT wind tunnel, and to examine the relationship between these systems and aerodynamic measurements such as static pressure and drag. This work is important not only for Volvo Cars but also for the automotive industry as a whole, as providing accurate measurements for designing automotive vehicles allows automobile manufacturers to create optimized designs and reduce emissions. With

automobile manufacturers focusing more and more on electric vehicles, measured drag becomes even more important as it represents the largest source of energy losses for these types of vehicle.

1.4 Goals

The goal of this project is to improve the performance of the Volvo Cars PVT wind tunnel. This has been divided into the following three sub-goals:

1. Examine and quantify the influence of various ground effect simulation systems on the static pressure gradient.
2. Reduce the influence of ground effect simulation systems on the static pressure gradient without significantly impacting their performance in terms of minimizing the boundary layer.
3. Determine how changes to ground effect simulation systems influence drag measurements.

1.5 Research Methodology

The research carried out in this project consists of an in-depth analysis of the design and construction of the Volvo PVT along with its upgrade in 2006. It also includes an investigation of automotive wind tunnels currently in use around the globe to understand what influence the boundary layer control systems have on the static pressure gradient along a test section. It is hoped that this review of both construction and design will help point to which parts of the test section and what systems should be considered when capturing data. With that information in mind, a systematic approach to gathering data will be used, attempting to isolate which of the ground simulation systems dominate the influence on the static pressure gradient. From this, it is hoped that the influence can also be identified in the drag measurements, giving a sense of how much an effect the variation of the static pressure can have on the drag coefficient. The data will be captured using various measurement tools commonly found in wind tunnels, such as pitot tubes, boundary layer rakes, omniprobes and pressure patches.

1.6 Delimitations

This thesis will not attempt to numerically simulate the PVT or any of the ground simulation systems. There will be no recommendations or analysis to redesign the main features of the tunnel itself outside of the test section. This thesis will not cover recommendations for general wind tunnel design. The focus of this thesis is purely on the test section in the PVT and in particular, its ground simulation system.

1.7 Structure

Chapter 2 presents relevant background information about automotive wind tunnels, along with a review of relevant literature related to automotive wind tunnels and the Volvo PVT in particular. Chapter 3 discusses fundamental fluid mechanics related to wind tunnel analysis and specifically the boundary layer. Chapter 4 discusses the experimental methodology used to investigate the Volvo PVT wind tunnel, and Chapter 5 presents and discusses the results of the investigation. Chapter 6 concludes the thesis with a further discussion of the results presented in Chapter 5, along with ideas for future projects to continue improving the Volvo PVT wind tunnel.

Chapter 2

Background

This chapter provides basic background information about automotive wind tunnels and their design. The different types of wind tunnels and the different types of test sections will be described in detail along with their relevance to the Volvo Cars PVT.

2.1 Automotive wind tunnel design

Although there are many different types of wind tunnels, for automotive vehicles, there are only two that are reasonable to use. These two are defined by their return design, or by how the air moves into and out of the tunnel.

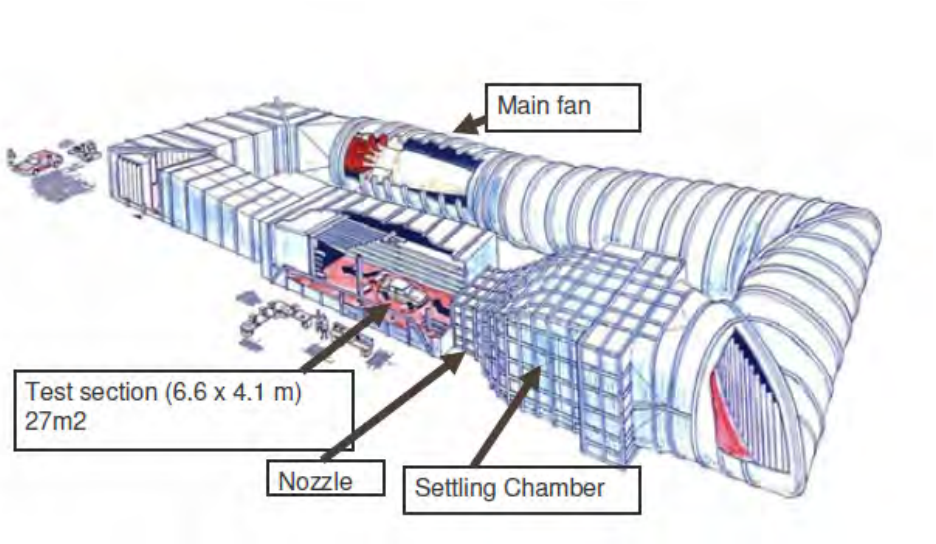

Figure 2.1: Overview of the Volvo PVT wind tunnel, a closed return wind tunnel with a slotted wall test section, courtesy of Volvo Cars.

2.1.1 Eiffel-type: open return

The Eiffel-type wind tunnel is an open return wind tunnel named after its creator Gustave Eiffel. The wind tunnel takes air directly from the environment at its inlet and sucking it into the test section, where it then continues to the fan and into the outlet. One of the key features of the original design was the diffuser, which Eiffel patented in 1918 and reduced the required power by a factor of 3 [5]. This type of wind tunnel are no longer developed for automotive purposes, as their disadvantages outweigh their benefits [2].

2.1.1.1 Advantages

The main advantage of an Eiffel-type wind tunnel is how inexpensive it is to build compared to its counterpart. Since the total length and size of the wind tunnel is significantly shorter than the Göttingen type, the construction costs are reduced [2]. This also comes with a smaller footprint for the facility, which can also reduce the cost if the price of land is considered.

2.1.1.2 Disadvantages

Eiffel-type wind tunnels do have several significant drawbacks. The main one is that local weather can influence the conditions in the test section if one has a Eiffel-type with an inlet directly to the atmosphere. This significantly impacts the practicality of this type of tunnel in countries where the weather changes significantly throughout the year [2]. Flow quality is also a significant issue, with local winds influencing measurements within the test section even if the weather is acceptable that day for testing. However, there are a few examples of open return wind tunnels that were placed within a building to avoid the effects of weather. In addition, significant effort must be taken to ensure that no debris enters the system. Eiffel-type tunnels are also very loud, making them not suitable to be built near residences [2].

2.1.2 Göttingen-type: closed return

In a Göttingen-type tunnel the air is driven within a closed circuit by a fan. This type of tunnel is named after the university at which it was first developed under the supervision of Ludwig Prandtl. At each corner of the circuit curved streamlined deflectors are used to ensure the smoothness and uniformity of the air flowing through the circuit [6]. These tunnels are in general more costly to construct than their counterpart, however provide better flow quality as mentioned by Prandtl and his cohorts in his report on the Göttingen-type tunnel in 1920 [6]. Modern Göttingen tunnels utilize an important feature from Gustave Eiffel's original design and that is the diffuser which significantly reduced the power requirement [5].

2.1.2.1 Advantages

The Göttingen-type tunnel has a distinct advantage in its low-power requirement. The cost of the motor and fan is comparatively low, along with the operating costs, including electricity [2]. It also has a significant advantage in flow quality. Since air is controlled and kept within the tunnel, the effects of conditions outside the tunnel will not influence the measurements as much as its counterpart [2].

2.1.2.2 Disadvantages

One of the disadvantages with a Göttingen-type tunnel is its total cost to build. Prandtl mentions in his report that in relation to the cost of building the facility in Göttingen, the maximum budget had been surpassed [6]. Since it is a closed return system, the total length of the tunnel is much more than that of an open return tunnel. This is due to the requirement of having a closed circuit for the air flow to travel along, but also to the fact that one needs a large settling chamber. This significantly increases the cost of building [2]. An example of this can be seen in the building of the Honda Automotive Laboriatories of Ohio wind tunnel, which was reported to cost 124 million USD [7], and some wind tunnels have even higher investment budgets.

Another disadvantage is that the materials used in designing, testing, and building automobiles are sensitive to temperature. To account for this fact, many wind tunnels employ climate control systems, which require additional power and add another layer of complexity to the design and construction [2]. Clay models of vehicles are often used in testing shapes of vehicles and these models are quite sensitive to heat. Although not all wind tunnels take this into account, those that do have a clear advantage in the design process.

2.2 Test section design

The two defining characteristics of a test section are its size and the type of boundary employed. The cross section of the nozzle A_N and the length L between the nozzle and the collector define the size of the test section. For open jet test sections, the volume of the plenum is a third dimension that is important [2]. There are three different types of test section that are employed in the automotive industry today, and these are named after the type of boundary that the jet of air interacts with after the nozzle. The three types are closed wall, open jet, and slotted wall.

2.2.1 Closed wall

A closed wall test section is what most people imagine when thinking of a wind tunnel. The walls of the test section are of the same dimension as the nozzle, so it is in essence just a simple straight channel, usually with a rectangular form. A modern example of a wind tunnel that employs this type of test section is the General Motors full scale wind tunnel [8].

2.2.1.1 Advantages

The closed test section has a large usable length when compared to the open jet. It also has better flow stability, and there is no problem of low-frequency pumping found in open jet test sections [2].

2.2.1.2 Disadvantages

However, the closed test section has a few disadvantages when compared to an open jet. The first of which is the fact that, due to the closed nature of the test section, the boundary layer grows along the walls, thus reducing the effective test section area. This boundary layer increases the velocity and as a result decreases the pressure as one travels downstream from the nozzle. One can attempt to geometrically compensate for this by gradually expanding the cross section as the flow travels downstream; however, when a model is placed in the tunnel, this becomes only an approximation. The closed test section is also sensitive to solid and wake blockage effects, with the blockage correction approximately twice that of the open jet. High angles of yaw with a model can also cause boundary layer separation due to an adverse pressure gradient [2].

2.2.2 Open jet

An open jet test section differs from a closed wall test section in that the nozzle protrudes out into an open room with dimensions much larger than that of the nozzle. The idea with this type of test section is to attempt to mimic the flow field where the walls can be considered ”infinitely far away” and thus as close to open-air conditions as possible. This is not true in reality, and the plenum of an open jet test section can have considerable effects on the flow field of the jet exiting the nozzle if neglected. A variant of this test section, known as the $3/4$ open jet is the type that is mainly used in automotive wind tunnels.

2.2.2.1 Advantages

The main advantage of the open jet test section is said to be that it is more comparable to the ideal free-jet case. From this one might assume that the open-jet test section has a constant static pressure along the axis of the jet without any effort. This is not entirely true, and the dimensions of the test section, plenum, nozzle, and collector are carefully designed and tuned to ensure that the static pressure as constant as possible across the test area in the empty test section. Solid blockage effects and correction are small for open-jet test sections; nevertheless these interference effects cannot be considered in a vacuum as they are only one of several interference effects [2].

From an industry perspective, the open-jet wind tunnel is advantageous because of its ability to provide both flow and aero-acoustic measurement and analysis. This means that a company does not need to construct and design two separate wind tunnels; these tests can often be performed in tandem. Considering the high costs of designing, constructing, and running wind tunnels, it is understandable

that these are attractive options for many automotive companies. Kramer et al. conclude that the open jet wind tunnel is the most economical type due to its small cross section size [9], which means reduced construction costs.

Another clear advantage of the open-jet test section is in how easy it is to perform a multitude of measurements without disturbing the flow. Since the test section has a large plenum, measurement equipment can be placed in such a way that does not interfere with the flow or vibrate due to the flow allowing for good measurements. Open-jets also provides ease of accessibility for model placement along with allowing for easy flow visualization using, for example, Particle Image Velocimetry (PIV) [2].

2.2.2.2 Disadvantages

The largest disadvantage of the open jet test section is its limited usable length. As the jet of air leaves the nozzle and travels downstream, it mixes with the still air of the plenum, creating a shear layer in the flow. This mixing strips the core of the jet, the core being defined as the region of the flow where the velocity is equal to the desired velocity in the tunnel. Thus, as the jet travels downstream, the cross section of the flow at which the velocity is equal to the free-stream velocity shrinks considerably [2].

This mixing also gives rise to other drawbacks. If one observes the mixing region between the jet and the quiescent air in the plenum, a turbulent mixing process is seen. This mixing is more intense than the mixing found in a turbulent boundary layer along a wall, which leads to higher losses due to friction than in the case with a wall. This increases the power requirements of the system [2].

A third disadvantage observed in open jet test sections is that it is sensitive to low-frequency oscillations in the flow. From aero-acoustics it is seen that in expansion chambers a self-sustaining oscillations can occur at certain flow speeds. The plenum of the open jet test section acts as a very large expansion chamber in this case, and this can cause a low-frequency pumping or surge in flow [2]. However, this effect is typically mitigated by using Helmholtz resonators and does not cause issues in modern wind tunnels when addressed properly.

2.2.3 Slotted wall

First proposed by Wieghardt and Vandrey in their paper *Experiments on a slotted-wall working section in a wind tunnel* [10], a slotted wall test section is a hybrid of open jet and closed wall test sections. It has a plenum; however, it has walls that follow the test section as a closed test section would. The plenum in a slotted wall test section tends to be much smaller than their open-jet counterparts. These walls are perforated with slots that run the length of the wall. These slots are on not only the lateral walls but also the ceiling. The idea is that the plenum behind the slotted walls allows for streamline expansion as in the ideal open air, however, mitigates the disadvantages of the open jet test section by still having walls that run the length of the test section [2]. Slotted wall wind tunnels are not nearly as widespread as closed or open jet wind tunnels, and within the automotive industry the two most well-known are the Toyota Gazoo Racing (TGR) wind tunnel and Volvo Cars PVT wind tunnel.

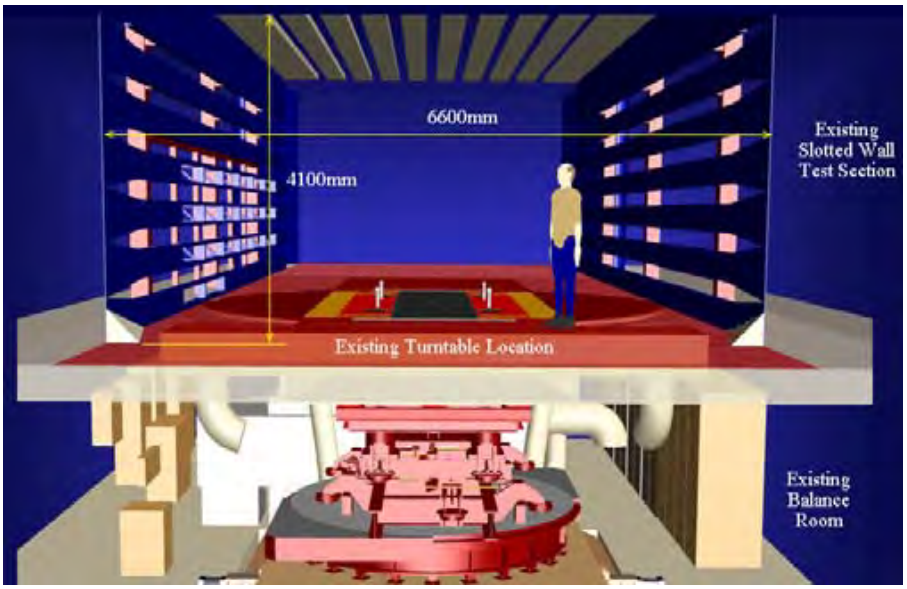

Figure 2.2: Image illustrating the slotted wall test section and force balance in the Volvo PVT wind tunnel, courtesy of Volvo Cars.

2.2.3.1 Advantages

The advantages of a slotted wall wind tunnel lie in the fact that it mitigates the disadvantages of the open jet and closed test section types. In the context of automotive wind tunnels, the slotted wall wind tunnel is shown to have good results for larger blockage ratios compared to open or closed test sections that have accurate test results up to blockage of 21.4% [11]. This is also confirmed by Flay et al. in their report on the performance of slotted wall test sections at high yaw angles for ground vehicles [12]. Slotted wall wind tunnels also tend to have better flow quality than open jet wind tunnels and have a longer usable length [2].

2.2.3.2 Disadvantages

A disadvantage of slotted walls is that they still require a correction of the flow to get accurate measurements. A proposed correction method was given in a Master's Thesis by M. Eng titled *Investigation of Aerodynamic Correction Methods Applied to a Slotted Wall Wind Tunnel*. This thesis was performed at Volvo Cars PVT, and provided a correction method that worked at the time [13]. However, it was found to be lacking later on, and Volvo switched to a new correction method developed in-house by the aerodynamics team.

Another disadvantage of having a slotted wall test section is that it is not nearly as suitable for aeroacoustic measurements as the $3/4$ open jet test section. The small size of the plenum, along with acoustic reflections from the slotted walls, makes it difficult to obtain the proper measurements. Optical access from outside the high-speed flow is very limited as well, as most probes or traverses

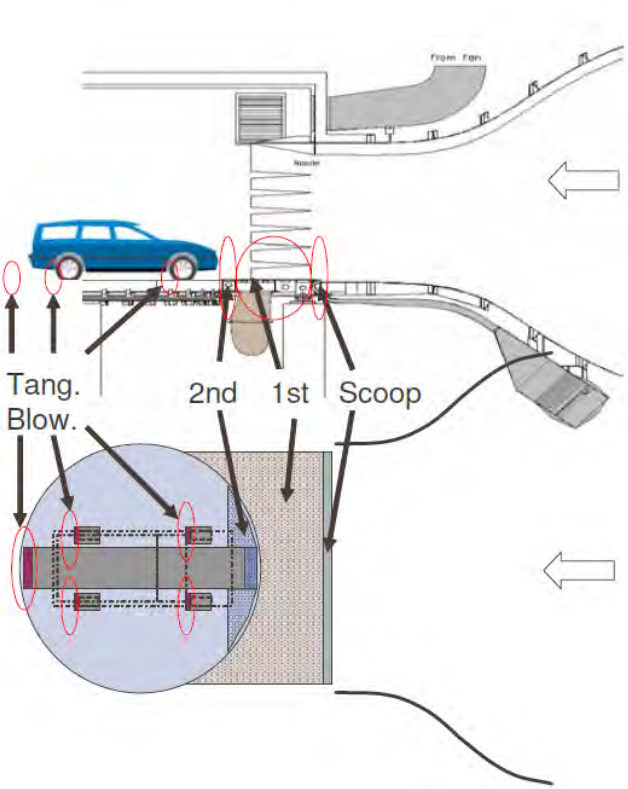

Figure 2.3: Diagram showing the various systems that make up the ground effect simulation system in the Volvo PVT wind tunnel, courtesy of Volvo Cars.

would influence the flow in some way due to the size constraints of the test section.

2.3 Ground simulation systems

As outlined in the beginning of the chapter, to truly simulate a vehicle moving on the open road, one needs to control the boundary layer in the test section of a wind tunnel. GESS are ubiquitous in modern automotive wind tunnels and have three main categories of control; suction, tangential blowing and moving ground. BLCS consist of the first two categories, while Moving Ground Plane (MGP) is the last.

2.3.1 Boundary layer removal systems

The first part of the BLCS system involves removing the boundary layer through suction, the different suction systems fall under the umbrella of BLRS. The second part involves re-energizing the boundary layer through tangential blowing, bringing the velocity profile closer to the standard block seen in the

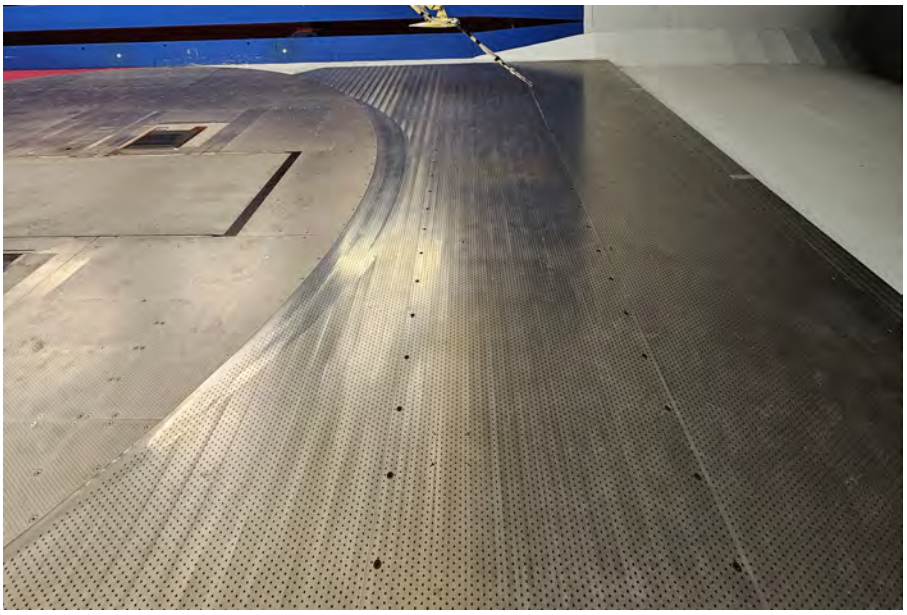

Figure 2.4: Image showing the distributed suction systems in the Volvo PVT wind tunnel. The first pre-suction and second pre-suction zones can be seen, with the first pre-suction having larger holes and spanning the entire width of the test section. The second pre-suction zone is limited to the turntable. The leading edge of the scoop can also be seen looking at the upper right corner of the metal plate. Image taken by the author, published with the permission of Volvo Cars.

free-stream.

2.3.1.1 Boundary layer scoop

The first type of control typically used in automotive wind tunnels is boundary layer suction. This typically involves multiple suction systems and regions. Starting far upstream, the first system that the flow encounters when moving into the nozzle is a boundary layer scoop. The scoop is used to remove the boundary layer that grows along the wind tunnel as the flow moves through the loop, and ensures that this boundary layer does not grow into the test section. The scoop often is a step in the nozzle that sucks the boundary layer into it, leaving a uniform velocity profile entering the nozzle and test section. The flow that is removed by the scoop is reinjected back into the flow elsewhere in the wind tunnel, and where the flow is re-injected can vary from tunnel to tunnel. In the Volvo Cars PVT wind tunnel, the scoop flow is re-injected above the nozzle.

2.3.1.2 Distributed suction

After the scoop, distributed suction zones are used to remove any boundary layer that grows from the nozzle to the vehicle in the test section. The design of these zones can be simple, usually consisting

of a perforated plate placed upstream of where the test object will be positioned. A more complex design would involve additional distributed suction along the underside of the vehicle, however, this adds significant complexity and expense [14].

The design of the perforations can differ, and some tunnels employ different densities of perforation for different suction zones. The Volvo PVT wind tunnel for example has two suction zones, the suction plate in zone one has larger holes while the plate in zone two has smaller holes. Zone two is also divided into a center and an outer zone, the specifications of which can be found in the table 2.1 below. These plates and their placement in the test section can vary from tunnel to tunnel, and are a critical point in designing a test section due to their influence on the static pressure gradient. The flow that is removed by these systems is re-injected into the flow just like the scoop, with the point of re-injection varying from tunnel to tunnel.

System	Hole size	Hole spacing	Pattern	Open area ratio	Max flow rate
1st Pre-suction	5 mm	16 mm	60° staggered pitch	8.9%	7.7 m^3/s
2nd Pre-suction - Center	2 mm	9 mm	60° staggered pitch	4.5%	0.45 m^3/s
2nd Pre-suction - Outer	2 mm	9 mm	60° staggered pitch	4.5%	1.6 m^3/s

Table 2.1: Table showing the different characteristics of the pre-suction zones employed in the Volvo PVT wind tunnel.

2.3.2 Tangential blowing

Since the suction plates can significantly influence the static pressure gradient, these systems are usually kept far upstream of the region where the vehicle to be tested would be placed. This means that there is unavoidable boundary layer growth downstream of these suction regions. This growth is small in comparison to what it would be without these systems though. One way to modify the boundary layer profile so it has as close to a uniform profile as possible is to reenergize the boundary layer by blowing air into it using Tangential Blowers (TB). The velocity profile in a boundary layer gets its shape due to the fact that the velocity is zero at the point of contact with the ground, however by introducing a flow at that point the displacement thickness can be reduced. These systems are usually placed upstream of the moving ground plane in the test section, however in the Volvo PVT wind tunnel they are placed downstream. The characteristics of the TB system used in the Volvo PVT wind tunnel is shown below in table 2.2.

Tangential blower	Slot height	Slot width	Max flow rate
WDU	0.6 mm	600 mm	0.08 m^3/s
Center belt	1.0 mm	1000 mm	0.15 m^3/s

Table 2.2: Table outlining the key characteristics of the tangential blowers in the Volvo PVT wind tunnel.

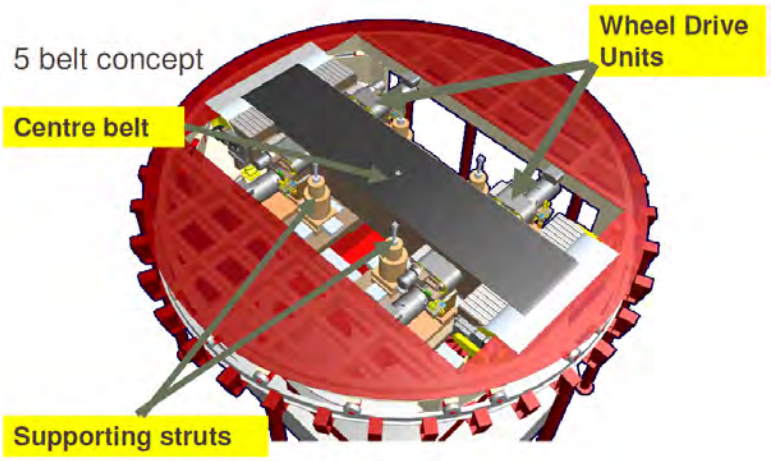

Figure 2.5: The five belt system used in the Volvo PVT wind tunnel, courtesy of Volvo Cars.

2.3.3 Moving ground plane

A critical component of simulating the ground for a car moving on an open road is that the ground should also move, for automobile wind tunnels this is done using a MGP. This accomplishes two things; one, it controls the boundary layer as the boundary layer will have a velocity profile closer to the free-stream, and two, it moves the tires of the vehicle which is an important part of testing its aerodynamics. The interaction of the wheels with the air under the vehicle is not negligible when calculating drag and is important for an accurate measurement of the forces on the vehicle, as the wheels and the wheel houses can account for up to a quarter of the total drag [15]. Rotating the wheels also changes the overall flow around the car, and has significant influence in the wake where the rotation of the wheels changes the balance of the flow, altering both drag and lift forces. This phenomenon holds substantial implications for the aerodynamic design of the vehicle when attempting to optimize the shape of vehicle, particularly in optimizing the design of the rear end of the car to reduce drag. Properly simulating the movement of the wheels can lead to significant changes in the measured C_D value of a vehicle, Elofsson et al. reported average changes of ten to twenty counts when comparing simulating the movement of the wheels to having the wheels at a standstill [4]. The ground is simulated using a moving belt underneath the vehicle, and there are a few different configurations used in the automotive industry today.

The first type is a one-belt system. This system has a large belt on which the vehicle sits and gives the best representation of the open-road case. However, there is a drawback to this system as the vehicle needs to be fixed to the center of the test section. With a single belt, there is no way to lock the vehicle from the ground, which means that arms or stings extending from the walls or ceiling of the test section must be used to keep it in place. These arms, as expected, influence the flow around the vehicle and have negative effects on the measurements [16]. These types of moving ground system are usually employed by Formula One racing teams, as these high-performance vehicles are so low to

the ground that very high accuracy is needed when simulating the ground.

The second type is a three-belt system. This system has one large belt moving under the vehicle, and two outer belts that run under the wheels of the vehicle. This allows the vehicle to be fixed in place from below, removing the need for stabilizing arms as in the one-belt system.

The third type is a five-belt system. This system has one large belt under the vehicle like in the three-belt system but has 4 separate small belts for the wheels. The main advantages of the 5 belt system are the struts that attach to the underside of the vehicle and the Wheel Drive Unit (WDU)s. The forces on the vehicle are measured only through the struts and the WDUs, which allows for precice measurements. The parasitic drag forces on the WDUs and the stuts are small which makes this system ideal for measuring drag. To adapt to different wheel bases and track widths, the belts under the WDUs can be moved. This is the most popular choice for the moving ground simulation system for passenger vehicles for most automotive wind tunnels used in designing passenger vehicles and is the moving ground system of choice for the Volvo Cars PVT wind tunnel.

2.4 Related works

The related works to this thesis encompass a variety of academic articles related to the theory of automotive wind tunnels and their test section types, along with technical reports related to the Volvo PVT wind tunnel and reports related to other automotive wind tunnels.

2.4.1 Volvo Cars PVT Wind Tunnel

The first major related work for this thesis is the work by Sternéus et al. [14] regarding the addition of the ground simulation system to the Volvo PVT in 2006. The report summarizes and analyzes the work done by Aiolos, the company contracted to perform the upgrade and certification of the wind tunnel. The full 2006 upgrade included a moving ground system, tangential blowers, boundary layer removal system, and a new fan. Several important observations were noted here, the first of which is related more historically to a cooperation between Volvo and Jaguar Racing. In 2004 it was reported that Jaguar Racing (which then became Red Bull Racing by 2006) would be given access to a third wind tunnel for their Formula 1 racing team. Since Volvo was a Ford subsidiary at the time, this cooperation influenced the design of the 2005-2006 upgrade of the wind tunnel. This cooperation specifically influenced the adjustment of the BLRS and the placement and adjustment of the tangential blower system.

Sternéus et al. [14] reports that the static pressure gradient is acceptable with regard to the new BLRS completely removing the boundary layer compared to the old system; however, there is a spike in the gradient in front of where the vehicle would sit. This implies that the upgrade had an effect on the static pressure gradient, as this spike was not seen before the upgrade. This gives further reasons to investigate the BLRS and their tuning closely. The tunnel data reports a displacement thickness $\delta^* = 0.35$ mm with the tunnel in *aero* mode with all systems on. This is considered to be very high

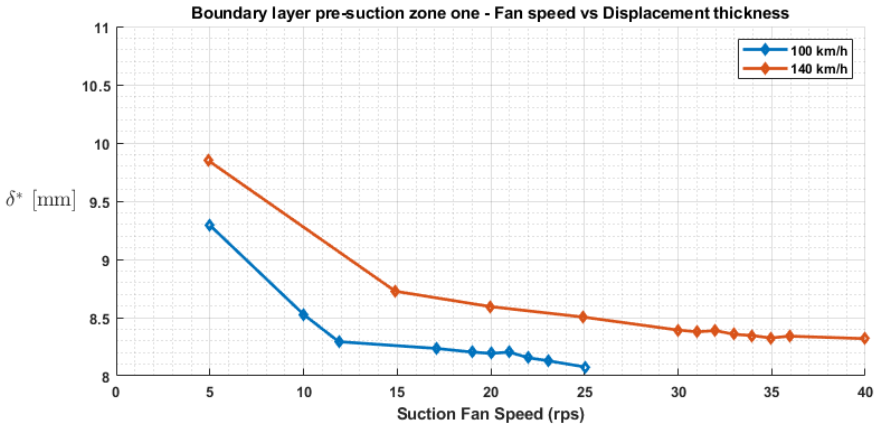

Figure 2.6: Plot showing the relationship between the boundary layer pre-suction zone one's fan speed and measured displacement thickness at the center of the turntable for two different wind speeds with second boundary layer pre-suction off. Data taken from the upgrade commissioning report by Aiolos [17], courtesy of Volvo Cars.

performance even by the standards in 2024. This will become clear later on when comparing the targets of more modern wind tunnels and will be a key point in the trade-off between displacement thickness and static pressure gradient.

The work done by Sternéus et al. [14] prompted an investigation into the full details of the report provided by the Aiolos Corporation for the commissioning of the PVT upgrade. This report contains an overview of all the work done by Aiolos and their verification of the new systems added in the upgrade. The most important parts of this report for this thesis are the methods and values used to tune BLRS and how they were calibrated.

During the experiments carried out by the author, it was questioned why the specific suction values of BLRS were selected by Aiolos. When comparing the suction values reported for each subsystem of the BLRS by the computers in the control room of the PVT with the calibration curves provided by Aiolos, it was observed that the chosen values were at the higher end of the range of potential suction values. The difference in displacement thickness seen above in figure 2.6 between the maximum suction value reported and a value of about $40 - 60\%$ less was negligible, and on the scale of fractions of a millimeter [17]. This brought into question whether these high values provided any value for Volvo. To explain this choice, the author once again looks to the historical context. Since it was known that Jaguar Racing was going to be using the PVT for developing its Formula 1 car, the only rational reason for choosing such high suction values is that the boundary layer will have much greater influence on the super low hyper performance vehicles in Formula 1 racing. Thus, the suction values were set according to these requirements by the Formula 1 team, and never changed for almost two decades.

Jaguar Racing and their cooperation with Volvo ended shortly after the upgrade of the PVT, leaving Volvo with a wind tunnel that was tuned in some aspects for Formula 1 cars while producing and testing

consumer passenger vehicles. This fact alone gives enough ground to warrant an investigation into the influence of the suction on the flow in the wind tunnel and its influence on the measured values in both an empty tunnel but also with a vehicle present.

2.4.2 Boundary layer removal systems and gradient effects in wind tunnels

Ground simulation systems became more and more sophisticated in the early 2000s, leading to the adoption of suction systems and moving ground systems becoming the standard for automotive wind tunnels. Wiedemann et al. [18] investigated the effects of these systems and attempted to see if the influences of the systems on the flow can be separated and analyzed individually.

The experiments performed by Wiedemann and his colleagues were performed on two different $1:5$ scale models in the IVK Model Wind Tunnel. By changing the suction values higher and lower than their baseline values, the influence of the suction on the static pressure and drag coefficient was found. Wiedemann et al. describes the influence as consisting of two parts; one part due to the ground simulation, that is, the reduction in the thickness of the boundary layer influencing the flow under the model and one part due to the static pressure gradient; which changes due to the unintended additional pressure gradient from suction [18].

In the data shown by Wiedemann et al. [18], the suction systems change the shape of the static pressure curve and create a peak roughly where the suction zone ends. The authors plotted the change of drag coefficient ΔC_D with respect to the ratio of suction velocity w to free-stream velocity U, $\frac{w}{U}$, and found that for ratios beyond roughly $0.1 - 0.2$ there was a linear growth in the ΔC_D reported. The exponential component of the curve was then found to be due to the growth of the boundary layer at low suction rates, and thus, for a high enough rate the relationship between suction rate and ΔC_D becomes linear. Wiedemann et al. conclude that to offset the effect of gradient-induced drag on the C_D measurements one could move the model further downstream or reduce the suction velocity. However, both of these ideas will increase the thickness of the boundary layer, which could lead to further adverse effects; however, this is mitigated if the belt is placed directly after where the suction ends such as in the case of the center belt in the Volvo PVT. Tangiential blowing is briefly mentioned as a potential solution to mitigate the effect of a thicker boundary layer due to reduced suction [18].

The findings in this paper are important to this thesis as it gives credence to the theory that suction rates play an important role in both the measured values of the static pressure along the test section but also the shape of the curve. The data presented to the author at the start of this project showed a peak in static pressure upstream of the turntable center. Finding both a reason for this peak and confirming that it can be changed through the suction rates of the BLRS gives further reason to attempt the same study for the Volvo PVT.

A few years later, Wickern et al. [19] performed a study similar to that done by Wiedemann et al. [18], however, in a full-scale wind tunnel. Conducted in the Audi $3/4$ open jet wind tunnel, *Gradient Effects on Drag Due to Boundary-Layer Suction in Automotive Wind Tunnels* focuses on the influence

the suction rate has on the measured C_D. Wickern et al. performed both experimental and numerical studies in the wind tunnel with the results showing that the gradient effect of having too much suction dominates the contribution of ΔC_D that BLRS has on the measurements.

At the standard rate of suction, 7% of the free-stream velocity, the displacement thickness in the wind tunnel was measured as $\delta^* = 1$ mm. Three different vehicle types were tested; sedan, squareback and van. For all three types, it was seen that increasing suction above the standard value contributed to a linear increase in C_D, although with slightly different slopes correlated with the sensitivity of each vehicle type to the rate of suction change. The values of ΔC_D range from 0.005 to 0.013 for suction rates $0.07 \leq \frac{w}{U} \leq 0.23$ in the test case with the sedan with w being the suction velocity and U the free-stream velocity [19].

This paper like the previous one shows that an investigation into the suction rates for the Volvo PVT is necessary. If the results here are similar to the results found in the Volvo PVT it would mean that a significant amount of the excess drag reported when comparing the PVT to other wind tunnels could be due to the excess suction. The Volvo PVT has a displacement thickness of around 0.35 mm, so a threefold increase in the displacement thickness would put the Volvo PVT at the same displacement thickness as the Audi wind tunnel, with the hopes of seeing the same linear decrease in ΔC_D due to suction [19]. However, one thing to keep in mind is that the size of the wind tunnel nozzle used in this study is considerably smaller than that of the Volvo Cars PVT. It is not guaranteed that one should see a similar influence on the flow in the PVT.

In March of 1988 a collaborative study between Volvo, Porsche and the German-Dutch Wind Tunnel (DNW) was executed, studying the effects that boundary layer control systems have on measurements taken on automobiles. This study was carried out experimentally at all 3 wind tunnels and is one of the first studies carried out on this topic. The Porsche and Volvo wind tunnels were slotted wall wind tunnels equipped with basic boundary layer suction systems using a perforated plate before the turn table. The DNW wind tunnel used tangential blowing to control the boundary layer. Several different vehicles were tested, with different configurations for each vehicle. The vehicles tested were the Mira notch, wagon, and slant back, Volvo 760 GLE wagon, notch and slant back, Mazda Cosmo, Porsche 928 S, 924 S, 944 Turbo, 911 Carrera, and 956 C [20]. The same boundary layer control settings were used for each vehicle tested.

Berndtsson et al. [20] find in their analysis that for both types of boundary layer control system, there is an increase in measured C_D for decreasing displacement thickness. This effect is different for different types of cars though, and the authors split the vehicles into two groups, passenger cars, and racing cars. It is noted that for the racing car category, the sensitivity of the change in C_D was higher compared to passenger cars as the displacement thickness goes to 0. This makes sense as these cars tend to have much lower ground clearance than a passenger car and therefore the effect of changes in the boundary layer is more pronounced.

Looking at the suction systems, for the Porsche tunnel an increase of $\Delta C_D/C_{D_o} = 2 - 3.7\%$ (C_{D_o} is the measured drag with control systems off) was observed while in the Volvo tunnel an increase of $1.3 - 2.8\%$ was recorded when compared to having the systems off. When comparing the tangential

blowing with the suction system for a test case with the Porsche 956 there was a noted decrease in measured drag when using the suction system versus the tangential blowers. Due to this difference, Berndtsson et al. [20] recommend a follow up study be done to investigate the differences between the systems. The authors also recommend that a parameter study of the suction rate be performed for boundary layer suction systems, which, as seen above, will be done later by Wiedemann et al. [18]. A Reynolds number sensitivity was confirmed in the measurements of both types of boundary layer control system, with the different passenger cars having a similar sensitivity while the different racing car models had considerable differences.

The analysis presented by Berndtsson et al. [20] is one of the earliest works on the topic of the influence of boundary layer control systems on drag measurements. This work was important in laying the foundations for future analyzes such as the work by Wiedemann et al. [18], however, it is hard to know exactly how well the results translate to modern wind tunnels. The wind tunnels used in this paper had no moving ground systems and still wheels during the tests, where the flow is re-injected from the suction systems and what wind speed calibration method is used can affect the results. The boundary layer thickness without using BLCS also differs and can affect the flow differently when comparing different wind tunnels. Suction systems and tangential blowers also have different effects on the flow, as suction systems reduce the mass flow rate and on average slow the flow while remaining in the wind tunnel tangential blowers speed up the flow on average.

In his doctoral thesis, *Evaluation and modeling of the flow in a slotted wall wind tunnel*, Ljungskog [21] goes into depth on the design and analysis of the Volvo PVT. His work was divided into 4 subtopics:

1. The effect of tangential blowing on the aerodynamic forces of a passenger vehicle.
2. Quantifying uncertainty in flow measurements in a slotted wall wind tunnel.
3. Flow angularity in a slotted wall wind tunnel.
4. Inclusion of the physical geometry of the wind tunnel for improving prediction in Computational Fluid Dynamics (CFD).

This work is the one of the more recent experimental work done on the Volvo PVT and is very relevant to this thesis. It provides up-to-date flow quality measurement data using modern probes, and attempts to account for the slight flow angularity and asymmetry across the y axis in the tunnel. After a number of different experiments, the investigators concluded that the angularity and asymmetry of the flow can be due to some sort of residual vorticity from the fan, no concrete cause or correlation is found in the other parts of the wind tunnel, such as the turbulence wind screens [21].

Ljungskog reports in the investigation of the tangential blowers that there seems to be an asymmetry between the left and right blowers, but also concludes that the tangential blowers are effective at reducing the displacement thickness behind the wheel drive units. An asymmetry was

also found later on in the experiments done by the author which corroborates Ljungskogs findings [21].

Ljungskog found no correlation between wind speed on static pressure or flow angularity. He concludes that the asymmetry in the static pressure and the induced flow angularity could be caused by residual vortices of the fan that interact with the third corner of the wind tunnel, but comments that to confirm this fact, additional measurements must be made in the wind tunnel itself [21].

Ljungskog, however, does not perform any experiments pertaining specifically to BLRS, or its influences on the static pressure or other variables. This provides additional grounds to investigate BLRS with modern measurement equipment, analyze the results, and compare with previous reports, as he did in his investigations.

2.4.3 Wind speed determination methods

When calculating the pressure coefficient it is incredibly important to have a good measure of the free-stream dynamic pressure. For a wind tunnel, this is usually calculated in one of two ways, the *nozzle* method or the *plenum* method. Nijhof et al. [22] goes into detail on the difference between these two methods in automotive wind tunnels.

A general overview of the two methods is shown with explanations of how they differ fundamentally along with equations that describe the calculated pressure differences. A quick summary of the difference between the two methods is that the nozzle method attempts to keep the volume flux constant at the nozzle, while the plenum method keeps the flow velocity at the jet boundary constant when blockage is introduced in the test section. Nijof et al. [22] further detail that specifically for the nozzle method, the static pressure of the flow increases with increasing blockage, which is not the case for the plenum method. Since the flow velocity at the jet boundary is kept constant, the undisturbed static pressure is equal to the pressure in the plenum, and thus the measured plenum pressure can be used as the reference static pressure.

For closed wall wind tunnels only the nozzle method can be used as there is no plenum, for open jet wind tunnels and slotted wall wind tunnels both nozzle or plenum method can be used. In an ideal zero blockage case both methods return the same results as that is the conditions under which they are calibrated; however, Nijhof et al. [22] concludes that differences emerge when blockage is introduced into the test section with major differences seen at high blockage conditions. The authors find that in contrast to previous investigations into the subject, the plenum method was less sensitive to blockage effects compared to the nozzle method and thus should be preferred for measurements. The C_p values for $-2\text{ m} \leq x \leq 2\text{ m}$ were recorded in the test section for the two methods, and the results of the experiments show that depending on the position of the vehicle. The reported value of C_p varies significantly in the nozzle method, where the curves for the plenum method collapse as long as the vehicle is far enough from the nozzle exit plane. The authors mention that boundary layer control systems can also have an influence on tunnel calibration, and that significant errors can result when using the nozzle method, as the nozzle method attempts to keep the volume flux constant. Boundary

layer suction systems modify the volume flux in or near the nozzle exit plane, which can affect the calibration of such systems [22]. The experiments performed during this thesis showed no significant difference in C_D for different BLCS configurations when using the nozzle or plenum method. That is to say that no configuration showed a larger reduction in C_D when using the plenum method when comparing it to other configurations.

Although a slotted wall wind tunnel is not tested in this paper, one can infer that the findings of an open jet wind tunnel will have some correlation to the effects seen in a slotted wall wind tunnel when choosing between the two methods. Considering the idea of modifying the suction rates of the boundary layer system, it seems that the plenum method would be optimal to use if it is shown to be a viable method for the Volvo PVT. Another concept worth noting here is the effect of the distance between the front of the vehicle and the nozzle exit plane for the plenum method. While this is not tested in this work, the author recommends that if Volvo Cars switches to using the plenum method, that a study be carried out on the positioning of the vehicle in the tunnel relative to the nozzle exit plane and the effects it has on the static pressure gradient and measured drag.

2.4.4 Reports on other automotive wind tunnels

In addition to examining work done on the Volvo PVT wind tunnel, the author examined work done on the construction, design, and upgrades of various other wind tunnels in the automotive industry. This was done to get a grasp of the design trends that exist in the industry and more specifically the parameters that are of the utmost importance when designing and tuning the systems in the wind tunnel. The following reports are on wind tunnels with open jet test sections; however, they all use and tuned their BLRS to reduce the gradient of the static pressure along the test section.

Nagel et al. [23] present the work done to design and tune the wind tunnel and its test section at the Ford Rolling Road Wind Tunnel Facility in Michigan. This $3/4$ open jet wind tunnel began operation in January 2022, and has many modern features found in a number of wind tunnels such as interchangeable 1 belt and 5 belt moving ground system, BLRS, two position adjustable nozzle and 6 component balance for measuring forces on the car.

The authors mention multiple times that the most important parameters that affect the static pressure gradient in the test section are the collector; its size, design, and distance to the rear of the vehicle in the test section, and the configuration of the BLRS. The report shows the static pressure curve along the center line from -3 m $\leq x \leq 5$ m at $z = 0.75$ m with steps of $\Delta x = 0.25$ m. The values appear to be in line with what is recommended for wind tunnels reporting a difference of $|\Delta C_p| \leq 0.002$ for one nozzle configuration and $|\Delta C_p| \leq 0.003$ for the other with the reference being taken as the value at the center of the turn table. The displacement thickness values were reported to be $\delta^* \leq 12$ mm at $x = 0$ m and $y = \pm 0.85$ m, where $x = 0$ m is at the centerline of the MGP [23].

Waudby-Smith et al. [24] describe the design, construction, and validation of a new $3/4$ open jet wind tunnel for automotive design in China. The tunnel was built for China Automotive Technology and Research Center (CATARC), which operates within the central government enterprise of China.

This tunnel features a two-position nozzle and the usual suite of boundary layer control systems with primary and secondary suction zones with tangential blowers just upstream of each component of the 5 belt MGP. The authors of the report put emphasis on the design of the collector and BLRS as the two important points concerning the static pressure gradient. The static pressure was reported to be within the limits of $|C_p| \leq 0.002$ with the static pressure gradient $\left|\frac{\partial C_p}{\partial x}\right| \leq 0.0015[\frac{1}{\text{m}}]$ from -3.5 m $\leq x \leq 4.5$ m at $y = [0 \text{ m}, \ \pm 1.8 \text{ m}]$ and $z = [0.7 \text{ m}, \ 1.4 \text{ m}, \ 2.0 \text{ m}]$. An interesting fact was seen here that the target for the displacement thickness at the center of the turntable was $\delta^* \leq 5$ mm, with values in the range of $1 - 1.6$ mm seen at the turntable center and upstream at $x = -2.5$ m with $y \leq \pm 0.70$ m.

When comparing this with the displacement thickness at the center of the turn table in the Volvo PVT wind tunnel reported by Sterneus et al. [14], this is much higher by a factor of around $3 - 5$. This inspired the author to investigate the possibility of reducing the suction rates of the BLRS in the Volvo PVT in hopes that the static pressure gradient would be reduced while still maintaining a displacement thickness below this value keeping the Volvo PVT in line with its industry counterparts.

Best et al. [25] details the construction and design of the new aeroacoustic Honda Automotive Laboratories of Ohio (HALO) wind tunnel in Marysville, Ohio. Having started operations in 2022, this closed return $3/4$ open jet wind tunnel has all the modern features that we have seen so far. It features a two-position nozzle system, an interchangeable single and five-belt moving ground plane (MGP), BLRS with adjustable scoop cover, and a six-component force balance together with acoustic equipment and treatments.

As seen in the other wind tunnel reports, Best et al. [25] emphasize the importance of the influence of the BLRS on the static pressure gradient. This wind tunnel uses a traditional scoop at the nozzle along with a combination of suction and blower slots within the test section upstream of the vehicle to control the boundary layer and its profile while keeping the influence on the static pressure gradient to a minimum. The axial static pressure is reported to be within the bounds of $|C_p| \leq 0.002$ within the testing area -3.5 m $\leq x \leq 4.5$ m. Best et al. also note that the boundary layer profile at different speeds is consistent and mention that the displacement thickness at the upstream wheel drive units was below 5 mm.

Buckisch et al. [26] describe the design and construction of the Daimler Aeroacoustic wind tunnel in operation at the Mercedes-Benz Technology Center in Sindelfingen, Germany. Beginning operations in 2013, this facility has a single position nozzle, five belt MGP, force balance, and BLRS. The BLRS is similar to the ones mentioned previously, with a nozzle scoop to remove the initial boundary layer from the flow in the circuit, a perforated suction zone upstream of the turntable, and a tangential blower and suction gap in front of the center belt. Buckisch et al. reported a static pressure of $|C_p| < 0.002$ and $\left|\frac{\partial C_p}{\partial x}\right| \leq 0.0007\frac{1}{\text{m}}$ over the span of -3.0 m $\leq x \leq 5.0$ m, with $\Delta x = 0.5$ m for $y = \pm 0.7$ and 0.5 m $\leq z \leq 1.0$ m, with wind speeds $U = [60, \ 90, \ 140, \ 200]$ km/h being tested [26].

The axial pressure gradient is remarkable, and provides a good target to aim for when tuning the systems in the Volvo PVT wind tunnel. Although not explicitly mentioned what factors contributed to performance, one can infer from previous reports that careful tuning of the BLRS and the design of

the nozzle and collector must have played a role. Unfortunately however, the authors make no mention of the boundary layer profile or the displacement thickness. If it can be shown that the Volvo PVT can reach the performance of the Daimler Aeroacoustic Wind Tunnel without sacrificing too much in the way of displacement thickness, that would be the ideal configuration.

2.5 Summary

After review of the works presented above, it is clear that the boundary layer control systems and the wind speed determination method have the potential to have a significant adverse effect on the static pressure and consequently the measured drag on the vehicle. The plenum method is the norm when it comes to measuring the dynamic pressure in open jet wind tunnels, and it would be of interest to see the effect of using that instead of the nozzle method in a slotted wall wind tunnel as data on the differences between these two methods for this specific type of test section have not been found. A study of suction rates, tangential blowing downstream of the moving belts and how they relate to C_D is also paramount to perform, as this seems to be a considerable contributing factor to the total C_D seen in the Volvo PVT.

The following relationships are defined from this review of previous works in the area, and form a basis of important parameters to consider during experimentation:

1. To simulate open-road conditions, some form of boundary layer control must be employed. The performance of these systems can be quantified by the boundary layer height δ and displacement thickness δ^*.

2. These systems influence the flow; depending on the suction rate, significant changes can be seen in the measured values of C_p.

3. This change in static pressure, seen in C_p influences the measured drag coefficient C_D. This influence can be represented as some ΔC_D, with the reference being the C_D value when the control systems are in a reference state, i.e. off.

4. The suction systems can also influence the dynamic pressure at the point or points where the wind speed is calibrated relative to the rest of the test section. This affects the wind speed determination and, therefore, also C_D.

5. There is a relationship between the desired δ^* and ΔC_D and one must balance the desired displacement thickness with what is considered acceptable for ΔC_D.

Chapter 3

Theory

3.1 Governing equations

The governing equations for incompressible fluid motion are the incompressible Navier-Stokes equations, which consist of the continuity and the momentum equations [27].

3.1.1 Mass conservation

The continuity equation, which describes the conservation of mass:

$$\frac{1}{\rho(\mathbf{x},t)}\frac{D}{Dt}\rho(\mathbf{x},t) + \nabla \cdot \mathbf{u}(\mathbf{x},t) = 0 \,, \tag{3.1}$$

where:

$$\frac{D}{Dt}\rho(\mathbf{x},t) \equiv \frac{\partial \rho}{\partial t} + \mathbf{u} \cdot \nabla \rho \,. \tag{3.2}$$

In this equation, ρ represents the density of the fluid, $\mathbf{u}$ is the velocity vector. $\mathbf{x}$ is the spatial coordinate and t is time. For flows in which the effects of compressibility are negligible or nonexistent, the continuity equation 3.1 can be further simplified since the total rate of change of density 3.2 is zero. With

$$\frac{D}{Dt}\rho(x,t) = 0 \tag{3.3}$$

equation 3.1 reduces to:

$$\nabla \cdot \mathbf{u}(\mathbf{x},t) = 0 \,. \tag{3.4}$$

This is valid for flows in which density changes are small. In general, a fluid is considered *incompressible* if the density does not change with pressure. The general rule of thumb is that liquids

are almost incompressible and can be considered incompressible for most cases. Gases are always considered compressible by definition, but for flow speeds less than around 100 m/s, the change of absolute pressure is small. Due to small changes in absolute pressure, density changes are considered negligible and the incompressible description of mass conservation can be used [27]. The flows in this work can be considered to be incompressible in nature, and as such the incompressible forms of the momentum and energy equations will be shown.

3.1.2 Momentum conservation

The momentum equation of the incompressible Navier-Stokes equations in vector form, describes the conservation of momentum is:

$$\frac{\partial \mathbf{u}}{\partial t} + \mathbf{u} \cdot \nabla \mathbf{u} = -\frac{1}{\rho}\nabla p + \mathbf{g} + \nu \nabla^2 \mathbf{u} \,. \tag{3.5}$$

Here, p is pressure, $\mathbf{g}$ represents the body forces acting on the fluid element and ν is the kinematic viscosity of the fluid [27].

3.2 Boundary layer

For near-wall flows, Prandtl theorized that the effect of viscosity is important, but becomes negligible as the distance from the wall increases. Prandtl proposed that a fluid particle at the surface of the wall will have zero relative velocity to the wall. As one moves away from the wall, the fluid velocity changes from zero to the free-stream velocity. This process is not instantaneous, it is gradual and creates a velocity gradient. Prandtl derived a modified version of the Navier-Stokes equation system for these near-wall flows [3].

The Navier-Stokes equation system for a steady incompressible two-dimensional boundary layer flow are [27]:

$$\frac{\partial u}{\partial x} + \frac{\partial v}{\partial y} = 0 \tag{3.6}$$

$$u\frac{\partial u}{\partial x} + v\frac{\partial u}{\partial y} = -\frac{1}{\rho}\frac{\partial p}{\partial x} + \nu\frac{\partial^2 u}{\partial y^2} \tag{3.7}$$

$$-\frac{\partial p}{\partial y} = 0 \tag{3.8}$$

u and v here are the velocities in the x (streamwise) and y (wall-normal) directions.

3.2.1 Boundary layer height and velocity profiles

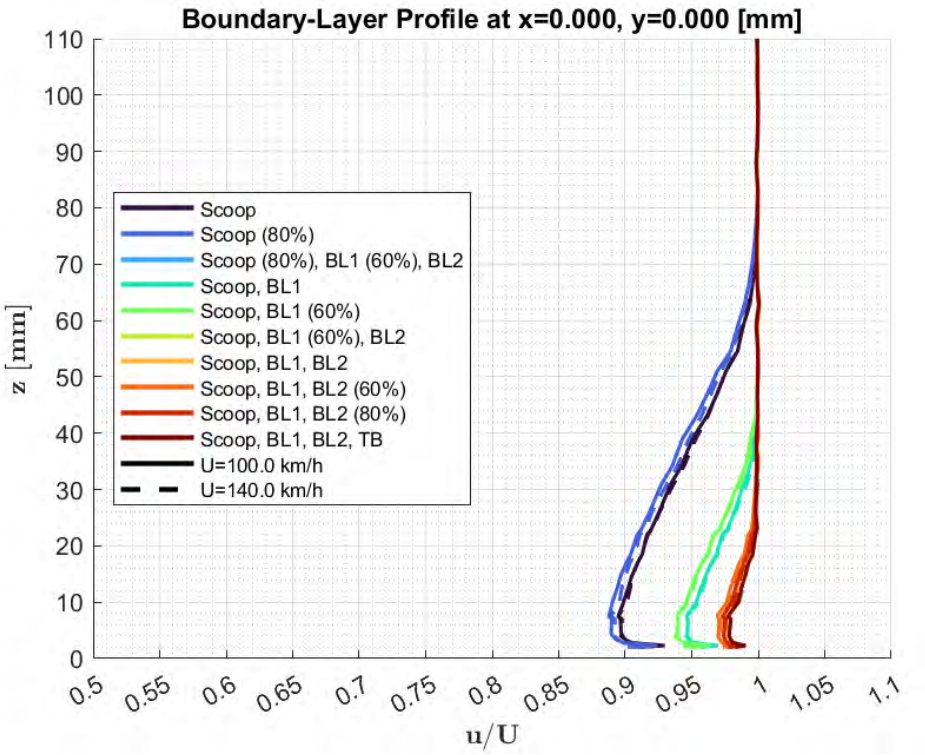

Figure 3.1: Boundary layer profiles for different BLRS configurations and free-stream velocity with data taken on the moving ground plane.

A question arises with boundary layer theory, that question is: Where is the divide between the free-stream flow and the boundary layer? The boundary layer region is defined by its height or distance from the wall, and this height is often defined as the height at which the velocity in the boundary layer reaches some value close to the free-stream flow. This value is often defined as $95 - 99\%$ of the free-stream velocity [27].

An important part of the boundary layer is the velocity profile of the boundary layer. The velocity profile can have varying shapes depending on the characteristics of the flow and the fluid flowing. Shown in figures 3.1 and 3.2, one can see examples from the experiments in the Volvo PVT of the boundary layer profiles at two different positions. One along the centerline and one at $y = 1930$ mm. u is the local velocity and U is the free-stream velocity, so u/U is the ratio of the local velocity to the free-stream velocity.

The data shown in figure 3.1 is taken on the moving belt of the moving ground plane, so the boundary layer profile first has a speed close to that of the moving ground. However, the incoming flow on the belt has a boundary layer to some extent even though the suction is applied upstream of the belt.

This results in a small decrease in velocity going away from the belt. After that the velocity increases until it reaches the free-stream velocity. Figure 3.2 shows a more ”traditional” looking profile, as the data was taken off the moving ground plane.

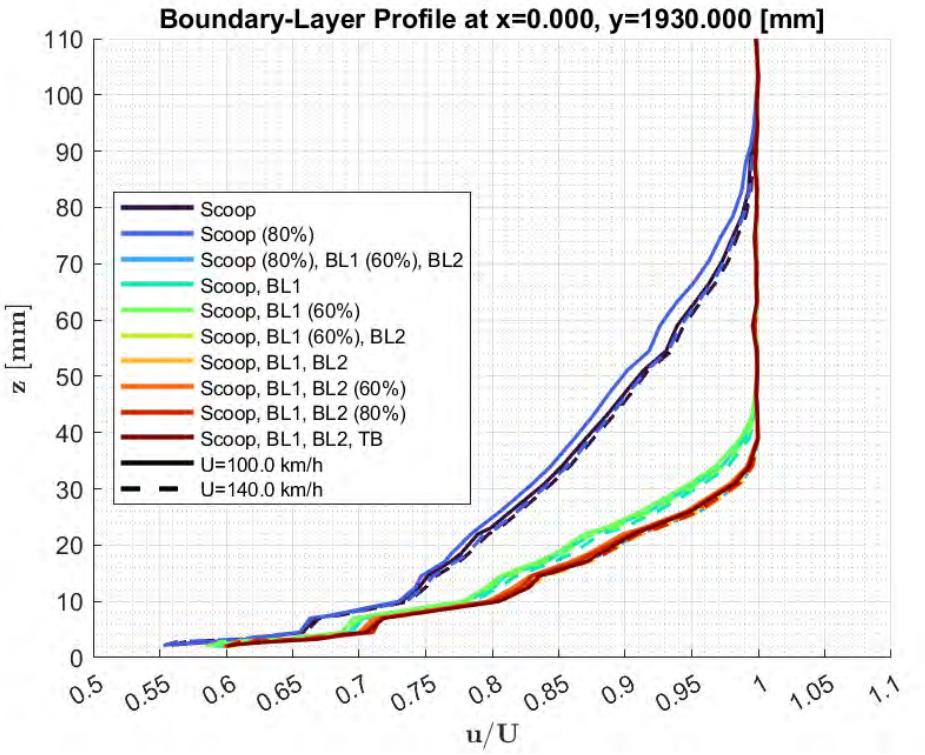

Figure 3.2: Boundary layer profiles for different BLRS configurations and free-stream velocity off of the moving ground plane.

3.2.2 Displacement and momentum thicknesses

While the definition of the boundary layer thickness can differ depending on how one defines δ, it can be useful to have more finite measures of the boundary layer. Two measures that are ubiquitous to boundary layer analysis are the displacement, and momentum thicknesses. The displacement and momentum thickness are two measures of how much the presence of a boundary layer influences the flow.

The displacement thickness δ^*, can be thought of as the distance that one would need to move a plate in the y direction to reduce the volume flow in an inviscid case to be equivalent to a flow influenced by the presence of a boundary layer. This thickness can be defined with the following equation [27]:

$$\delta^* = \int_0^\infty \left(1 - \frac{u}{U}\right) dy \, . \tag{3.9}$$

The momentum loss due to the presence of a boundary layer is defined by the following relation [27]:

$$\rho U^2 \theta = \int_0^\infty \rho u(U-u)dy \ . \tag{3.10}$$

The momentum thickness θ, is the distance that a surface which has a boundary layer flow forming on it must be displaced so that the total flow momentum is the same as in the case of an inviscid flow. This is defined by the following equation [27]:

$$\theta = \int_0^\infty \frac{u}{U}\left(1-\frac{u}{U}\right)dy \ . \tag{3.11}$$

The ratio of these two values is known as the shape factor H. Which is defined as [27]:

$$H = \frac{\delta^*}{\theta} \ . \tag{3.12}$$

The shape factor gives a measure of the shape of the boundary layer and can be useful in comparing different boundary layer profiles.

3.3 Pressure coefficient

The pressure coefficient is a non-dimensional measure of the pressure. This measure is used to compare the relative pressure in a point in a flow to some reference pressure, usually in the undisturbed free-stream.

It is defined by:

$$C_p = \frac{p_s - p_\infty}{q_\infty} = \frac{p_s - p_\infty}{\frac{1}{2}\rho U^2} \ . \tag{3.13}$$

Where p_s is the local static pressure, p_∞ is the static pressure of the undisturbed flow, ρ and U have the same definitions as previously discussed. The denominator is the dynamic pressure q_∞, and the numerator is the difference in static pressures between the point being analyzed and the free-stream [27].

If C_p is positive, it indicates that the pressure at that point is higher than the reference. There could be many causes for this but it signifies that something is causing the flow to decelerate. The opposite is true when C_p is negative, indicating a region where there is an acceleration in the flow.

3.4 Drag coefficient

The drag coefficient C_D is a non-dimensional measure of the resistance to moving a shape through a fluid. It is defined as:

$$C_D = \frac{F_D}{q_\infty A} = \frac{F_D}{\frac{1}{2}\rho U^2 A} \,. \tag{3.14}$$

Here F_D is the drag force measured on the object, and A is the cross-sectional area. Pressure and friction make up F_D and in bluff-body flows, such as the flow around a car, the pressure dominates over friction in its contribution to the total drag [28].

Chapter 4

Experimental methodology

A chain of relationships that govern the variables of interest was outlined in section 2.5. To quantify this relationship between the variables, a series of investigations was performed. These investigations can be broken down into three categories of tests. Tests investigating the static pressure and its gradient, tests investigating the boundary layer, and tests investigating the drag coefficient. All of these tests involved turning on and off the various boundary layer control systems or changing their suction values.

4.1 Static pressure C_p and the static pressure gradient $\frac{\partial C_p}{\partial x}$

A large study of static pressure and its gradient was carried out along the tunnel test section. These tests were performed by traversing the test section along a predefined set of 51 points. The sweeps were performed by a moving traverse in the tunnel with an omniprobe system attached to its tip. Two omniprobe systems were used; one omniprobe system with a bidant fork with a omniprobe on each prong, the other system was a single larger omniprobe on a long rod extending laterally from the tip of the traverse. A series of tests were also performed using pressure patches on both the walls of the test section and a Volvo C40.

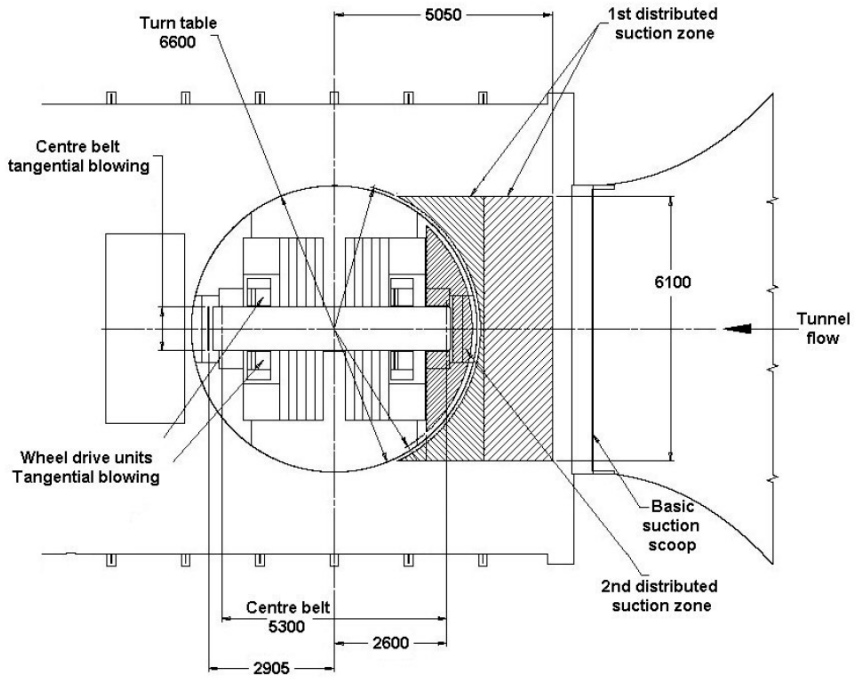

Figure 4.1: Overhead view of the Volvo PVT wind tunnel test section. The position of Boundary layer pre-suction zone one (BL1) and Boundary layer pre-suction zone two (BL2) are shown along with the scoop, MGP system and TB. Courtesy of Volvo Cars.

The data sweeps are performed according to the following coordinate map shown in figure 4.2, and these positions can be compared to figure 4.1 above to get an idea of where they are in the test section. Not seen clearly in the figure are the sweeps in z, which is why there are a few points stacked on top of each other in this image.

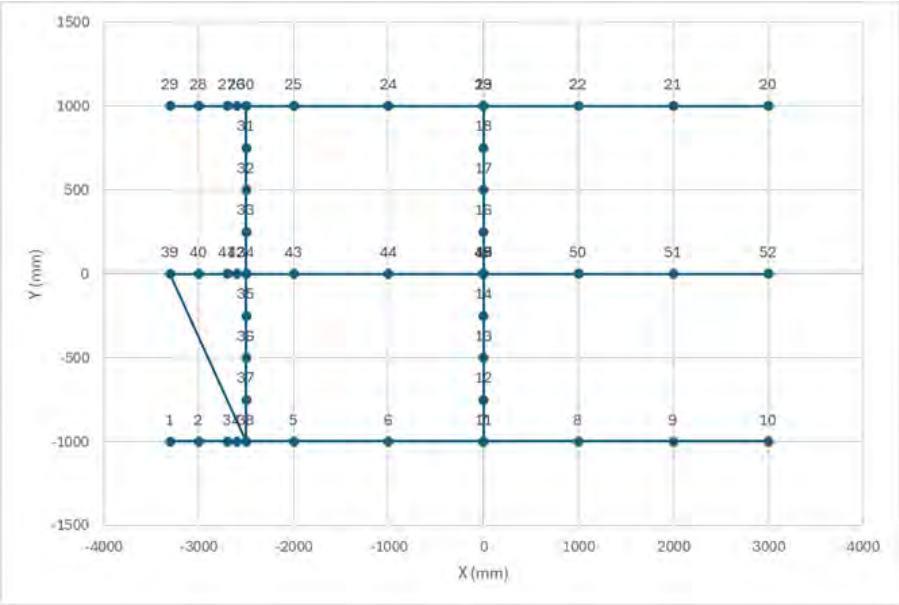

Figure 4.2: Map of positions measured for static pressure sweeps in the empty wind tunnel. $(x, y) = (0, 0)$ represents the center of the turn table in the test section.

At each point the traverse stops for a set amount of time, sampling flow data at a set frequency, and performing an average over those samples. That average becomes the recorded value for that point. This sweep took on average 70 minutes to complete. Many different configurations of both boundary layer control system settings and probe systems were tested, with a focus on capturing as much data as possible for a these configurations to ensure repeatability of the values.

For the initial tests preformed in the Volvo PVT wind tunnel, the dual probe system was used. Some concerns arose on the influence of the probes orientation on the measurements, so multiple tests were repeated with the probe at different angles relative the traverse. The angles tested were $90°$ and $180°$ from the original orientation shown below in figure 4.3. A benchmark test case was chosen to check for the repeatability of the measurements for both probe systems and the different rotations of the dual probe system. This benchmark case ran the scoop and the first boundary layer suction system at their standard settings, the values can be seen in table 4.2 in the row BL Mode 6.

Figure 4.3: Dual probe measurement system on the traverse used for static pressure measurements. The probe is in its ”standard” orientation in this image. Image taken by the author, published with permission of Volvo Cars.

Additional concerns were raised on the influence of the traverse on the measurements; it was postulated that its proximity to the dual probe system could potentially influence the measurements. Some differences were seen in the measured values for the axial static pressure for the different orientations of the dual probe system. The changes in the static pressure being examined are small and it is not far fetched to consider that the proximity of the traverse to the probes could affect the measurements. A separate omniprobe system was employed at a distance from the traverse to investigate this hypothesis, and is shown in figure 4.5. After numerous tests, it was concluded that there can be small variations from test to test depending on which probe or orientation is used but the shape of the curves is consistent. The gradient of the pressure coefficient is the variable of interest, so having consistent curves for each configuration of the boundary layer control systems is important.

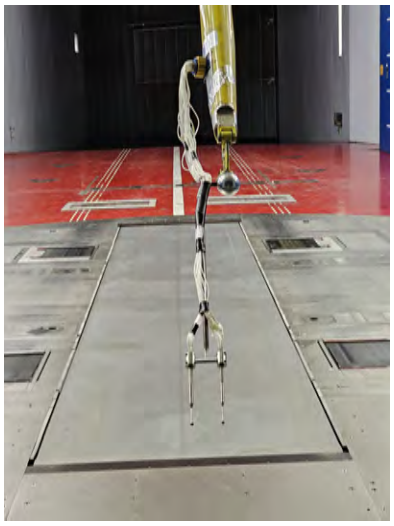

Figure 4.4: Dual probe measurement system on the traverse used for static pressure measurements. The probe is rotated 90° from its ”standard” orientation in this image. Image taken by the author, published with permission of Volvo Cars.

Data for static pressure along the walls of the test section and on the Volvo C40 being tested were also collected using pressure patches placed on the vehicle and on the walls of the test section. This data was gathered to see if there were any significant effects on the pressure at the walls of the test section and to see if there could be any link between that and the sides of the vehicle. All pressure patches were connected to pressure blocks that were connected to the wind tunnel computer system for data collection.

Figure 4.5: Omniprobe mounted on long pole away from the traverse, for testing the influence of the traverses proximity to the measurement device. Image taken by the author, published with permission of Volvo Cars.

Figure 4.6: Close up shot of the boundary layer rake employed for the experiments. Image taken by the author, published with permission of Volvo Cars.

4.2 Investigation of the boundary layer

Once enough data on the effect of the boundary layer control systems on the static pressure and its gradient was collected, the boundary layer was investigated. This investigation was carried out by placing a boundary layer rake shown above in figure 4.6 at specific points in the test section of the wind tunnel and alternating the boundary layer system configurations. Two x positions were chosen, one upstream of the center of the turntable near the position where the front of the vehicle would sit and one in the center of the turntable. For each of those x, nine y positions were investigated, giving a total of 18 points.

To place the rake at each of these positions, the rake and the beam to which it was attached was moved to a given position x_0 and y_0, with the beam centered at that coordinate. Once in place, the system was taped down to ensure no movement during the experiment. From there, three coordinates could be measured in quick succession, one for the position at the center of the beam, and two on either side at $y = y_0 \pm 400$ mm. This process was repeated a total of 6 times, and the coordinates can be seen below in table 4.1.

Figure 4.7: Boundary layer rake set up, the rake can be moved along the beam to specific locations and locked in place. Image taken by the author, published with permission of Volvo Cars.

	$x = 0$ mm	$x = -2275$ mm
$y =$	± 1930 mm	± 1930 mm
$y =$	± 1530 mm	± 1530 mm
$y =$	± 1130 mm	± 1130 mm
$y =$	± 400 mm	± 400 mm
$y =$	0 mm	0 mm

Table 4.1: Table of coordinates tested for the boundary layer measurements.

The upstream x position was chosen to be just behind the second boundary layer suction plate as having the structure holding the rake on the suction plate would block part of the suction and potentially interfere with the results. The lateral positions were also limited by the fact that the feet of the structure were large and could not be placed on the MGP.

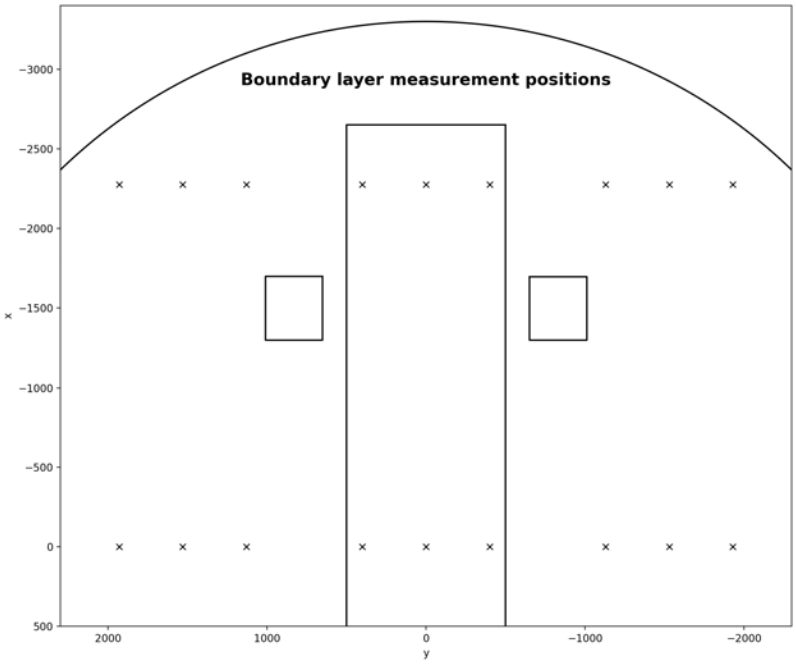

Figure 4.8: Figure showing the measurement positions for the boundary layer rake experiments.

4.3 Drag coefficient C_D

Once data on static pressure and boundary layer were collected in the empty test section, the final parameter to investigate was the drag coefficient. This was performed by mounting a number of pressure patches to a Volvo C40 and testing it in the wind tunnel with different speeds, boundary layer configurations and wind speed determination methods. The determination of the C_D coefficient is achieved by using the wind tunnel balance in conjunction with distinct wind speed calibrations tailored to each boundary layer configuration. Additionally, pressure patches offer additional data on what happens to the pressure in various configurations.

To analyze the different configurations, a parametric study was performed by varying different combinations of boundary layer control systems suction values to be compared to the original ”Aero” mode. The two tables below, tables 4.2 and 4.3, provide an overview of the 16 different configurations used in this series of experiments for the two wind speeds. The influence of the wind speed determination method on C_D was also investigated using the same probes and data used here and is described in more detail in section 4.4 below.

Figure 4.9: Picture of the Volvo C40 being tested with pressure patches mounted onto the body of the vehicle. Image taken by the author, published with permission of Volvo Cars.

Scoop	BL1	BL2	TB	BL Mode
0.8	0	0	0	1
1	0	0	0	2
1	0.6	0	0	3
1	1	0	0	4
1	0.87	0	0	5
1.15	0.87	0	0	6
1.15	1	0	0	7
1	1	0.5	0	8
1	1	0.6	0	9
1	1	0.8	0	10
1	1	1	0	11
1	0.6	1	0	12
0.8	0.6	1	0	13
0.8	0.6	0.6	0	14
1	0.6	0.6	0	15
1	1	1	1	16

Table 4.2: Table showing the suction values of the boundary layer control system for a wind speed of 100 km/h. Normalized against the standard ”Aero” mode, which is mode 16 in this table.

Scoop	BL1	BL2	TB	BL Mode
0.8	0	0	0	1
1	0	0	0	2
1	0.6	0	0	3
1	1	0	0	4
1	0.96	0	0	5
1.116	0.96	0	0	6
1.116	1	0	0	7
1	1	0.5	0	8
1	1	0.6	0	9
1	1	0.8	0	10
1	1	1	0	11
1	0.6	1	0	12
0.8	0.6	1	0	13
0.8	0.6	0.6	0	14
1	0.6	0.6	0	15
1	1	1	1	16

Table 4.3: Table showing the suction values of the boundary layer control system for a wind speed of 140 km/h. Normalized against the standard ”Aero” mode, which is mode 16 in this table.

4.4 Wind speed determination methods

To set and determine the wind speed exiting the nozzle, one must calculate the dynamic pressure $_{\infty}$. This can be done using two different methods, the nozzle and the plenum method. A general description of the two methods are as follows: The nozzle method keeps the volume flux at the nozzle constant, while the plenum method keeps the flow velocity at the jet boundary constant when blockage is introduced into the test section [22]. The velocity profiles for the two methods are illustrated in figure 4.10.

The nozzle method is used primarily in closed test section wind tunnels, but can be used in slotted wall or open jet test sections as well. This method measures the static pressure difference between the settling chamber and a position near the exit plane of the nozzle. It is assumed that the static pressure near the nozzle exit plane is the same as the test section for this method . The plenum method can be used in slotted wall or open jet test sections. It differs from the nozzle method in that it measures the static pressure in the plenum of the test section instead of at the nozzle exit plane and uses that to calculate the dynamic pressure [22].

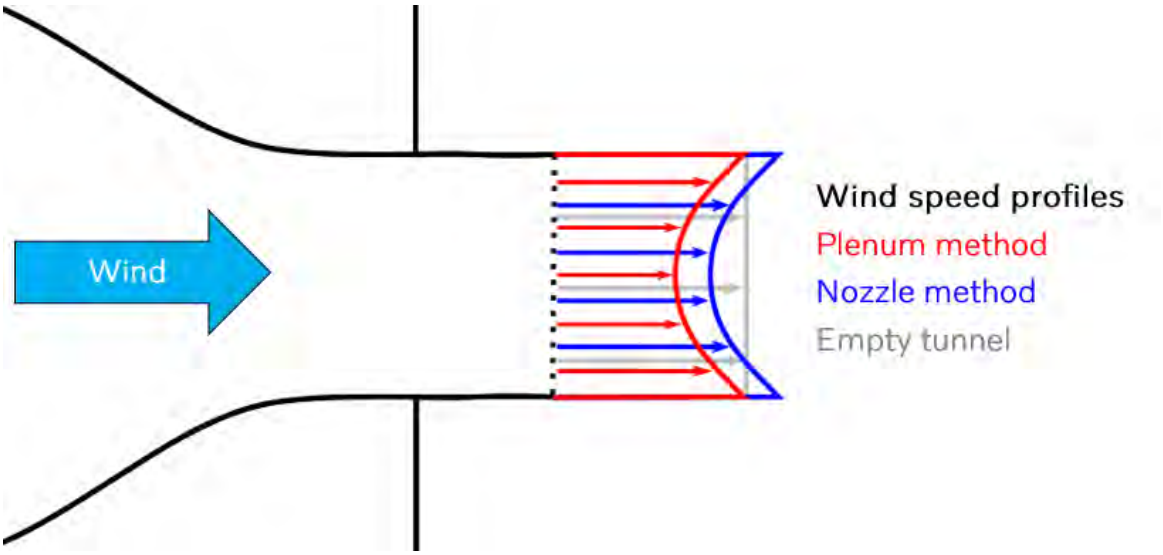

Figure 4.10: Figure showing an example of how the velocity profiles of the two wind speed determination methods differ with blockage introduced in the test section. The profiles are the same for both methods when the wind tunnel is empty [22].

Figure 4.11: Picture of the Pitot tube mounted in the wind tunnel for wind speed calibration. In the background can be seen the pressure patches mounted on the wall of the test section. Image taken by the author, published with permission of Volvo Cars.

To understand the effects that the wind speed method chosen for the wind tunnel had, a pressure spade was placed on each wall just inside the nozzle exit plane in line with the nozzle pressure sensor. For the plenum method, pressure patches were placed within the plenum on each side of the slotted wall test section. Then three nozzle modes were defined; Nozzle 1 for the ceiling sensor normally used in the PVT, Nozzle 2 for the average value measured through the left and right pressure patches that

were placed in the nozzle and Nozzle 3 for the weighted average of the three positions. This was done to see if there were any significant asymmetries in the nozzle that could lead to issues with the wind speed measurements.

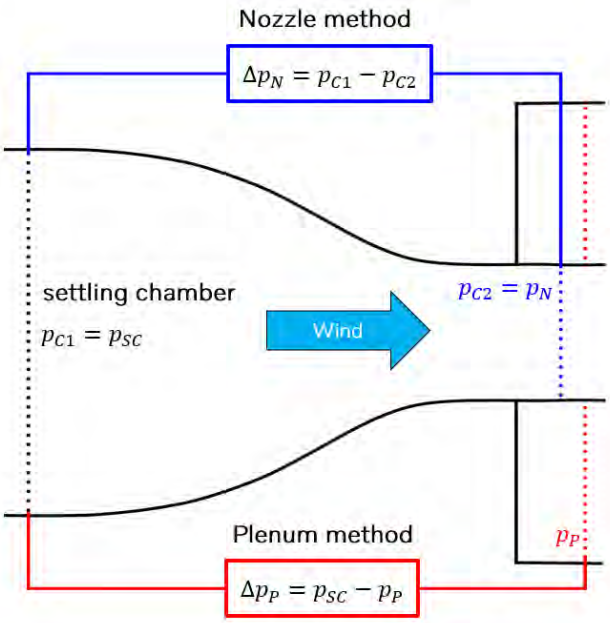

Figure 4.12: Schematic showing how the two different wind speed determination methods are calculated using sensors in a wind tunnel.

The wind speed U_∞ at the nozzle exit can be determined from the dynamic pressure using the following equation:

$$q_\infty = \frac{\rho U_\infty^2}{2} \tag{4.1}$$

To solve for U_∞, a relationship or definition for the dynamic pressure q_∞ is required. q_∞ can be estimated from a pressure difference and a constant k calibrated using a Pitot static tube in an empty test section [22]. The process for determining k is described in the commissioning report by Aiolos from 2006, and involves measuring the total and static pressure on the Prandtl probe and using the provided calibration coefficients for the probe.

The definition for the dynamic pressure becomes:

$$q_\infty = \Delta p \cdot k_q \tag{4.2}$$

where

$$k_q = a_{k_p} + b_{k_p} \cdot \Delta p \tag{4.3}$$

The pressure difference Δp is the difference defined by what wind speed determination method one uses. In the case of the nozzle method it is Δp_N and for the plenum method it is Δp_P [22]. The Volvo Cars PVT wind tunnel always measures the pressure difference between the settling chamber sensor p_{c1} and a sensor on the ceiling of the nozzle p_{c2}. The pressure blocks that connect the pressure patches are also connected to p_{c2}, so the pressure patches in the nozzle and plenum measure the pressure difference to p_{c2}. To use these sensors to determine the wind speed, the measurements of the wind tunnel sensors and the pressure patches are combined. For the nozzle method in figure 4.12 the following relationship is used to calculate the pressure difference between the settling chamber and the pressure patch:

$$\Delta p_{patch} = p_{patch} - p_{c1} \tag{4.4}$$

However, the pressure patches and p_{c1} are not directly linked, thus one must go through p_{c2}, which gives:

$$p_{patch} - p_{c1} = (p_{patch} - p_{c2}) - (p_{c1} - p_{c2}) \tag{4.5}$$

The first differential is measured by the pressure blocks added during the experiments and the second differential is measured by the built in wind tunnel pressure sensor systems. This relationship is used for calculating the nozzle and plenum differential pressures, Δ_{P_N} and Δ_{P_P}, to the pressure patches added to the nozzle and plenum.

Chapter 5

Results and Analysis

5.1 Summary of major results

By changing the wind speed determination method, turning off the tangential blowers and changing the suction ratios for the boundary layer control systems, a maximum change of $\Delta C_D = 0.020$ or twenty counts was observed. Considering that changes in the magnitude of five counts are considered very significant in the automotive industry, this is a remarkable result. No significant change was observed for the three different calculations of the nozzle method outlined above in section 4.4, so nozzle 3 with the standard ”Aero mode” configuration was chosen as the reference to use when comparing the plenum and nozzle methods.

The impact on the displacement thickness at the center of the turn table for the ”optimal reduction” case shown in figure 5.1 is minimal. While exact data for this exact case are is not available, this case is a combination of two other cases for which data was taken. The first case is defined as; 80% for the scoop, 60% for boundary layer pre-suction one and 100% for boundary layer pre-suction two of their ”Aero mode” settings and the second case is defined as 100% for the scoop, 100% for boundary layer pre-suction one and 60% for boundary layer pre-suction two of their ”Aero mode” settings. Both of these cases have tangential blowing off, and are compared to the case with ”Aero” settings with tangential blowing off. The first case shows an increase in displacement thickness of $\Delta\delta^* = .07$ mm, with the second showing $\Delta\delta^* = .14$ mm. The ”optimal reduction” is defined as 80% for the scoop and 60% for boundary layer pre-suction one and two of their ”Aero mode” settings with tangential blowing off.

There is an asymptotic trend in the relationship between suction rate and total displacement thickness, which is seen in the figures presented in subsection 5.3.3. The average change in the boundary layer across all measured points in terms of displacement thickness, momentum thickness, and shape factor are small and are presented in tables 5.3 and 5.4 in subsection 5.3.4. Reduction of suction shows a trend of flattening the static pressure gradient with respect to x, and is seen in all measured spanwise positions in the test section, this trend is clearly seen by the C_p curves presented

in section 5.4.

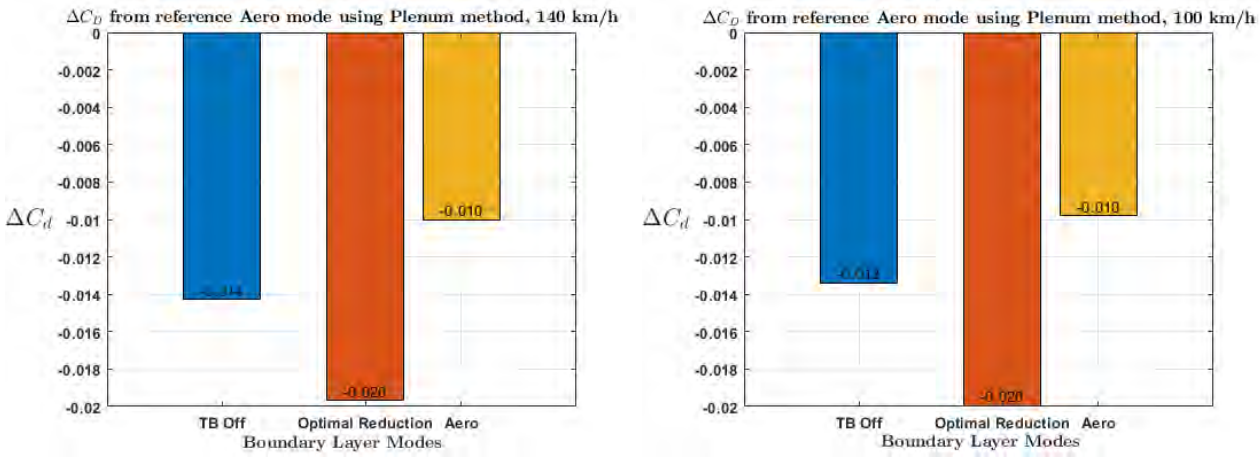

(a) Measured ΔC_D values for 140 km/h

(b) Measured ΔC_D values for 100 km/h

Figure 5.1: A comparison of the measured ΔC_D values for the Volvo C40 using the plenum method with different boundary layer control configurations at 100 km/h and 140 km/h, when compared to the reference ”Aero” mode using the nozzle method. TB Off corresponds to BL Mode 11, Optimal Reduction corresponds to BL Mode 14 and Aero corresponds to BL Mode 16 in table 4.2 and 4.3 respectively. The ”optimal reduction” is defined as 80% for the scoop and 60% for boundary layer pre-suction one and two of their ”Aero mode” settings with tangential blowing off. Values are rounded to the nearest count (0.001).

5.2 Drag coefficient - C_D

As observed in figure 5.1 above, changing the wind speed determination method from nozzle to plenum gave a 10 count reduction in the reported C_D value at 140 km/h for the standard ”Aero mode” configuration of the boundary layer control systems. This same change is seen when testing for a lower wind speed of 100 km/h. This follows the theory for the drag coefficient, as it should not be dependent on the wind speed, as had the value varied significantly, it would have put into question the validity of the results.

Turning off the tangential blowing system nets another 3 to 4 count reduction in C_D. At this point, the total reduction of ΔC_D is at 13 to 14 counts. Reducing the suction rates for the scoop, first and second boundary layer suction systems nets another reduction of 6 to 7 counts for the measured C_D. This brings the total reduction of C_D to 20 counts.

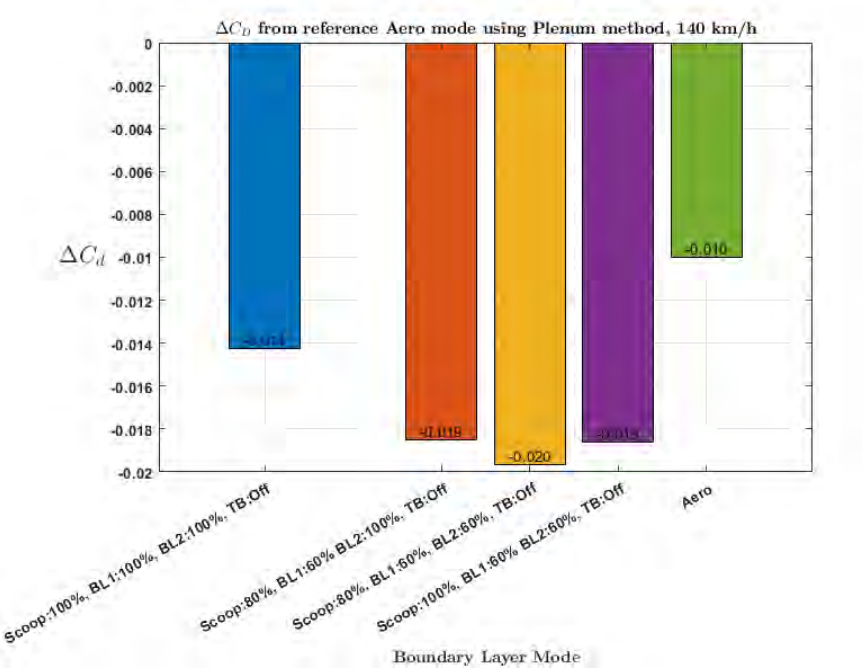

Figure 5.2: A comparison of the measured ΔC_D values for the Volvo C40 using the plenum method with different boundary layer control configurations at 140 km/h, when compared to the reference ”Aero” mode using the nozzle method. The settings are shown in the descriptions for the bars, with the ”optimal reduction” case from figure 5.1 seen in dark yellow.

Some variation can be seen between the similar configurations shown above in figure 5.2. The cost of this reduction in C_D will be shown in the next section with results on the boundary layer height and calculated displacement thickness. The displacement thickness and boundary layer data was unfortunately not captured for the ”optimal reduction” case, as this configuration was created after the boundary layer experiments. However, this configuration was a combination of two other configurations for which data exist, so the displacement thickness and boundary layer height should be within the bounds of these two configurations.

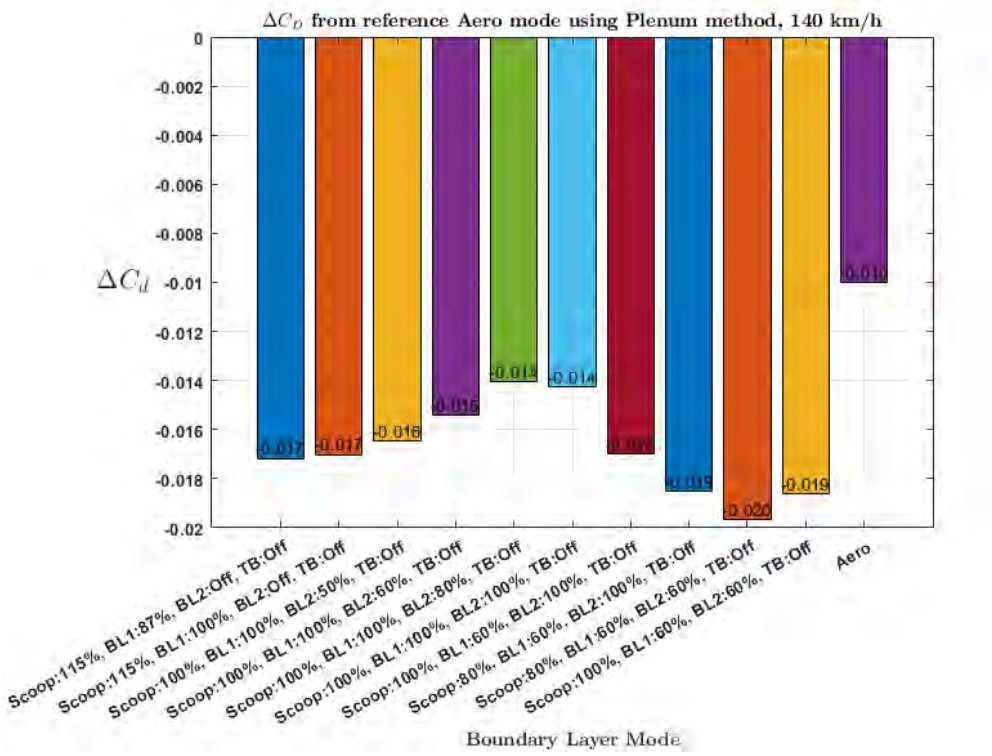

Figure 5.3: A comparison of the measured ΔC_D values for the Volvo C40 using the plenum method with different boundary layer control configurations at 140 km/h, when compared to the reference ”Aero” mode using the nozzle method. The settings are shown in the descriptions for the bars, with the ”optimal reduction” case from figure 5.1 seen labled ”Scoop: 80%, BL1: 60%, BL2: 60%, TB:Off”.

5.3 Boundary layer analysis

5.3.1 Boundary layer profiles

It can be seen in the boundary layer profiles presented here that there are three distinct groups that form based on the configuration used for the boundary layer control system. The first group represented by the blue and black lines in figure 5.4 is the boundary layer profiles when only the boundary layer scoop is activated, at suction values of 80% and 100% of their standard ”Aero” settings. The second group, represented by light green and cyan is the boundary layer profiles for when the scoop and boundary layer pre-suction one are activated, with variation on the suction rate of boundary layer pre-suction one. The third group, represented by the rest of the colors is the boundary layer profiles for when the scoop, boundary layer pre-suction one and two are activated with variations. The baseline case with the tangential blowers is also apart of this group, represented in dark red. Within the groups, it can be seen that reduced suction only causes minor differences, even with reductions of up to 40%. The

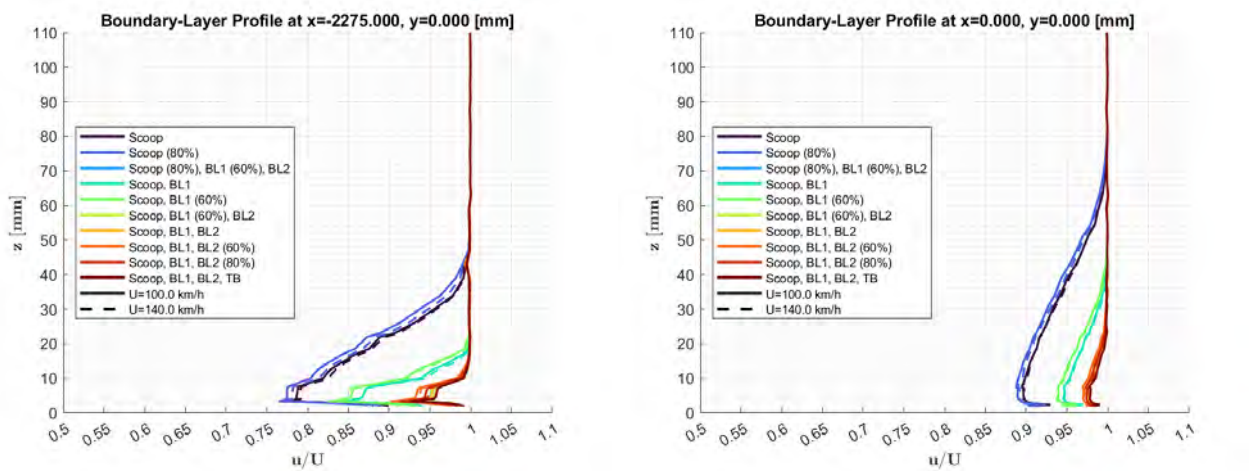

(a) Boundary layer profiles upstream of the turntable center, $x = -2275$ mm, $y = 0$ mm.

(b) Boundary layer profiles at the turntable center, $x = 0$ mm, $y = 0$ mm.

Figure 5.4: Boundary layer profiles upstream and at the turntable center for wind speeds 100 and 140 km/h.

influence of the moving ground system can be clearly seen above in figure 5.4 and 5.5, as it pulls the bottom of the boundary layer in. Moving farther out to $y = -1130$, the effect of the tangential blower is seen as it pushes the boundary layer out beyond the free-stream velocity before returning. At the two furthest points, $y = -1530$ and $y = -1930$, little change is seen in the boundary layer profile for all configurations. The differences between the two tightest groups appear to grow smaller at the extremes in y, while the group with only the scoop activated seems to keep its position away from the other two.

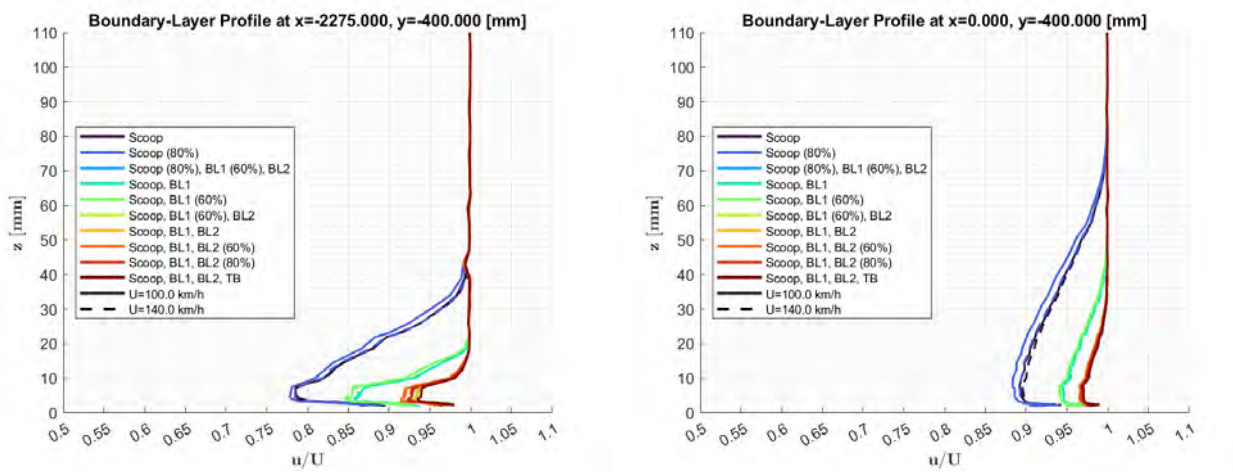

(a) Boundary layer profiles upstream of the turntable center, $x = -2275$ mm, $y = -400$ mm.

(b) Boundary layer profiles at the turntable center, $x = 0$ mm, $y = -400$ mm.

Figure 5.5: Boundary layer profiles upstream and at the turntable center for wind speeds 100 and 140 km/h, $y = -400$.

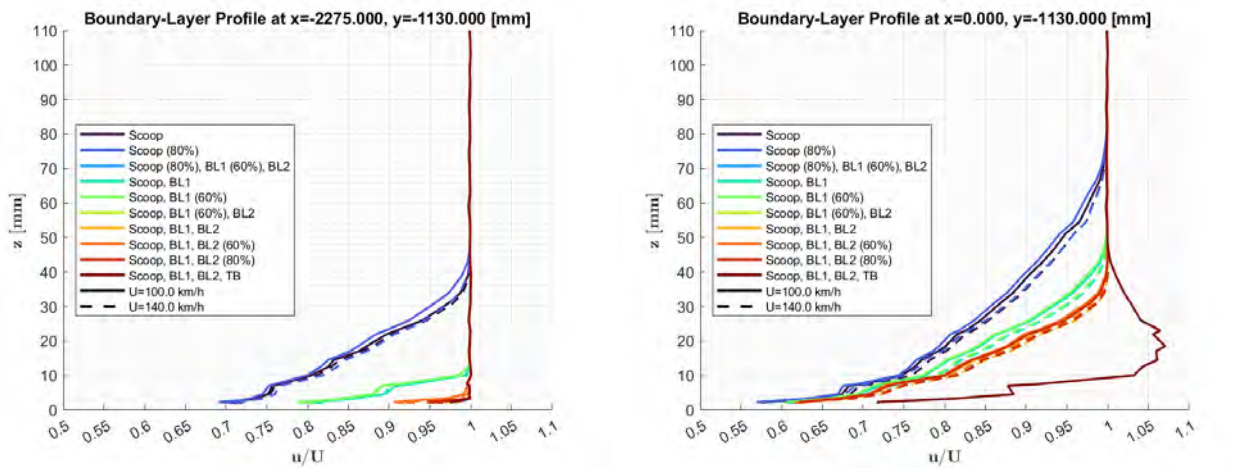

(a) Boundary layer profiles upstream of the turntable center, $x = -2275$ mm, $y = -1130$ mm.

(b) Boundary layer profiles at the turntable center, $x = 0$ mm, $y = -1130$ mm.

Figure 5.6: Boundary layer profiles upstream and at the turntable center for wind speeds 100 and 140 km/h, $y = -1130$.

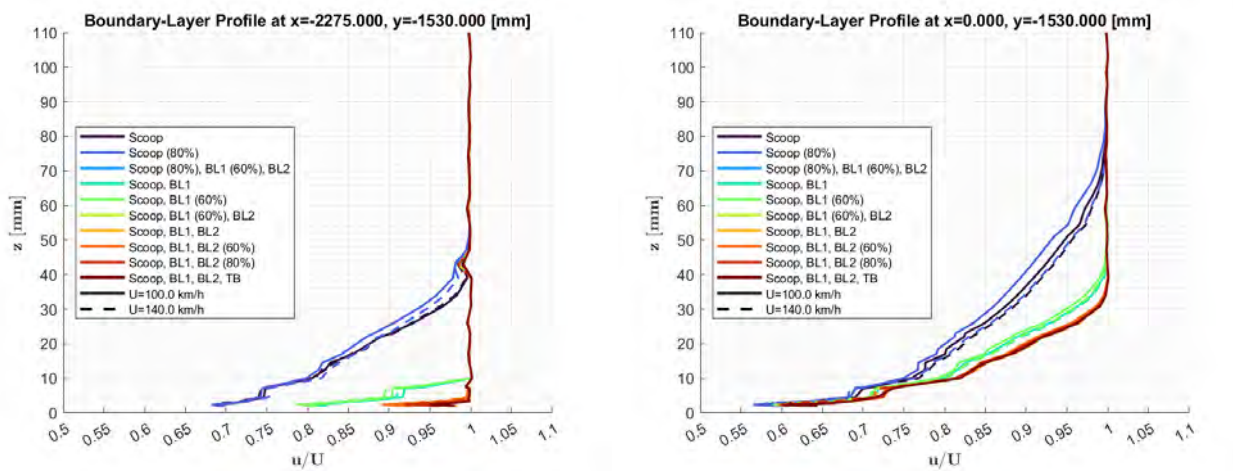

(a) Boundary layer profiles upstream of the turntable center, $x = -2275$ mm, $y = -1530$ mm.

(b) Boundary layer profiles at the turntable center, $x = 0$ mm, $y = -1530$ mm.

Figure 5.7: Boundary layer profiles upstream and at the turntable center for wind speeds 100 and 140 km/h, $y = -1530$.

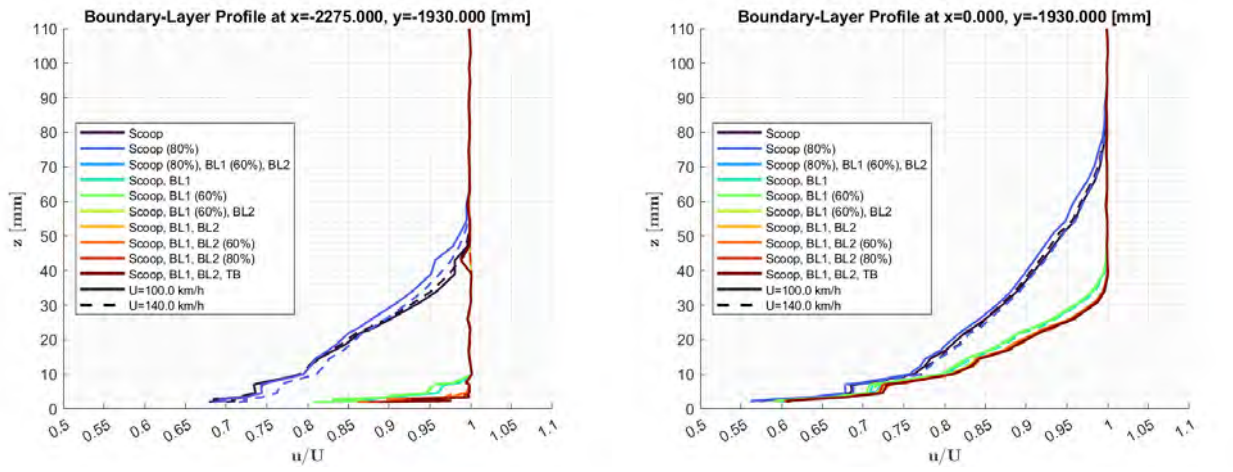

(a) Boundary layer profiles upstream of the turntable center, $x = -2275$ mm, $y = -1930$ mm.

(b) Boundary layer profiles at the turntable center, $x = 0$ mm, $y = -1930$ mm.

Figure 5.8: Boundary layer profiles upstream and at the turntable center for wind speeds 100 and 140 km/h, $y = -1930$.

5.3.2 Boundary layer height

Shown below are the various boundary layer heights recorded for the different configurations at different wind speeds and positions. Not shown are the results for the cases that only employed the

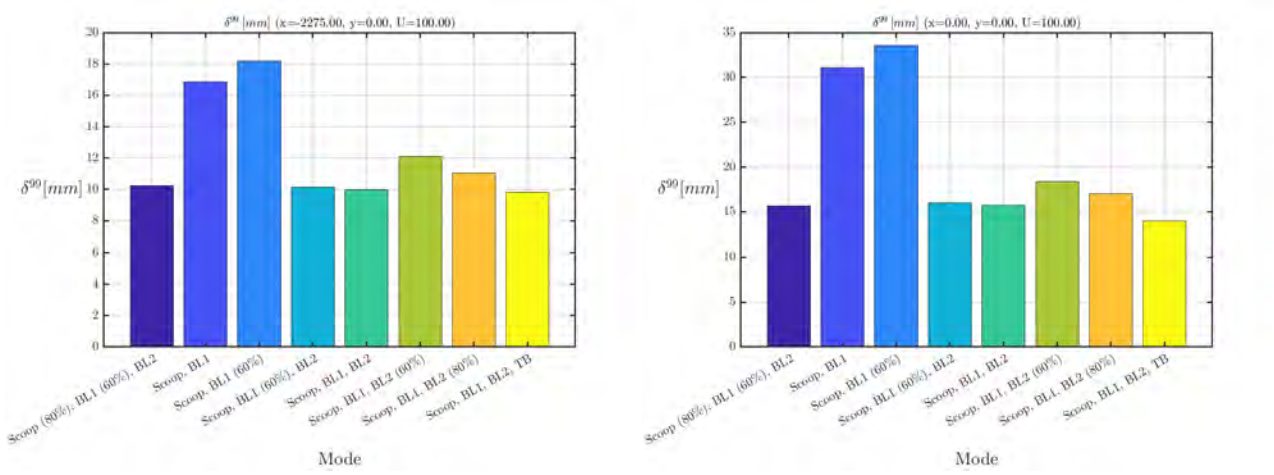

(a) Boundary layer height upstream of the turntable center, $x = -2275$ mm, $y = 0$ mm.

(b) Boundary layer height at the turntable center, $x = 0$ mm, $y = 0$ mm.

Figure 5.9: Boundary layer heights upstream and at the turntable center for wind speed 100 km/h.

scoop, as these are not as relevant and make the graphs difficult to read. The 100 km/h case is shown here, and the 140 km/h case follows the same pattern and has the same conclusions, with a slightly reduced boundary layer height. Here, the two groups can be compared more closely, and it can be seen that there is a large difference in boundary layer height for the cases using only the scoop and boundary layer suction zone one when measuring close to the center line. This difference is close to double on average, depending on the configuration of the boundary layer suction zone two. The difference becomes much smaller as one moves farther out in y, and the difference between heights measured at $x = -2275$ and 0 mm becomes more apparent. It seems that the boundary layer height stays quite low as one moves downstream if one measures on the moving ground system.

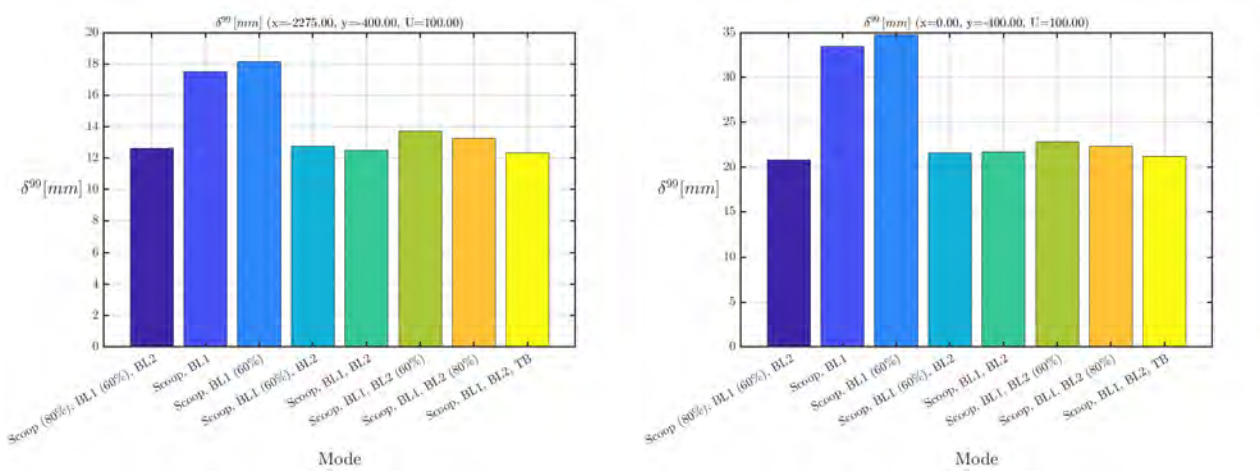

(a) Boundary layer height upstream of the turntable center, $x = -2275$ mm, $y = -400$ mm.

(b) Boundary layer height at the turntable center, $x = 0$ mm, $y = -400$ mm.

Figure 5.10: Boundary layer heights upstream and at the turntable center with $y = -400$ mm for wind speed 100 km/h.

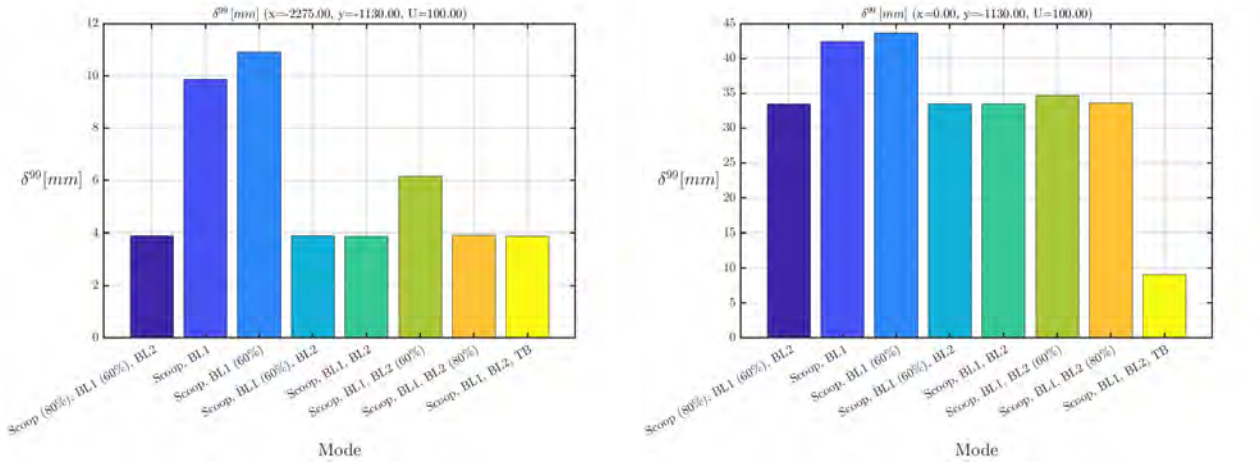

(a) Boundary layer height upstream of the turntable center, $x = -2275$ mm, $y = -1130$ mm.

(b) Boundary layer height at the turntable center, $x = 0$ mm, $y = -1130$ mm.

Figure 5.11: Boundary layer heights upstream and at the turntable center with $y = -1130$ mm for wind speed 100 km/h.

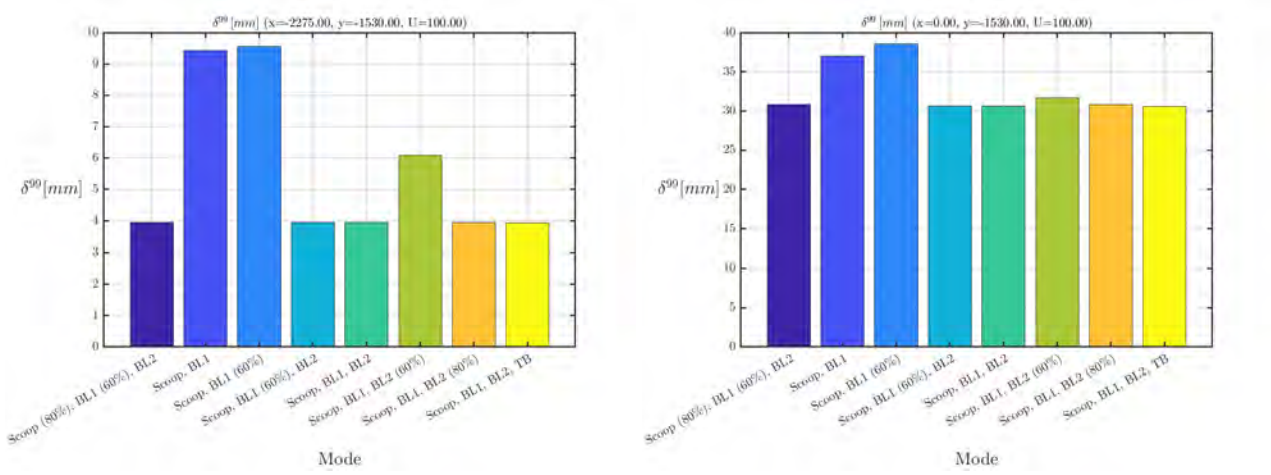

(a) Boundary layer height upstream of the turntable center, $x = -2275$ mm, $y = -1530$ mm.

(b) Boundary layer height at the turntable center, $x = 0$ mm, $y = -1530$ mm.

Figure 5.12: Boundary layer heights upstream and at the turntable center with $y = -1530$ mm for wind speed 100 km/h.

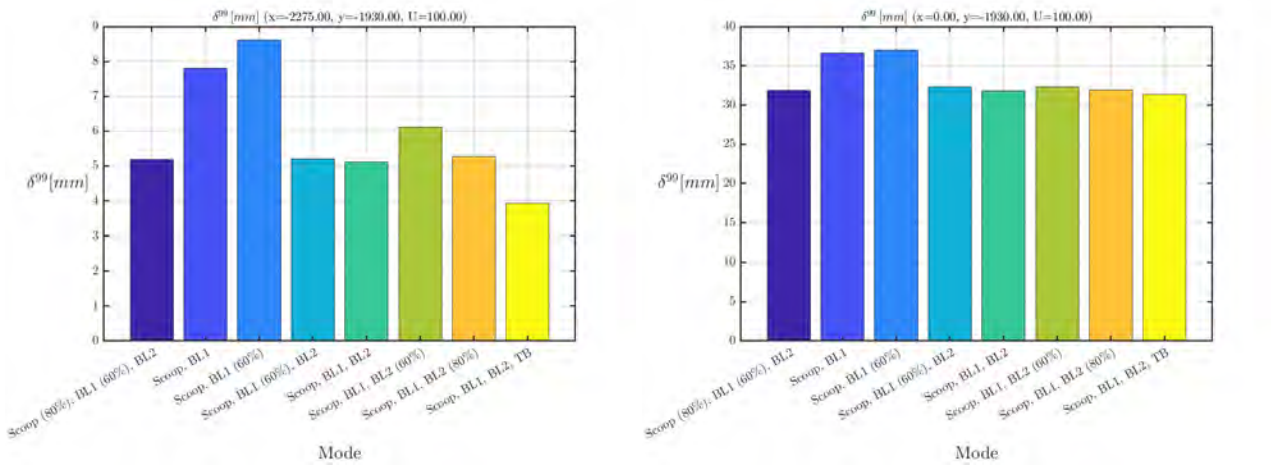

(a) Boundary layer height upstream of the turntable center, $x = -2275$ mm, $y = -1930$ mm.

(b) Boundary layer height at the turntable center, $x = 0$ mm, $y = -1930$ mm.

Figure 5.13: Boundary layer heights upstream and at the turntable center with $y = -1930$ mm for wind speed 100 km/h.

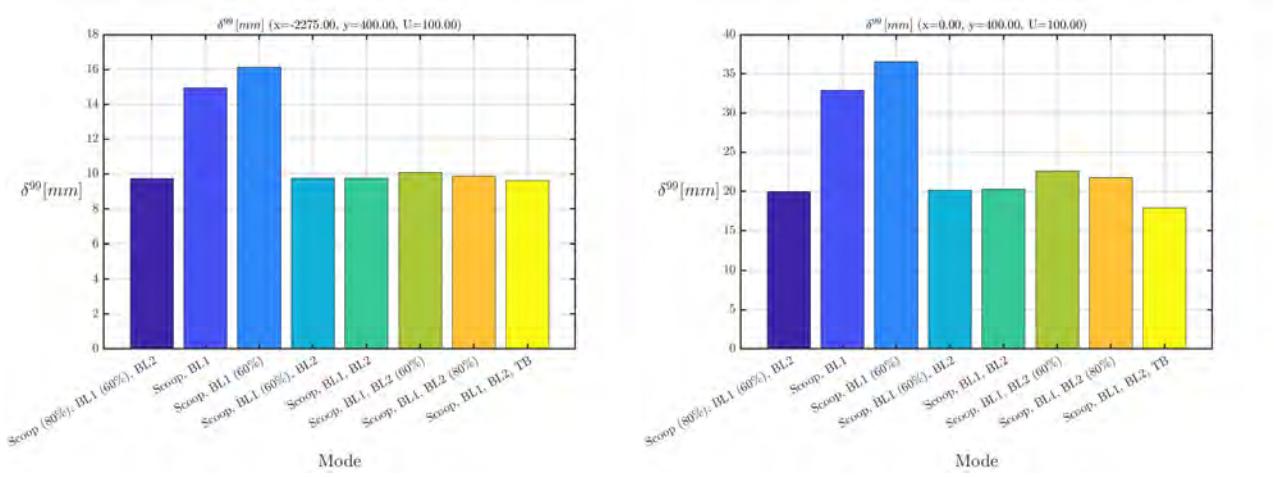

(a) Boundary layer height upstream of the turntable center, $x = -2275$ mm, $y = 400$ mm.

(b) Boundary layer height at the turntable center, $x = 0$ mm, $y = 400$ mm.

Figure 5.14: Boundary layer heights upstream and at the turntable center with $y = 400$ mm for wind speed 100 km/h.

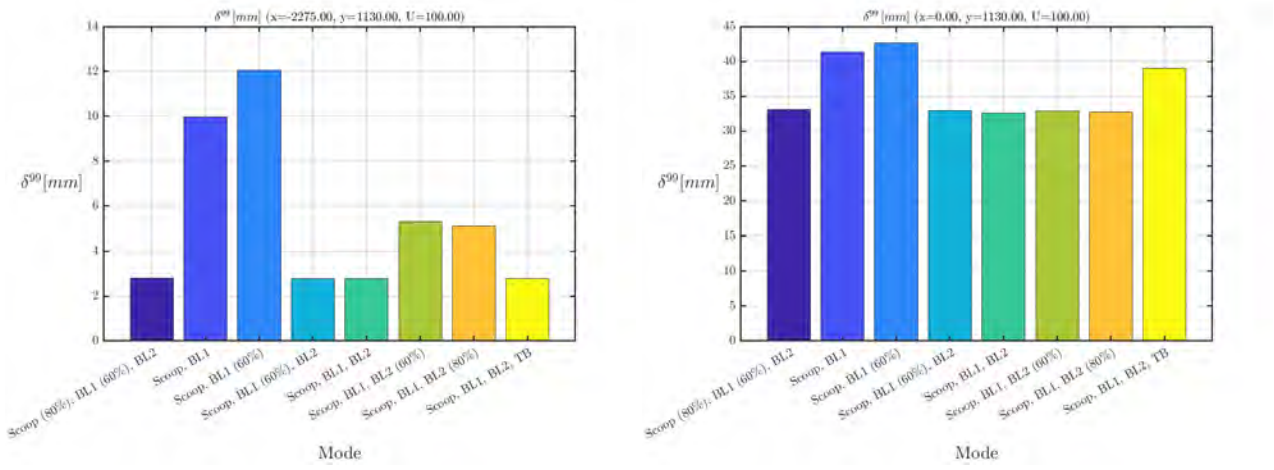

(a) Boundary layer height upstream of the turntable center, $x = -2275$ mm, $y = 1130$ mm.

(b) Boundary layer height at the turntable center, $x = 0$ mm, $y = 1130$ mm.

Figure 5.15: Boundary layer heights upstream and at the turntable center with $y = 1130$ mm for wind speed 100 km/h.

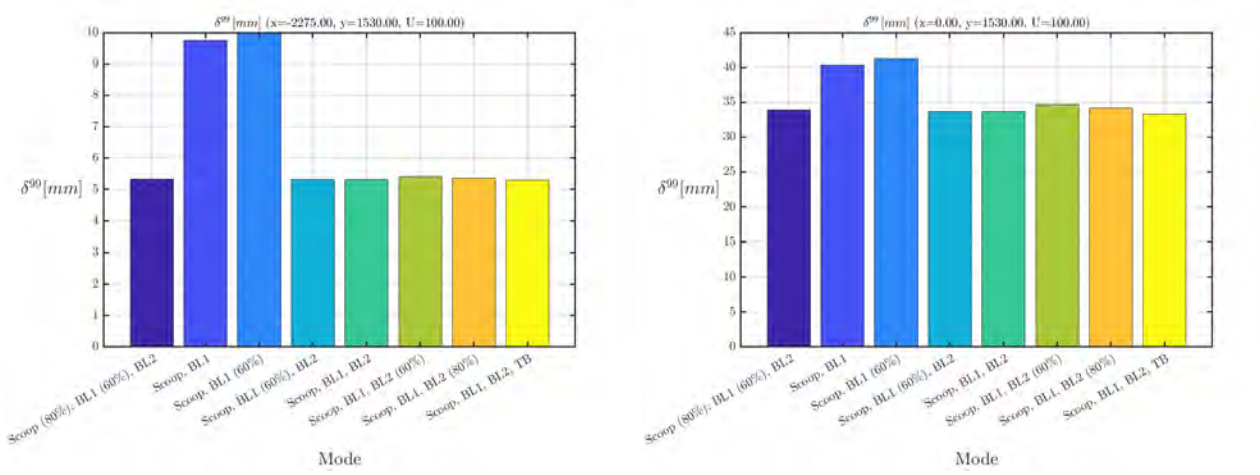

(a) Boundary layer height upstream of the turntable center, $x = -2275$ mm, $y = 1530$ mm.

(b) Boundary layer height at the turntable center, $x = 0$ mm, $y = 1530$ mm.

Figure 5.16: Boundary layer heights upstream and at the turntable center with $y = 1530$ mm for wind speed 100 km/h.

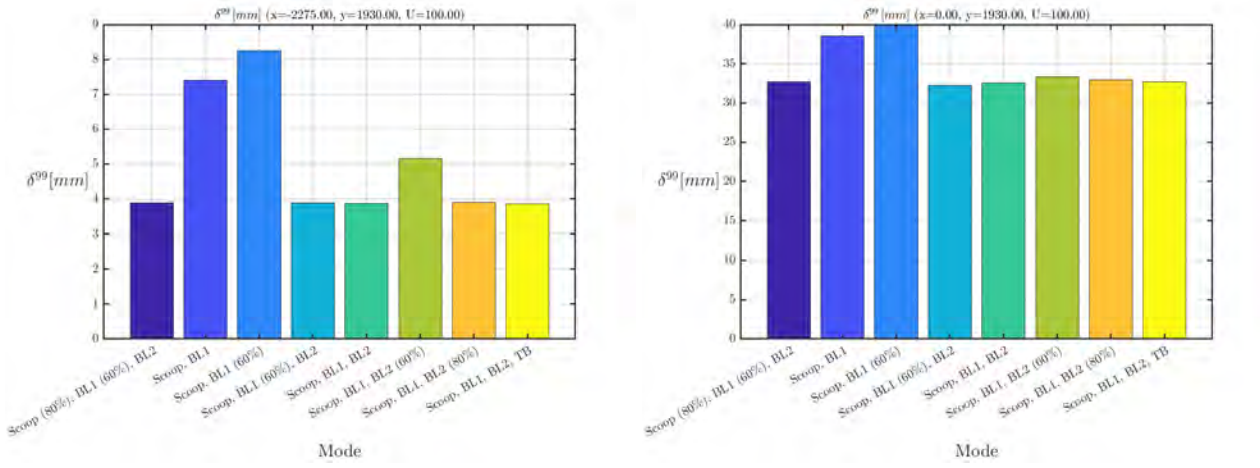

(a) Boundary layer height upstream of the turntable center, $x = -2275$ mm, $y = 1930$ mm.

(b) Boundary layer height at the turntable center, $x = 0$ mm, $y = 1930$ mm.

Figure 5.17: Boundary layer heights upstream and at the turntable center with $y = 1930$ mm for wind speed 100 km/h.

5.3.3 Displacement thickness

Referencing Figure 5.9 above, several noteworthy observations can be made. Initially, the boundary layer expands from approximately 10 mm to $15 - 16$ mm in height as the flow progresses downstream

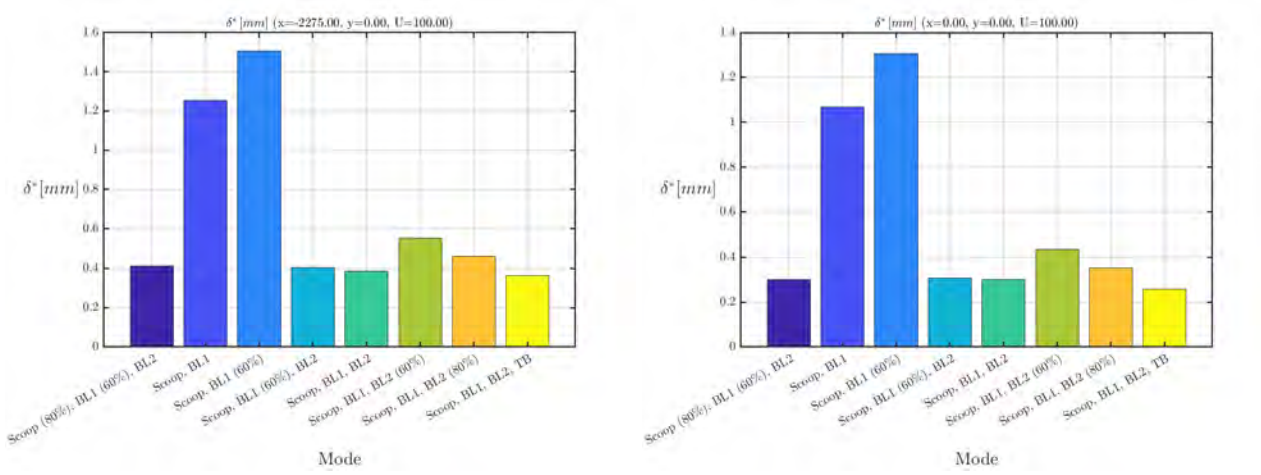

(a) Displacement thickness upstream of the turntable center, $x = -2275$ mm, $y = 0$ mm.

(b) Displacement thickness at the turntable center, $x = 0$ mm, $y = 0$ mm.

Figure 5.18: Displacement thickness upstream and at the turntable center for wind speed 100 km/h.

to the center of the turn table. The most notable observation, however, is the impact of boundary layer suction 2 on the boundary layer dynamics. Examining scenarios where the boundary layer 2 is operational, but the configuration of the scoop and/or boundary layer 1 varies, it becomes evident that reducing the suction rate in these two systems does not substantially increase the boundary layer height when the second suction system is active. This phenomenon is observed at both positions, and the boundary layer's growth as it advances downstream appears to remain relatively constant regardless of the suction systems' configuration. This relationship is reiterated in Figure 5.18 below, though the variations are considerably more pronounced.

Upon examining the variations in displacement thickness as depicted in Figure 5.19, the effect becomes markedly more pronounced. Of particular note are the considerable differences observed between scenarios with and without the activation of boundary layer two suction. This indicates that boundary layer suction system two exerts a significant influence on the boundary layer profile, even with reduced relative suction rates from the reference. This phenomenon is evident in the scenario with boundary layer 2 at 60% of its reference value. Although the tangential blowing system affects the displacement thickness along the center line, it is considerably less significant compared to the effect elicited by the suction systems.

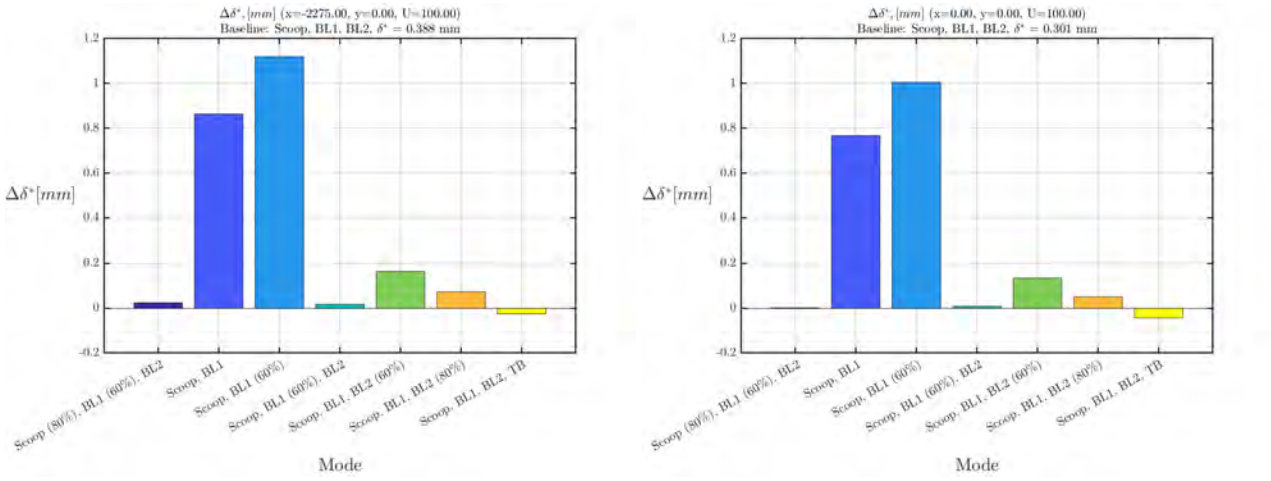

(a) $\Delta\delta^*$ upstream of the turntable center, $x = -2275$ mm, $y = 0$ mm.

(b) $\Delta\delta^*$ at the turntable center, $x = 0$ mm, $y = 0$ mm.

Figure 5.19: Deltas of displacement thickness with respect to standard "Aero" mode settings without tangential blowing upstream and at the turntable center for wind speed 100 km/h.

Looking laterally, at the same x positions but changing y to ± 400 mm, similar conclusions can be drawn. When comparing the figures 5.14 and 5.10, a slight asymmetry is seen in the heights of the boundary layer. This difference is more pronounced upstream of the turntable center, at $x = -2275$ mm.

Again, the same phenomena regarding the influence of boundary layer suction system 2 is seen here in figures 5.21 and 5.20. The differences are more pronounced in the displacement thickness as seen in the center-line comparison. There is around a 0.1 mm difference from $y = -400$ mm to $y = 400$ mm in all configurations,

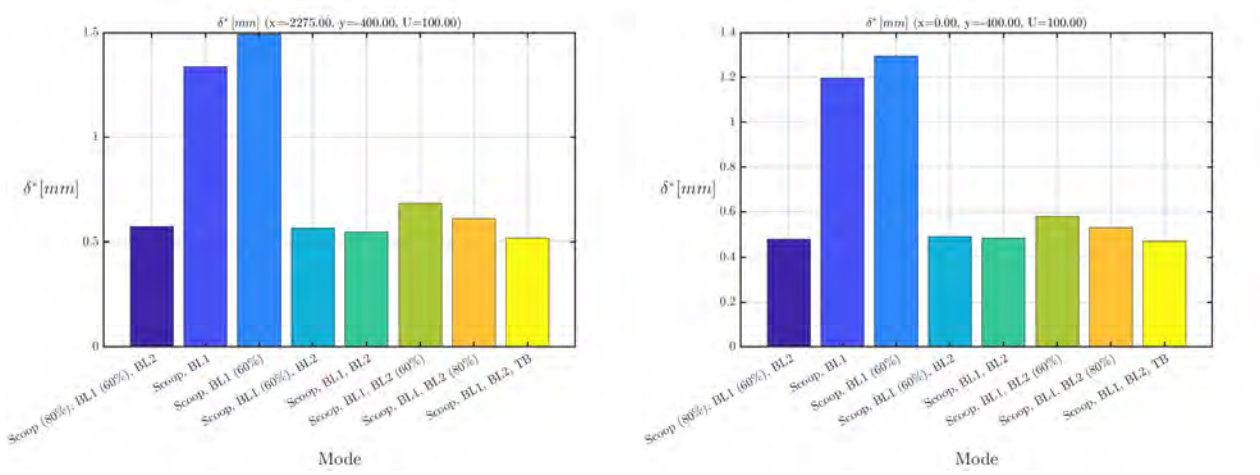

(a) Displacement thickness upstream of the turntable center, $x = -2275$ mm, $y = -400$ mm.

(b) Displacement thickness at the turntable center, $x = 0$ mm, $y = -400$ mm.

Figure 5.20: Displacement thickness upstream and at the turntable center with $y = -400$ mm for wind speed 100 km/h.

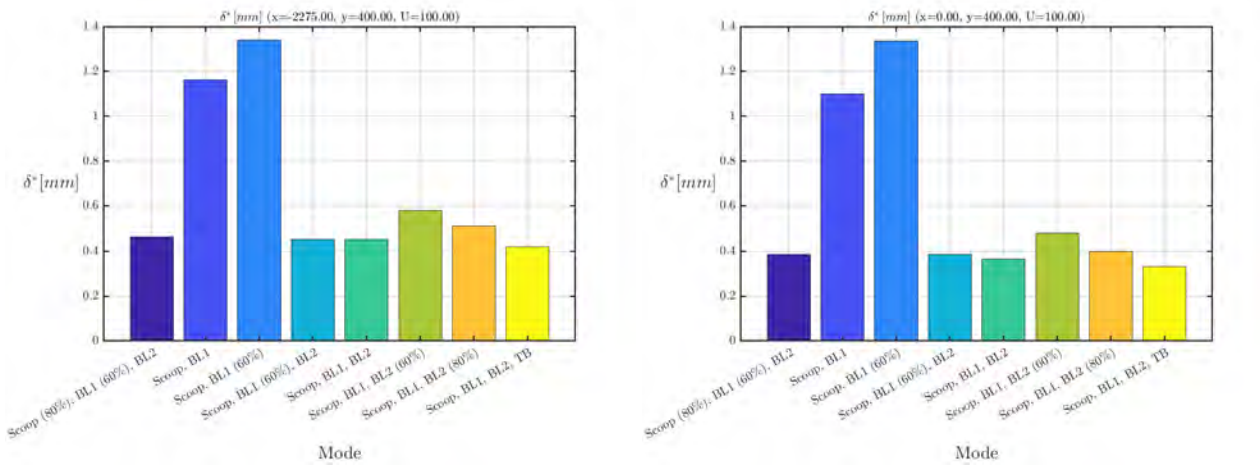

(a) Displacement thickness upstream of the turntable center, $x = -2275$ mm, $y = 400$ mm.

(b) Displacement thickness at the turntable center, $x = 0$ mm, $y = 400$ mm.

Figure 5.21: Displacement thickness upstream and at the turntable center with $y = 400$ mm for wind speed 100 km/h.

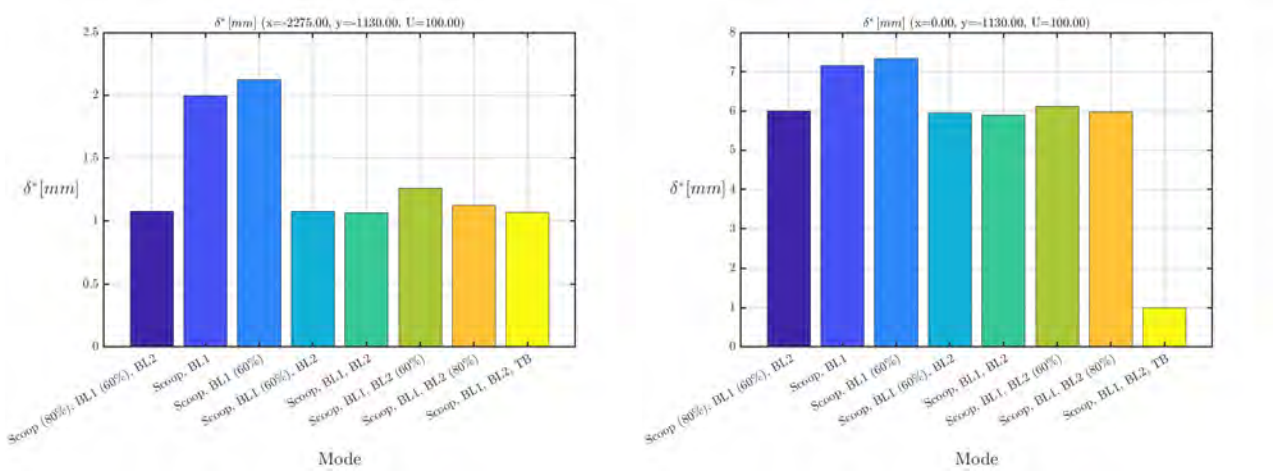

(a) Displacement thickness upstream of the turntable center, $x = -2275$ mm, $y = -1130$ mm.

(b) Displacement thickness at the turntable center, $x = 0$ mm, $y = -1130$ mm.

Figure 5.22: Displacement thickness upstream and at the turntable center with $y = -1130$ mm for wind speed 100 km/h.

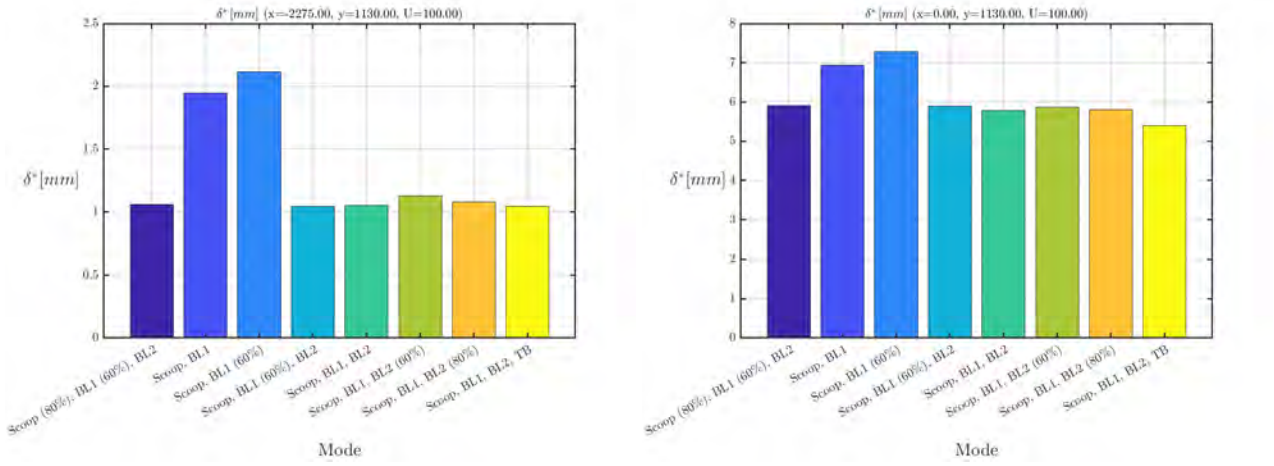

(a) Displacement thickness upstream of the turntable center, $x = -2275$ mm, $y = 1130$ mm.

(b) Displacement thickness at the turntable center, $x = 0$ mm, $y = 1130$ mm.

Figure 5.23: Displacement thickness upstream and at the turntable center for wind speed 100 km/h, $y = 1130$ mm .

An interesting observation is seen in the plot of the deltas of displacement thickness. In figure 5.24 it is seen that for one of the configurations at $x = 0$ mm, the reduction of the boundary layer systems suction gives a very slight reduction in the displacement thickness. This could be within the realm of measurement error. However, it is interesting to see the differences between the lateral positions

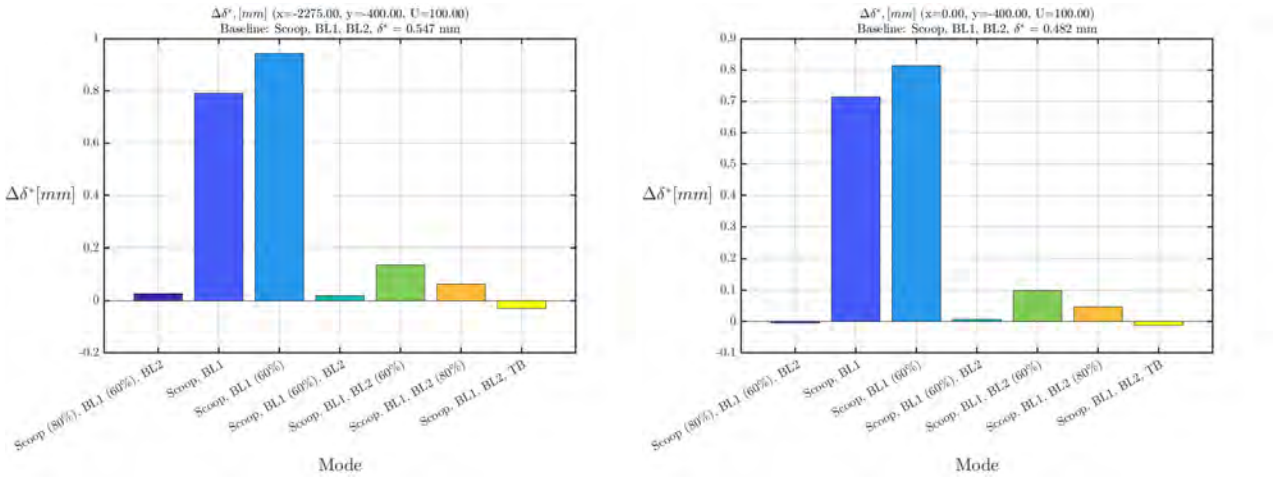

(a) $\Delta\delta^*$ upstream of the turntable center, $x = -2275$ mm, $y = -400$ mm.

(b) $\Delta\delta^*$ at the turntable center, $x = 0$ mm, $y = -400$ mm.

Figure 5.24: $\Delta\delta^*$ upstream and at the turntable center for wind speed 100 km/h, $y = -400$.

upstream and at the center of the turntable. There has always been a slight asymmetry in the flow in the Volvo PVT, and these results could be a consequence of this. These differences are small though, if one considers that they are of the magnitudes of tenths of a millimeter.

Equally interesting is if one considers the differences between deltas in both figures 5.24 and 5.25 at coordinates $y = \pm 400$ mm and $x = -2275$ mm one sees a decrease in the displacement thickness as one goes from -400 mm $\leq y \leq 400$ mm, with the case "Scoop, BL1(60%), BL2" standing out. However, looking at the deltas at $y = \pm 400$ mm and $x = 0$ mm, we see the opposite. This is quite curious and warrants questioning if this is due to measurement error or some other effect in the wind tunnel.

Looking even farther out in the span-wise direction, the same patterns emerge with asymmetries across the span-wise direction. Examining the figures 5.15 and 5.11 there is a clear outlier here. The standard case with tangential blowing at $x = 0$ mm stands out and there is a large difference in the height of the boundary layer when comparing the two positions y. This level of asymmetry is not seen in the other cases, and is most likely an outlier, however, should be investigated closer. The same trends are seen in the displacement thicknesses, and shown in figures 5.23 and 5.22.

Looking further in y, the differences start to become more negligible. There is not a large difference in the total displacement thickness at positions $y = \pm 1530$ and $y = \pm 1930$. This can be seen by comparing figures 5.28 and 5.30, and by looking at the differences presented in figures 5.29 and 5.31 with the positive y counterpart seen in figures 5.32, 5.34, 5.33 and 5.35.

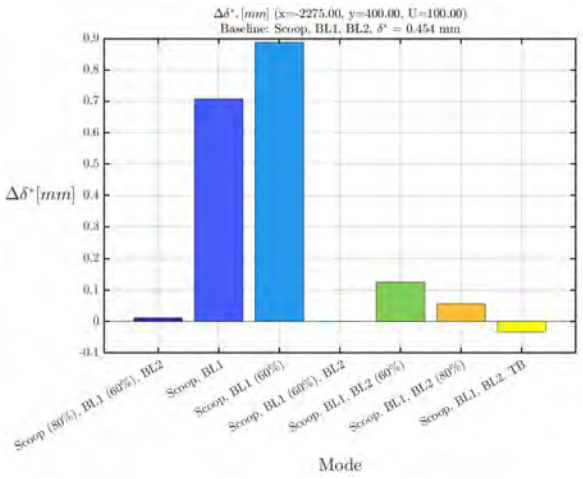

(a) $\Delta\delta^*$ upstream of the turntable center, $x = -2275$ mm, $y = 400$ mm.

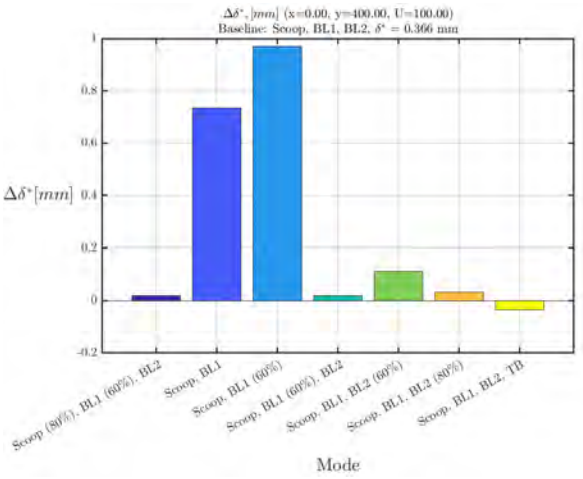

(b) $\Delta\delta^*$ at the turntable center, $x = 0$ mm, $y = 400$ mm.

Figure 5.25: $\Delta\delta^*$ upstream and at the turntable center for wind speed 100 km/h, $y = 400$.

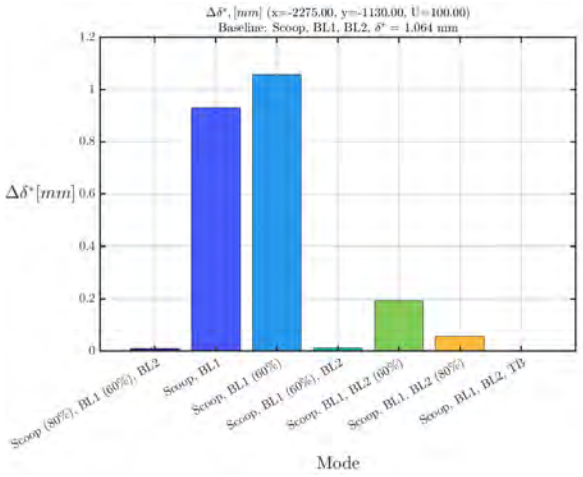

(a) $\Delta\delta^*$ upstream of the turntable center, $x = -2275$ mm, $y = -1130$ mm.

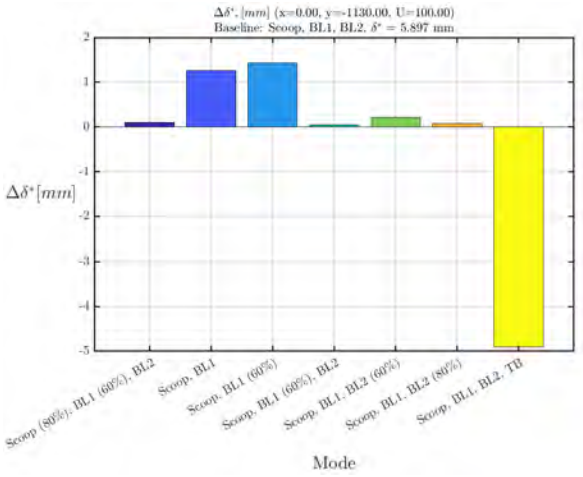

(b) $\Delta\delta^*$ at the turntable center, $x = 0$ mm, $y = -1130$ mm.

Figure 5.26: $\Delta\delta^*$ upstream and at the turntable center for wind speed 100 km/h, $y = -1130$ mm.

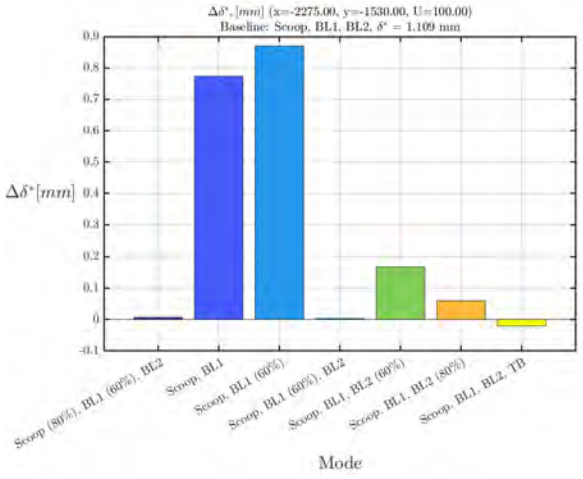

(a) $\Delta\delta^*$ upstream of the turntable center, $x = -2275$ mm, $y = -1530$ mm.

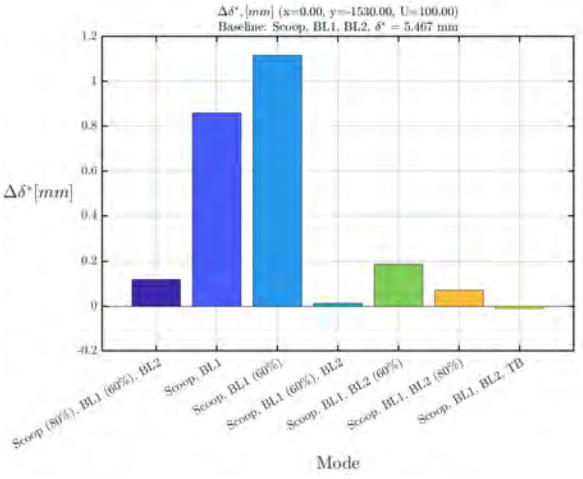

(b) $\Delta\delta^*$ at the turntable center, $x = 0$ mm, $y = -1530$ mm.

Figure 5.29: $\Delta\delta^*$ upstream and at the turntable center with $y = -1530$ mm for wind speed 100 km/h.

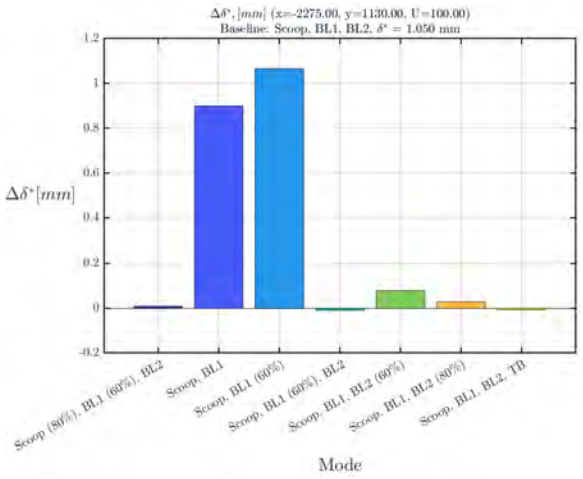

(a) $\Delta\delta^*$ upstream of the turntable center, $x = -2275$ mm, $y = 1130$ mm.

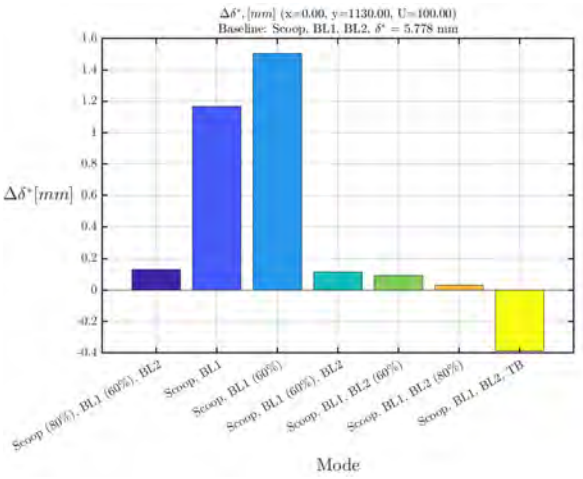

(b) $\Delta\delta^*$ at the turntable center, $x = 0$ mm, $y = 1130$ mm.

Figure 5.27: $\Delta\delta^*$ upstream and at the turntable center for wind speed 100 km/h, $y = 1130$ mm.

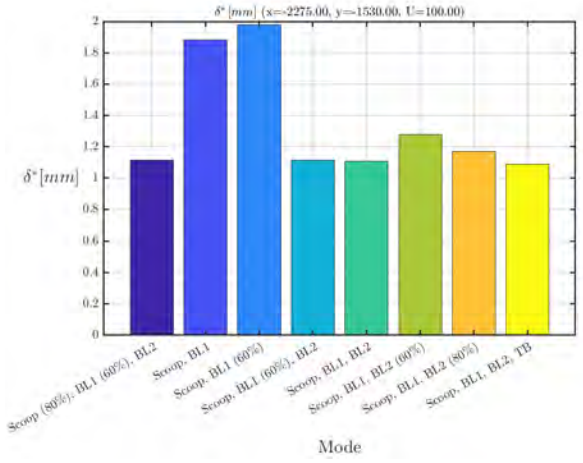

(a) Displacement thickness upstream of the turntable center, $x = -2275$ mm, $y = -1530$ mm.

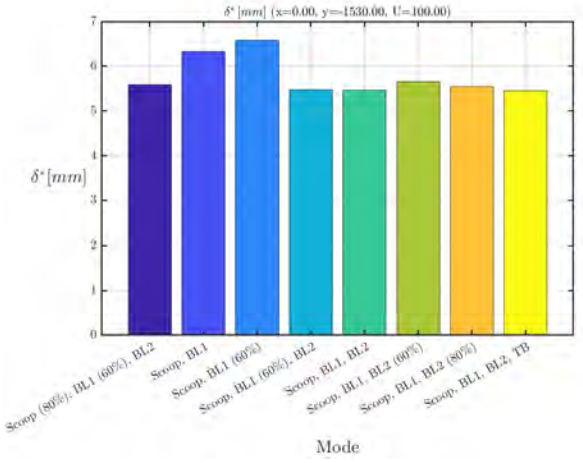

(b) Displacement thickness at the turntable center, $x = 0$ mm, $y = -1530$ mm.

Figure 5.28: Displacement thickness upstream and at the turntable center with $y = -1530$ mm for wind speed 100 km/h.

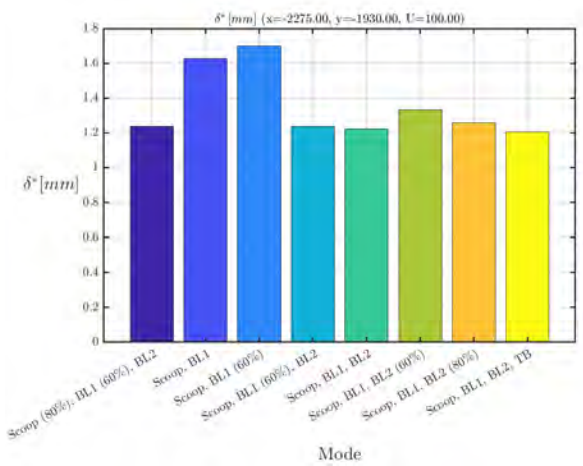

(a) Displacement thickness upstream of the turntable center, $x = -2275$ mm, $y = -1930$ mm.

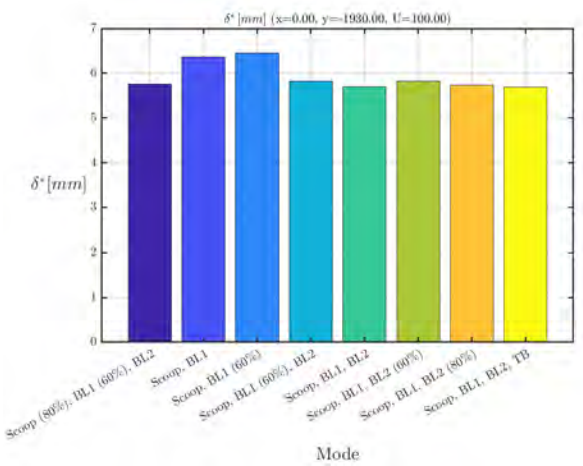

(b) Displacement thickness at the turntable center, $x = 0$ mm, $y = -1930$ mm.

Figure 5.30: Displacement thickness upstream and at the turntable center with $y = -1930$ mm for

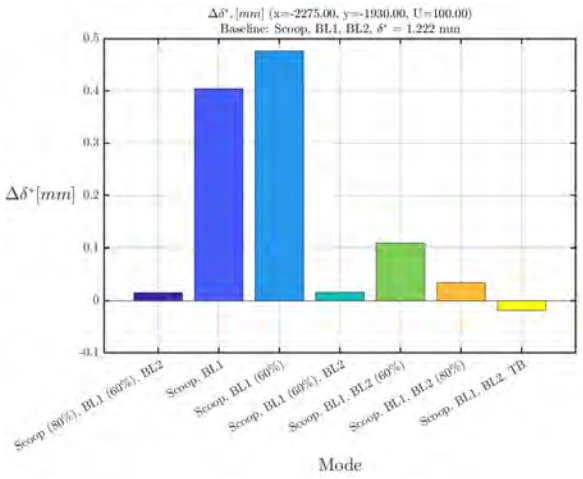

(a) $\Delta\delta^*$ upstream of the turntable center, $x = -2275$ mm, $y = -1930$ mm.

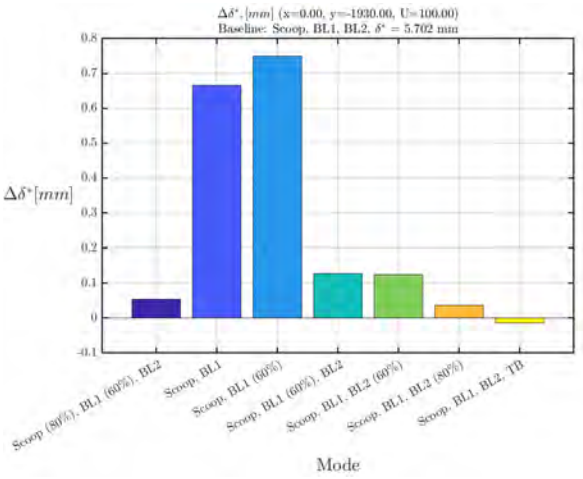

(b) $\Delta\delta^*$ at the turntable center, $x = 0$ mm, $y = -1930$ mm.

Figure 5.31: $\Delta\delta^*$ upstream and at the turntable center with $y = -1930$ mm for wind speed 100 km/h.

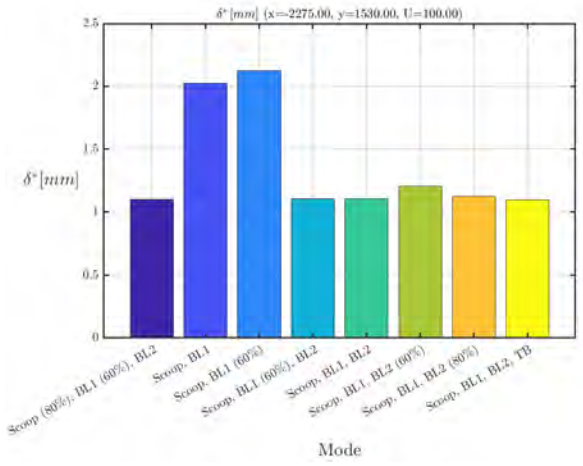

(a) Displacement thickness upstream of the turntable center, $x = -2275$ mm, $y = 1530$ mm.

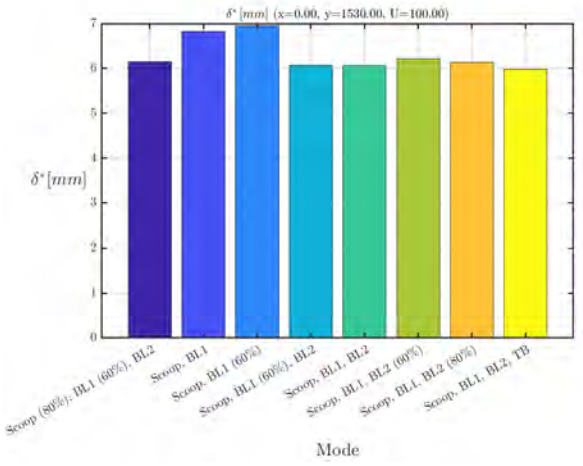

(b) Displacement thickness at the turntable center, $x = 0$ mm, $y = 1530$ mm.

Figure 5.32: Displacement thickness upstream and at the turntable center with $y = 1530$ mm for wind speed 100 km/h.

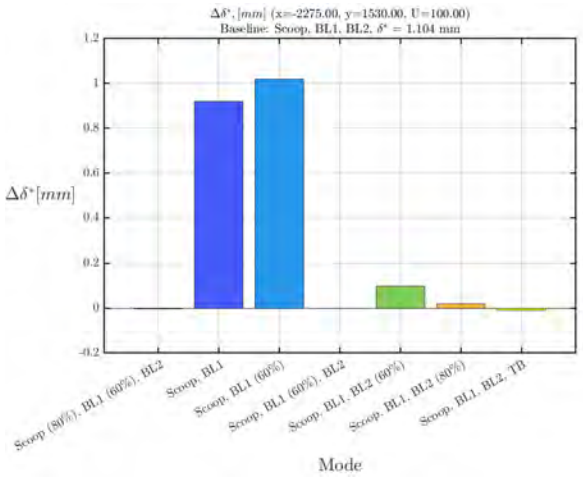

(a) $\Delta\delta^*$ upstream of the turntable center, $x = -2275$ mm, $y = 1530$ mm.

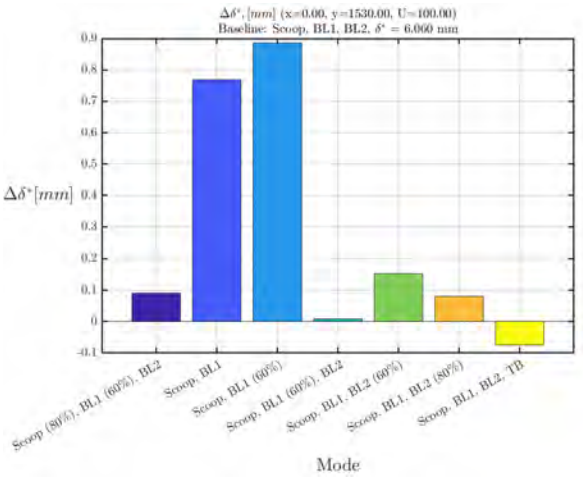

(b) $\Delta\delta^*$ at the turntable center, $x = 0$ mm, $y = 1530$ mm.

Figure 5.33: $\Delta\delta^*$ upstream and at the turntable center with $y = 1530$ mm for wind speed 100 km/h.

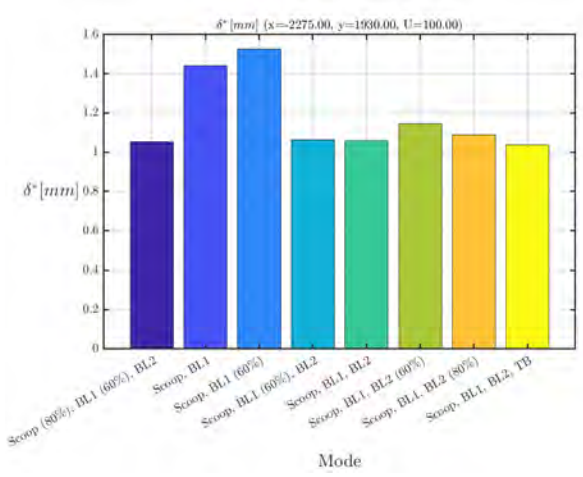

(a) Displacement thickness upstream of the turntable center, $x = -2275$ mm, $y = 1930$ mm.

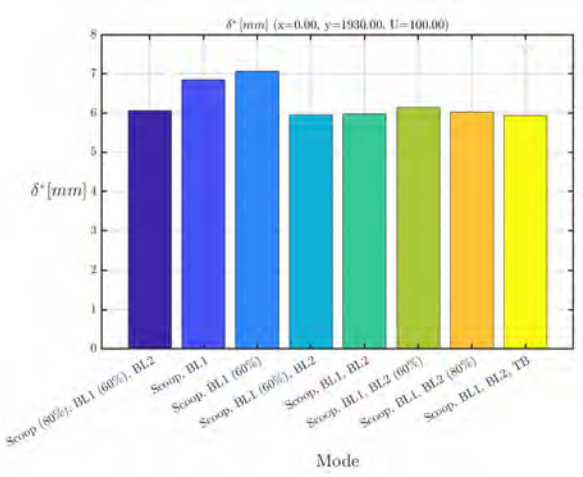

(b) Displacement thickness at the turntable center, $x = 0$ mm, $y = 1930$ mm.

Figure 5.34: Displacement thickness upstream and at the turntable center with $y = 1930$ mm for wind speed 100 km/h.

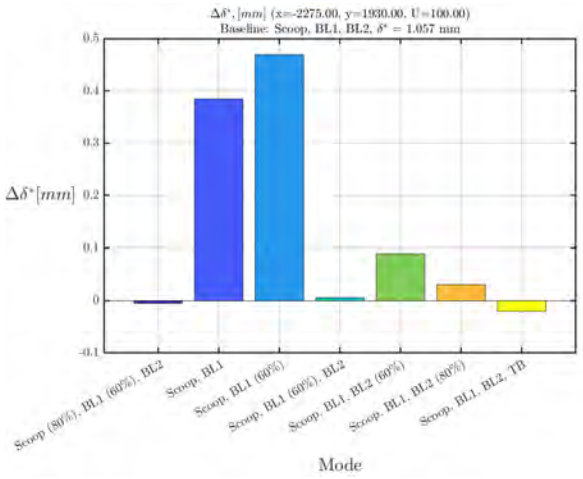

(a) $\Delta\delta^*$ upstream of the turntable center, $x = -2275$ mm, $y = 1930$ mm.

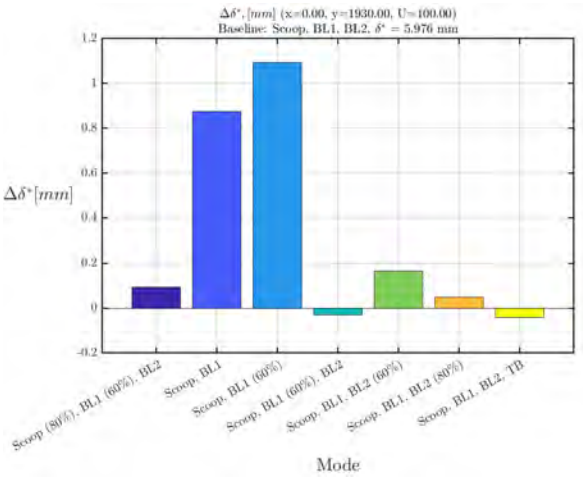

(b) $\Delta\delta^*$ at the turntable center, $x = 0$ mm, $y = 1930$ mm.

Figure 5.35: $\Delta\delta^*$ upstream and at the turntable center with $y = 1930$ mm for wind speed 100 km/h.

5.3.4 Shape factor

To compare the differences in the shape of the boundary layer profile in a more quantifiable way, the shape factor was calculated for each configuration by calculating the displacement and momentum thicknesses. Each configuration was then compared with the baseline mode "Scoop, BL1, BL2" for each position. Tables 5.1 and 5.2 show an example of this for the center of the turntable for 100 and 140 km/h. The tables for the other positions can be found in appendix A.1.

Mode	δ^* [mm]	θ [mm]	H	$\Delta\delta^*$[mm]	$\Delta\theta$ [mm]	ΔH
Scoop	3.6957	3.4187	1.0810	3.3278	3.0558	0.0671
Scoop (80%)	4.1425	3.8087	1.0877	3.7746	3.4458	0.0737
Scoop (80%), BL1 (60%), BL2	0.4003	0.3949	1.0138	0.0324	0.0320	-0.0001
Scoop, BL1	1.1205	1.0803	1.0372	0.7526	0.7174	0.0233
Scoop, BL1 (60%)	1.3364	1.2804	1.0437	0.9685	0.9176	0.0298
Scoop, BL1 (60%), BL2	0.3865	0.3811	1.0142	0.0186	0.0182	0.0003
Scoop, BL1, BL2	0.3679	0.3629	1.0139	0.0000	0.0000	0.0000
Scoop, BL1, BL2 (60%)	0.5095	0.5001	1.0190	0.1416	0.1372	0.0051
Scoop, BL1, BL2 (80%)	0.4399	0.4331	1.0156	0.0719	0.0702	0.0017
Scoop, BL1, BL2, TB	0.3454	0.3413	1.0122	-0.0225	-0.0216	-0.0017

Table 5.1: Boundary layer analysis $x = 0$ mm and $y = 0$ mm at 100 km/h.

Mode	δ^* [mm]	θ [mm]	H	$\Delta\delta^*$[mm]	$\Delta\theta$ [mm]	ΔH
Scoop	3.6785	3.4066	1.0798	3.3250	3.0576	0.0668
Scoop (80%)	3.9816	3.6708	1.0847	3.6281	3.3218	0.0717
Scoop (80%), BL1 (60%), BL2	0.3589	0.3542	1.0133	0.0054	0.0052	0.0003
Scoop, BL1	1.0743	1.0354	1.0376	0.7208	0.6864	0.0246
Scoop, BL1 (60%)	1.3245	1.2692	1.0436	0.9710	0.9202	0.0306
Scoop, BL1 (60%), BL2	0.3647	0.3600	1.0133	0.0112	0.0110	0.0003
Scoop, BL1, BL2	0.3535	0.3490	1.0130	0.0000	0.0000	0.0000
Scoop, BL1, BL2 (60%)	0.4839	0.4753	1.0181	0.1304	0.1263	0.0051
Scoop, BL1, BL2 (80%)	0.4118	0.4057	1.0151	0.0583	0.0567	0.0021

Table 5.2: Boundary layer analysis $x = 0$ mm and $y = 0$ mm at 140 km/h.

The average of the differences calculated for all measured positions is shown in tables 5.3 and 5.4 for wind speeds of 100 and 140 km/h, respectively. There is some change in the shape factor depending on the configuration. For configurations employing all the systems to some degree, there was minimal change, while configurations that set some of the systems to zero had noticeably higher changes. Something worth noting is the difference in the change of the shape factor for the two cases involving boundary layer pre-suction two at 60% and 80%. Reducing the suction rate from 80% to 60% increased the change in the shape factor by 0.008 for the 100 km/h case. The scale of this change is still very small; however, comparatively it is a large jump from 0.0044 to 0.0124. A similar trend is also observed in the 140 km/h case.

Mode	$\Delta\delta^*$ [mm]	$\Delta\theta$ [mm]	ΔH
Scoop	4.2996	3.5409	0.0983
Scoop (80%)	4.9161	4.0460	0.0999
Scoop (80%), BL1 (60%), BL2	0.0449	0.0327	0.0017
Scoop, BL1	0.7297	0.6145	0.0470
Scoop, BL1 (60%)	0.8816	0.7370	0.0542
Scoop, BL1 (60%), BL2	0.0228	0.0170	0.0018
Scoop, BL1, BL2	0.0000	0.0000	0.0000
Scoop, BL1, BL2 (60%)	0.1054	0.0866	0.0124
Scoop, BL1, BL2 (80%)	0.0375	0.0308	0.0044
Scoop, BL1, BL2, TB	-0.3104	-0.2603	-0.0508

Table 5.3: Average change in shape factor, displacement thickness and boundary layer thickness across all positions at 100 km/h.

Mode	$\Delta\delta^*$ [mm]	$\Delta\theta$ [mm]	ΔH
Scoop	4.1537	3.4419	0.0912
Scoop (80%)	4.3251	3.5893	0.0894
Scoop (80%), BL1 (60%), BL2	0.0530	0.0393	0.0008
Scoop, BL1	0.6993	0.5934	0.0458
Scoop, BL1 (60%)	0.8507	0.7186	0.0525
Scoop, BL1 (60%), BL2	0.0271	0.0211	0.0001
Scoop, BL1, BL2	0.0000	0.0000	0.0000
Scoop, BL1, BL2 (60%)	0.1061	0.0897	0.0113
Scoop, BL1, BL2 (80%)	0.0368	0.0318	0.0038

Table 5.4: Average change in shape factor, displacement thickness and boundary layer thickness across all positions at 140 km/h.

5.4 Static pressure: C_p and $\frac{\partial C_p}{\partial x}$

5.4.1 Variation of boundary layer pre-suction one

5.4.1.1 Pressure coefficient: C_p

Looking at the data for C_p along the test section, when varying the suction rate of boundary layer pre-suction one shows a clear reduction of peak pressure in front of where the vehicle would sit. This effect is seen most dramatically in figures 5.36 and 5.37. There is some spanwise variation though, which is seen clearly by comparing the results shown in figures 5.37 and 5.38.

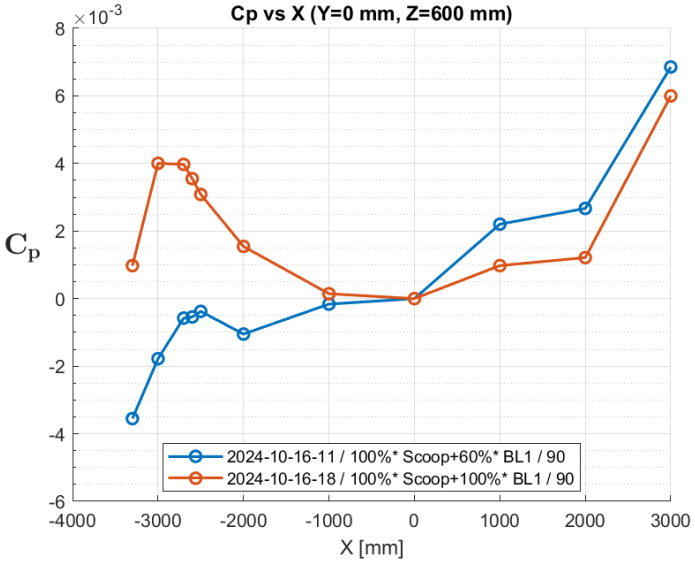

Figure 5.36: C_p measured along the centerline of the test section. The number at the end of the legend indicates the orientation of the probe in degrees from its original position.

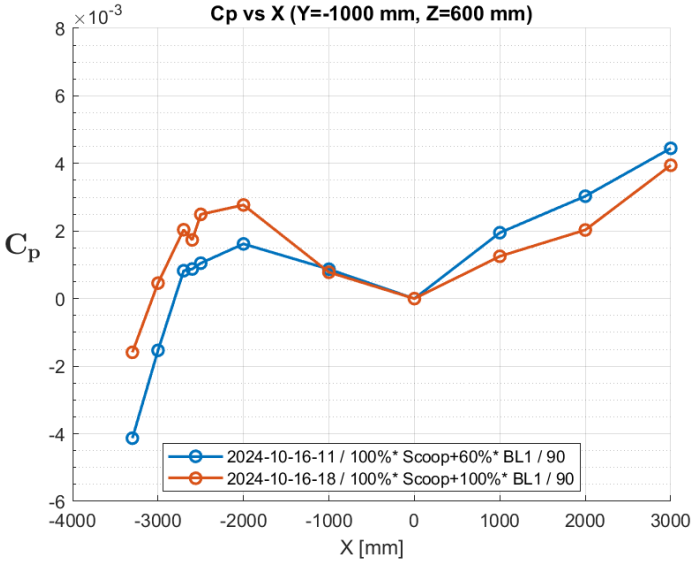

Figure 5.37: C_p measured along the x axis at $y = -1000$ mm in the test section. The number at the end of the legend indicates the orientation of the probe in degrees from its original position.

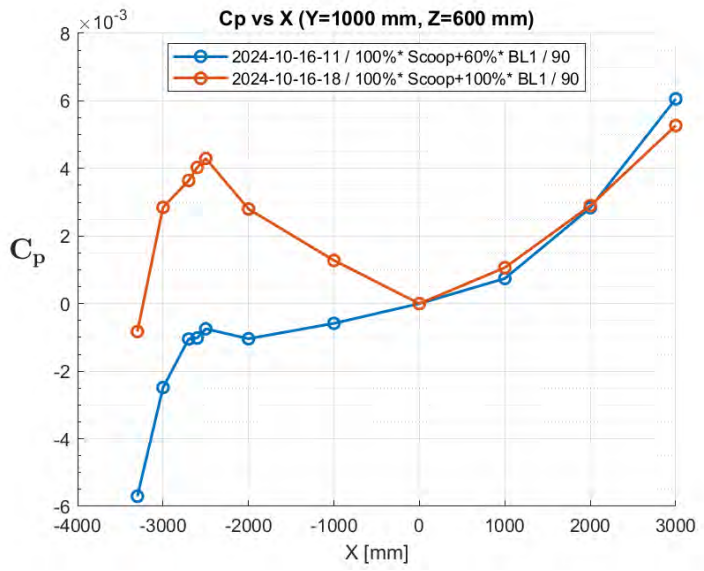

Figure 5.38: C_p measured along the x axis at $y = 1000$ mm in the test section. The number at the end of the legend indicates the orientation of the probe in degrees from its original position.

5.4.1.2 Gradient of pressure coefficient: $\frac{\partial C_p}{\partial x}$

Looking at the gradient of the pressure coefficient for this case, the conclusions in the previous section are reinforced. In all three spanwise positions the gradient is closer to zero along the test section than the case with standard suction. Again, there is a spanwise difference when comparing figures 5.40 and 5.41, with figure 5.41 more closely matching the data shown along the centerline in figure 5.39.

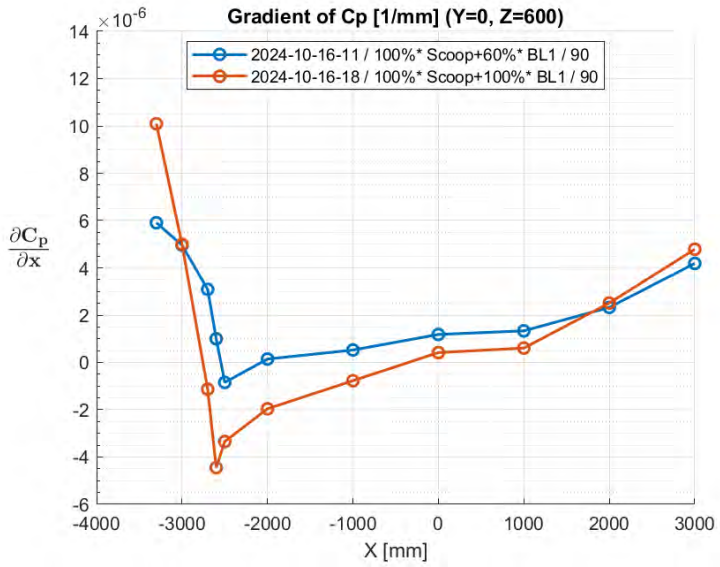

Figure 5.39: Gradient of C_p with respect to x calculated along the centerline of the test section. The number at the end of the legend indicates the orientation of the probe in degrees from its original position.

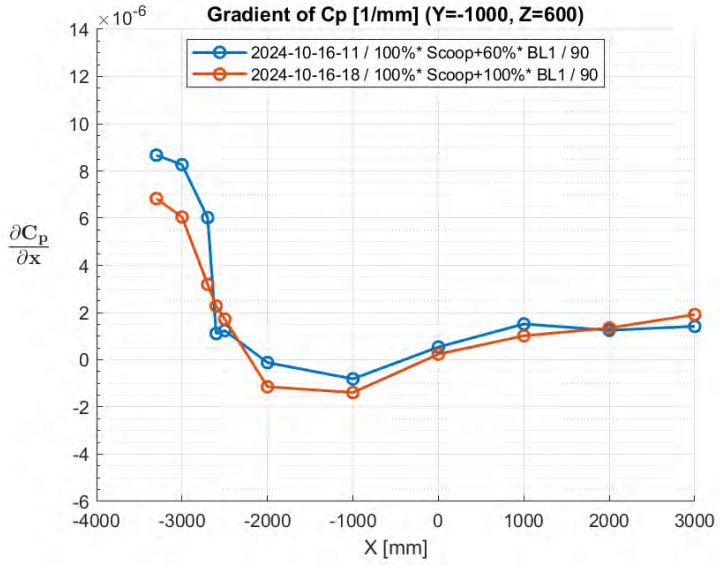

Figure 5.40: Gradient of C_p with respect to x at $y = -1000$ in the test section. The number at the end of the legend indicates the orientation of the probe in degrees from its original position.

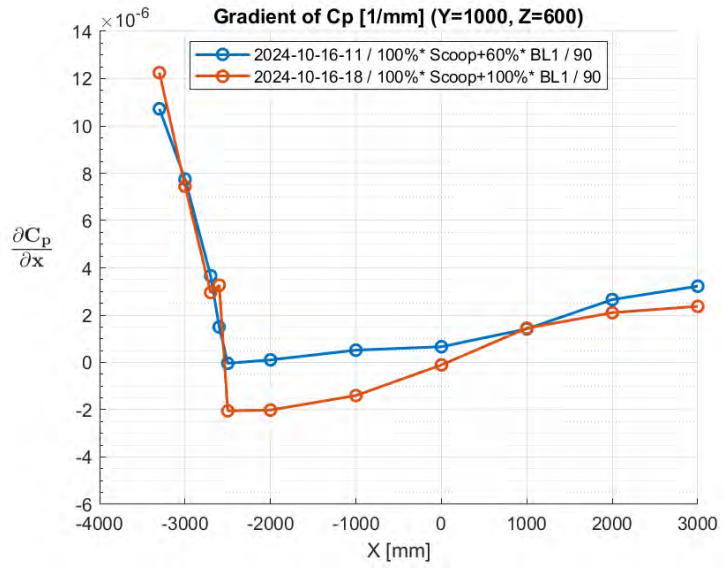

Figure 5.41: Gradient of C_p with respect to x at $y = 1000$ in the test section. The number at the end of the legend indicates the orientation of the probe in degrees from its original position.

5.4.2 Variation of boundary layer pre-suction two

5.4.2.1 Pressure coefficient: C_p

To compare the effect that suction reduction for boundary layer pre-suction two has on the pressure coefficient, four similar cases were chosen from the test campaigns. These figures are more qualitative in nature, as the data used here is from various test days, probe types, and probe orientations. Shown in figures 5.42, 5.43, a similar trend is seen as discussed in the previous section. The curve for the centerline and for $y = 1000$ follow the same pattern while $y = -1000$ shows deviations from this trend with the orange curve being an outlier, as it has more suction in total compared to the yellow curve from the same day. It seems that $y = -1000$ is a sensitive point in the test section, however more testing would be needed to conclusively prove this point.

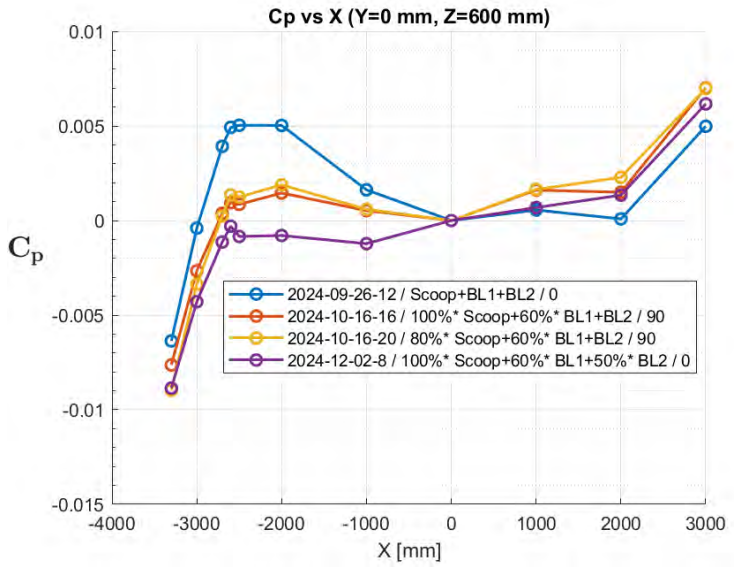

Figure 5.42: C_p measured along the centerline of the test section. The number at the end of the legend indicates the orientation of the probe in degrees from its original position.

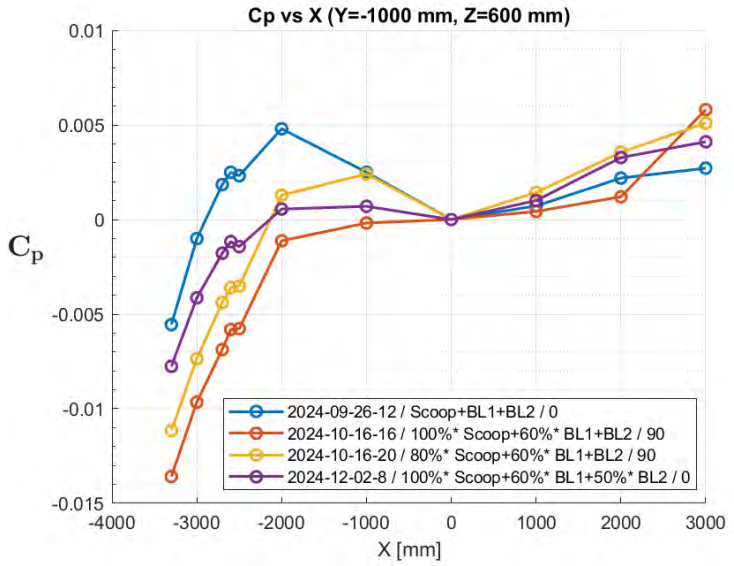

Figure 5.43: C_p measured along the x axis at $y = -1000$ mm in the test section. The number at the end of the legend indicates the orientation of the probe in degrees from its original position.

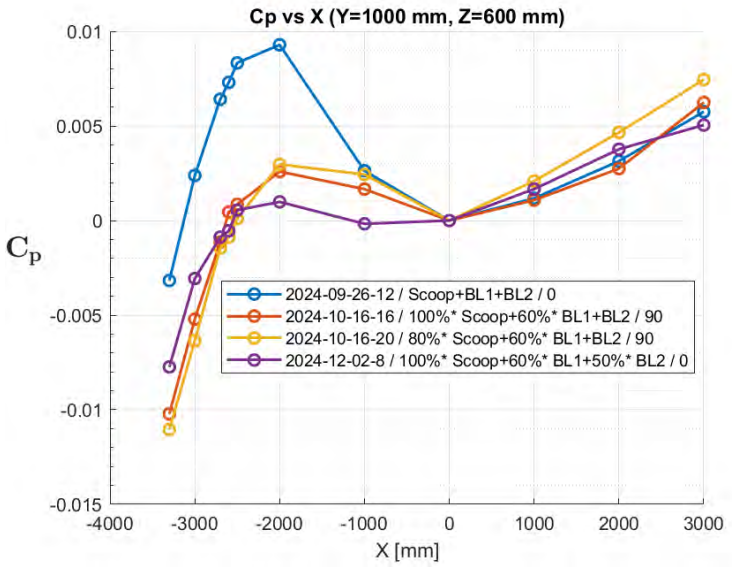

Figure 5.44: C_p measured along the x axis at $y = 1000$ mm in the test section. The number at the end of the legend indicates the orientation of the probe in degrees from its original position.

5.4.2.2 Gradient of pressure coefficient: $\frac{\partial C_p}{\partial x}$

In figures 5.45, 5.46 and 5.47 a more clear picture is seen. While the curves at $y = -1000$ continue to deviate from the trends, the centerline and $y = 1000$ show that the reduced suction configurations seem to have less of a gradient than the standard configuration.

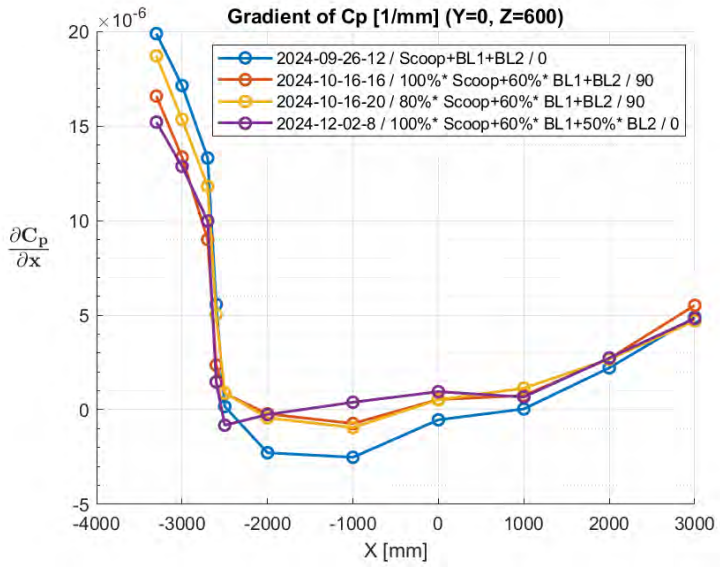

Figure 5.45: Gradient of C_p with respect to x calculated along the centerline of the test section. The number at the end of the legend indicates the orientation of the probe in degrees from its original position.

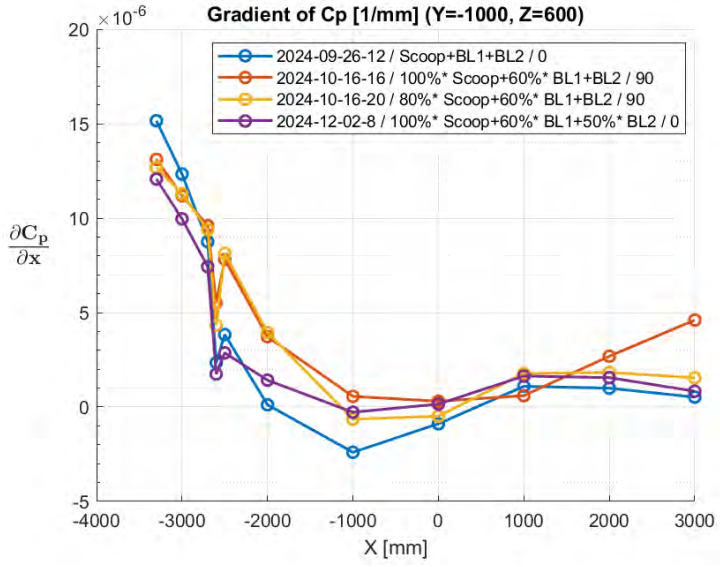

Figure 5.46: Gradient of C_p with respect to x at $y = -1000$ in the test section. The number at the end of the legend indicates the orientation of the probe in degrees from its original position.

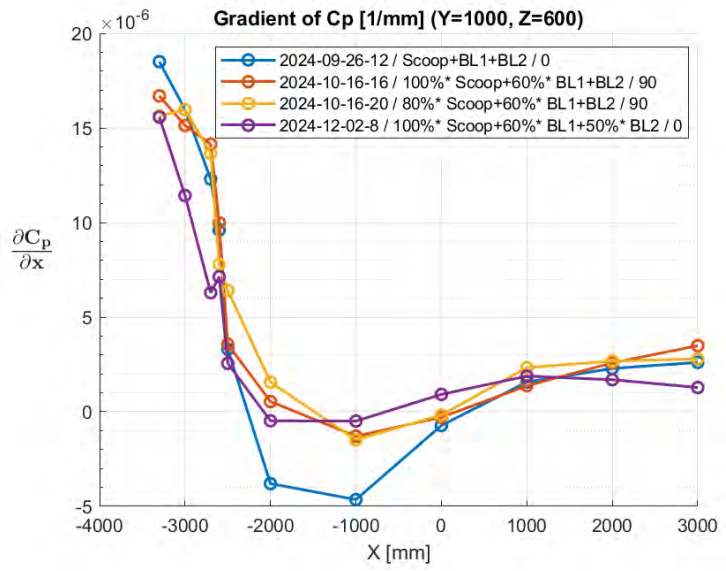

Figure 5.47: Gradient of C_p with respect to x at $y = 1000$ in the test section. The number at the end of the legend indicates the orientation of the probe in degrees from its original position.

5.5 Discussion

As mentioned in the beginning of this chapter, reducing the measured C_D by 0.020 by changing the wind speed determination method, reducing the suction of the boundary layer control system and deactivating the tangiential blowing system is remarkable. There is a clear link between the measured C_D and the amount of suction used in the boundary layer control system. However, what is more fascinating is that the performance of the boundary layer control system is largely unaffected by large reductions in suction. The more optimal settings found by this study reduced the suction of major parts of the system by up to 50% and only increased the displacement thickness in the center of the turntable by approximately 0.15 mm.

Although the displacement thickness does increase, it is not by a large amount and the displacement thickness does not become larger than what is seen in other wind tunnels as outlined in the literature review. There appears to be an asymptotic relationship between the amount of suction used and the amount of displacement thickness reduced, with excess amounts having a negative effect on the measured C_D. There may be some ”global optimal configuration” that is precisely on the border of where this asymptotic relationship starts to disappear and the negative performance on the boundary layer becomes must greater. There is definitely potential for even further improvement, and the results so far serve as a good baseline for future work. It would be interesting to do a focused study starting with the optimal suction settings shown here and incrementally reducing them by a few percentage points to see where performance becomes too poor to use.

It is interesting to see that while the perceived differences in the pressure coefficient were often small in the analysis of the configurations of the boundary layer control system, the final result in the measured C_D is impressive. Ensuring that the C_p curve remains as flat as possible in the region where the vehicle is located appears to be the key to reducing the measured C_D. The second pre-suction system, named ”Boundary Layer 2” or ”BL2” played a significant role in keeping the curve flat without letting the boundary layer grow too freely as it traveled downstream. There is also potential for more in-depth studies of the suction systems themselves. Looking at pressure differences across the suction plate and through the ducts of the suction system could be interesting to see if there are anomalies that reveal themselves there.

Chapter 6

Conclusions and Future work

6.1 Conclusions

The automotive industry continues to grow, and with that, the requirements for efficiency also grow. These requirements come from both the market, as buyers look to get more miles for their money, and from governments looking to reduce emissions to reach climate goals. As companies make the switch to increasing their production of electric vehicles, the C_D of the vehicle takes center stage, as the drag represents the lions share of energy losses from the vehicle during operation. Measurement C_D is paramount in this regard, and while the shape and design of the vehicle play a large role in the absolute values of C_D, this thesis has shown that the characteristics of the wind tunnel being used can also have a substantial influence.

The results of this thesis are substantial and unexpected from the authors' point of view. At the start of the project, the author hoped to provide some positive impact for the Volvo Cars PVT and help influence its future design; however, they were unsure of what the magnitude of that impact would be. A pivotal moment in the thesis was during an early test session in which the author questioned why the company that worked on the Volvo PVT upgrade had set the suction rates at such a high value, when the impact on displacement thickness was negligible. This was the first major break for the thesis and set the focus for all subsequent tests. The author believes without a doubt that they met and exceeded their goals with this project. The author also believes that there is still more room for improvement based on the findings presented in this report.

6.2 Limitations

The most limiting factors for the author during the thesis were time and location. The number of test sessions that could be performed during the duration of the thesis was limited due to the fact that the author lived in another city. Had the author lived in Göteborg, it would have been easier to iterate on the findings and potentially get closer to fine-tuning the boundary layer control system to a "ultimate

optimal configuration". Not living close to the test site also made it so that testing had to be done in large blocks, and scheduling wind tunnel time around other members of the team so that the author does not disturb the work of the company brought some challenges as well.

Living closer to Volvo Torslanda would have also facilitated a more systematic approach to gathering data, as it would have been easier to run quick tests in between other teams booked testing days. This would have enabled much more data to be gathered for the many different configurations for the boundary layer control system, and also allowed for more fine tuned comparisons. The optimal configuration found in this thesis was the result of squeezing in a final test based on looking at data from the wind tunnel on the fly, and making a decision based on intuition. It would have been possible to iterate with a few more configurations similar to this one had the author lived closer.

6.3 Future work

An experiment that Volvo could be interested in carrying out is a sensitivity study on the distance between the vehicle and the exit plan of the nozzle and how it affects the measurements. In a study conducted previously on wind speed determination methods, Nijhof et al. mentions that vehicle positioning in the tunnel can also have effects on the measurements [22]. The author believes that there is a sensitive point near where the front of the vehicle is placed and wonders what the measurements would have shown if the vehicle had been moved a half meter to a meter downstream in the test section.

Another interesting study would be incrementally reducing the suction further from the optimal found in this report. The optimum of this report can serve as a baseline from which another parametric study is done by reducing in steps of one to five percent instead of 20 to 40. The author believes that there is potential for further improvement of the performance by fine-tuning the systems even further. However, it is not known how much more room for improvement there is, but the author speculates that there could potentially be another reduction of one to five count in C_D with the right configuration.

Further investigations into the design of the suction systems could also be of merit, such as investigating the effect the position where the removed boundary layer flow reenters the wind tunnel. Another potential investigation could be to examine the mass flow through the suction plates at different suction rates. This could be a way to find at what point the asymptotic behavior appears. The study could potentially be performed using CFD, and then verified in the wind tunnel with experimental data.

Quite a lot of research is done on the effect of suction on boundary layers; however, the link between static pressure and BLRS is puzzling. This could potentially be a good project for an academic lab to investigate. The Fluid Physics Lab at KTH has a long history of research on boundary layer suction and asymptotic boundary layers, and this question could potentially be a good research topic for the lab.

References

[1] B. August, "Does an Electric Car Need to Be Efficient? Why It Matters," *Recurrent Auto*, 2023, accessed: March 10, 2025. [Online]. Available: https://www.recurrentauto.com/research/does-an-electric-car-need-to-be-efficient-why-it-matters [Page 1.]

[2] W.-H. Hucho, *Aerodynamics of Road Vehicles : From Fluid mechanics to Vehicle Engineering*, 4th ed. Warrendale, PA: Society of Automotive Engineers, 1998. ISBN 0-7680-0029-7 [Pages 1, 7, 8, 9, 10, and 11.]

[3] L. Prandtl and U. S. N. A. C. for Aeronautics, *Motion of Fluids with Very Little Viscosity*, ser. Technical memorandum. National Advisory Committee for Aeronautics, 1928. [Online]. Available: https://books.google.se/books?id=VM3pSgAACAAJ [Pages 2 and 26.]

[4] P. Elofsson and M. Bannister, "Drag Reduction Mechanisms Due to Moving Ground and Wheel Rotation in Passenger Cars," in *SAE 2002 World Congress Exhibition*. SAE International, Mar. 2002. doi: https://doi.org/10.4271/2002-01-0531. [Online]. Available: https://doi.org/10.4271/2002-01-0531 [Pages 3 and 15.]

[5] B. Chanetz, "A Century of Wind Tunnels since Eiffel," *Comptes Rendus Mécanique*, vol. 345, no. 8, pp. 581–594, 2017. doi: https://doi.org/10.1016/j.crme.2017.05.012. [Online]. Available: https://www.sciencedirect.com/science/article/pii/S1631072117300888 [Page 7.]

[6] L. Prandtl, "Göttingen Wind Tunnel for Testing Aircraft Models," 1920. [Online]. Available: https://api.semanticscholar.org/CorpusID:108058373 [Pages 7 and 8.]

[7] Honda. (2022) Honda Opens New World-Class Wind Tunnel in Ohio. [Online]. Available: https://hondanews.com/en-US/releases/honda-opens-new-world-class-wind-tunnel-in-ohio [Page 8.]

[8] N. Tortosa, P. Nagle, and T. Brooker, "General Motors Full Scale Wind Tunnel Upgrade," in *WCX SAE World Congress Experience*. SAE International, Apr. 2020. doi: https://doi.org/10.4271/2020-01-0687. [Online]. Available: https://doi.org/10.4271/2020-01-0687 [Page 8.]

[9] C. Kramer, H. Gerhardt, and L. Janssen, "Flow Studies of an Open Jet Wind Tunnel and Comparison with Closed and Slotted Walls," *Journal of Wind Engineering and Industrial Aerodynamics*, vol. 22, no. 2, pp. 115–127, 1986. doi: https://doi.org/10.1016/0167-6105(86)90078-4. [Online]. Available: https://www.sciencedirect.com/science/article/pii/0167610586900784 [Page 10.]

[10] F. Vandrey and K. Wieghardt, "Experiments on a Slotted-Wall Working Section in a Wind Tunnel," 1955. [Page 10.]

[11] J. Barlow, W. Rae, and A. Pope, *Low-Speed Wind Tunnel Testing*. Wiley, 1999. ISBN 9780471557746. [Online]. Available: https://books.google.se/books?id=nUHWDwAAQBAJ [Page 11.]

[12] R. G. J. Flay, G. M. Elfstrom, and P. J. F. Clark, "Slotted-Wall Test Section for Automotive Aerodynamic Tests at Yaw," in *SAE International Congress and Exposition*. SAE International, feb 1983. doi: https://doi.org/10.4271/830302. [Online]. Available: https://doi.org/10.4271/830302 [Page 11.]

[13] M. Eng, "Investigation of Aerodynamic Correction Methods Applied to a Slotted Wall Wind Tunnel" ," Master's thesis, Technische Universität Berlin, 2009. [Page 11.]

[14] J. Sternéus, T. Walker, and T. Bender, "Upgrade of the Volvo Cars Aerodynamic Wind Tunnel," *SAE Transactions*, vol. 116, pp. 1089–1099, 2007. [Online]. Available: http://www.jstor.org/stable/44687874 [Pages 14, 16, 17, and 23.]

[15] G. Wickern, K. Zwicker, and M. Pfadenhauer, "Rotating Wheels - Their Impact on Wind Tunnel Test Techniques and on Vehicle Drag Results," in *SAE International Congress and Exposition*. SAE International, Feb. 1997. doi: https://doi.org/10.4271/970133. [Online]. Available: https://doi.org/10.4271/970133 [Page 15.]

[16] B. Hetherington and D. B. Sims-Williams, "Support Strut Interference Effects on Passenger and Racing Car Wind Tunnel Models," in *SAE 2006 World Congress Exhibition*. SAE International, Apr. 2006. doi: https://doi.org/10.4271/2006-01-0565. [Online]. Available: https://doi.org/10.4271/2006-01-0565 [Page 15.]

[17] T. Bender, "Commissioning Report: PVT Ground Simulation Upgrade," Volvo Cars, Tech. Rep., 2006. [Page 17.]

[18] J. Wiedemann, O. Fischer, and P. Jiabin, "Further Investigations on Gradient Effects," in *SAE 2004 World Congress & Exhibition*. SAE International, mar 2004. doi: https://doi.org/10.4271/2004-01-0670. [Online]. Available: https://doi.org/10.4271/2004-01-0670 [Pages 18 and 20.]

[19] G. Wickern, S. Dietz, and L. Luehrmann, "Gradient Effects on Drag Due to Boundary-Layer Suction in Automotive Wind Tunnels," *SAE Transactions*, vol. 112, pp. 768–784, 2003. [Online]. Available: http://www.jstor.org/stable/44745450 [Pages 18 and 19.]

[20] A. Berndtsson, W. T. Eckert, and E. Mercker, "The Effect of Groundplane Boundary Layer Control on Automotive Testing in a Wind Tunnel," in *SAE International Congress and Exposition*. SAE International, feb 1988. doi: https://doi.org/10.4271/880248. [Online]. Available: https://doi.org/10.4271/880248 [Pages 19 and 20.]

[21] E. Ljungskog, *Evaluation and Modeling of the Flow in a Slotted Wall Wind Tunnel*, ser. Doktorsavhandlingar vid Chalmers Tekniska Högskola. Department of Mechanics and Maritime Sciences, Division of Vehicle Engineering and Autonomous Systems, Chalmers University of Technology, 2019. ISBN 9789179052195. [Online]. Available: https://books.google.se/books?id=adx0zQEACAAJ [Pages 20 and 21.]

[22] B. C. Nijhof and G. Wickern, "Reference Static and Dynamic Pressures in Automotive Wind Tunnels," in *SAE 2003 World Congress & Exhibition*. SAE International, mar 2003. doi: https://doi.org/10.4271/2003-01-0428. [Online]. Available: https://doi.org/10.4271/2003-01-0428 [Pages 21, 22, 40, 41, 42, 43, and 80.]

[23] P. Nagle, T. Brooker, G. Bari, J. Walter, J. Toth, and S. Skinner, "The Ford Rolling Road Wind Tunnel Facility," *SAE International Journal of Advances and Current Practices in Mobility*, vol. 5, no. 6, pp. 2138–2159, Apr. 2023. doi: 10.4271/2023-01-0654 Number: 2023-01-0654. [Online]. Available: https://www.sae.org/publications/technical-papers/content/2023-01-0654/ [Page 22.]

[24] P. Waudby-Smith, T. Bender, C. Sooriyakumaran, Y. Zhang, H. Wang, F. Zhao, G. Fan, J. Sun, and X. Liu, "The New China Automotive Technology and Research Center Aerodynamic-Acoustic and Climatic Wind Tunnels," SAE International, Warrendale, PA, SAE Technical Paper 2024-01-2541, Apr. 2024, iSSN: 0148-7191, 2688-3627. [Online]. Available: https://www.sae.org/publications/technical-papers/content/2024-01-2541/ [Page 22.]

[25] S. Best, G. Bari, T. Brooker, G. Flynt, J. Walter, and E. Duell, "The Honda Automotive Laboratories of Ohio Wind Tunnel," *SAE International Journal of Advances and Current Practices in Mobility*, vol. 5, no. 6, pp. 2116–2137, apr 2023. doi: https://doi.org/10.4271/2023-01-0656. [Online]. Available: https://doi.org/10.4271/2023-01-0656 [Page 23.]

[26] R. Buckisch, B. Schwartekopp, and J. Pfisterer, "Daimler Aeroacoustic Wind Tunnel: 5 Years of Operational Experience and Recent Improvements," SAE International, Warrendale, PA, SAE Technical Paper 2018-01-5038, Sep. 2018, iSSN: 0148-7191, 2688-3627. [Online]. Available: https://www.sae.org/publications/technical-papers/content/2018-01-5038/ [Page 23.]

[27] P. K. Kundu, I. M. Cohen, and D. R. Dowling, *Fluid Mechanics*, fifth edition. ed. Waltham, MA: Academic Press, 2014 - 2012. ISBN 0-12-382101-0 [Pages 25, 26, 27, 28, and 29.]

[28] J. D. Anderson, *Fundamentals of Aerodynamics*, 1st ed. New York: McGraw-Hill Education, 1985. [Page 30.]

Appendix A

Additional tables

A.1 Boundary layer

A.1.1 100 km/h

Mode	δ^* [mm]	θ [mm]	H	$\Delta\delta^*$[mm]	$\Delta\theta$ [mm]	ΔH
Scoop	5.6219	4.5836	1.2265	5.2845	4.2539	0.2032
Scoop (80%)	6.3838	5.2721	1.2108	6.0464	4.9424	0.1875
Scoop (80%), BL1 (60%), BL2	0.3592	0.3502	1.0257	0.0218	0.0205	0.0024
Scoop, BL1	0.6662	0.6156	1.0822	0.3288	0.2859	0.0589
Scoop, BL1 (60%)	0.7356	0.6745	1.0906	0.3982	0.3448	0.0673
Scoop, BL1 (60%), BL2	0.3518	0.3431	1.0255	0.0144	0.0134	0.0022
Scoop, BL1, BL2	0.3374	0.3297	1.0233	0.0000	0.0000	0.0000
Scoop, BL1, BL2 (60%)	0.4249	0.4088	1.0393	0.0875	0.0791	0.0160
Scoop, BL1, BL2 (80%)	0.3620	0.3518	1.0292	0.0246	0.0220	0.0059
Scoop, BL1, BL2, TB	0.3381	0.3308	1.0220	0.0007	0.0011	-0.0013

Table A.1: Boundary layer analysis $x = -2275$ mm and $y = -1930$ mm at 100 km/h.

Mode	δ^* [mm]	θ [mm]	H	$\Delta\delta^*$[mm]	$\Delta\theta$ [mm]	ΔH
Scoop	4.8434	3.9698	1.2201	4.5335	3.6642	0.2057
Scoop (80%)	5.4925	4.5179	1.2157	5.1826	4.2124	0.2014
Scoop (80%), BL1 (60%), BL2	0.3209	0.3161	1.0152	0.0110	0.0105	0.0009
Scoop, BL1	0.9139	0.8237	1.1096	0.6040	0.5181	0.0952
Scoop, BL1 (60%)	1.0031	0.8950	1.1208	0.6931	0.5894	0.1065
Scoop, BL1 (60%), BL2	0.3129	0.3081	1.0156	0.0030	0.0025	0.0013
Scoop, BL1, BL2	0.3100	0.3056	1.0143	0.0000	0.0000	0.0000
Scoop, BL1, BL2 (60%)	0.4183	0.4032	1.0377	0.1084	0.0976	0.0233
Scoop, BL1, BL2 (80%)	0.3489	0.3416	1.0214	0.0390	0.0360	0.0071
Scoop, BL1, BL2, TB	0.3148	0.3108	1.0130	0.0048	0.0052	-0.0014

Table A.2: Boundary layer analysis $x = -2275$ mm and $y = -1530$ mm at 100 km/h.

Mode	δ^* [mm]	θ [mm]	H	$\Delta\delta^*$[mm]	$\Delta\theta$ [mm]	ΔH
Scoop	4.4549	3.6508	1.2203	4.2829	3.4802	0.2117
Scoop (80%)	4.8611	3.9816	1.2209	4.6890	3.8111	0.2123
Scoop (80%), BL1 (60%), BL2	0.2097	0.2080	1.0083	0.0377	0.0374	-0.0003
Scoop, BL1	0.9177	0.8128	1.1291	0.7457	0.6422	0.1206
Scoop, BL1 (60%)	0.9998	0.8728	1.1456	0.8278	0.7022	0.1370
Scoop, BL1 (60%), BL2	0.1977	0.1960	1.0088	0.0257	0.0255	0.0002
Scoop, BL1, BL2	0.1720	0.1706	1.0086	0.0000	0.0000	0.0000
Scoop, BL1, BL2 (60%)	0.2839	0.2721	1.0434	0.1118	0.1015	0.0348
Scoop, BL1, BL2 (80%)	0.1893	0.1858	1.0189	0.0173	0.0152	0.0103
Scoop, BL1, BL2, TB	0.1906	0.1892	1.0074	0.0186	0.0187	-0.0012

Table A.3: Boundary layer analysis $x = -2275$ mm and $y = -1130$ mm at 100 km/h.

Mode	δ^* [mm]	θ [mm]	H	$\Delta\delta^*$[mm]	$\Delta\theta$ [mm]	ΔH
Scoop	4.0099	3.4200	1.1725	3.3898	2.8233	0.1333
Scoop (80%)	4.4048	3.7308	1.1806	3.7847	3.1341	0.1415
Scoop (80%), BL1 (60%), BL2	0.6584	0.6331	1.0399	0.0383	0.0364	0.0007
Scoop, BL1	1.3351	1.2134	1.1003	0.7151	0.6167	0.0611
Scoop, BL1 (60%)	1.4895	1.3432	1.1089	0.8694	0.7465	0.0698
Scoop, BL1 (60%), BL2	0.6705	0.6456	1.0386	0.0505	0.0489	-0.0005
Scoop, BL1, BL2	0.6201	0.5967	1.0392	0.0000	0.0000	0.0000
Scoop, BL1, BL2 (60%)	0.7203	0.6836	1.0537	0.1002	0.0869	0.0145
Scoop, BL1, BL2 (80%)	0.6832	0.6540	1.0446	0.0631	0.0573	0.0055
Scoop, BL1, BL2, TB	0.6094	0.5884	1.0357	-0.0107	-0.0083	-0.0035

Table A.4: Boundary layer analysis $x = -2275$ mm and $y = -400$ mm at 100 km/h.

Mode	δ^* [mm]	θ [mm]	H	$\Delta\delta^*$[mm]	$\Delta\theta$ [mm]	ΔH
Scoop	4.1493	3.5352	1.1737	3.6962	3.0957	0.1430
Scoop (80%)	4.7452	4.0006	1.1861	4.2922	3.5610	0.1554
Scoop (80%), BL1 (60%), BL2	0.4829	0.4682	1.0314	0.0298	0.0286	0.0007
Scoop, BL1	1.2367	1.1239	1.1004	0.7837	0.6843	0.0698
Scoop, BL1 (60%)	1.4834	1.3332	1.1127	1.0304	0.8937	0.0820
Scoop, BL1 (60%), BL2	0.4651	0.4509	1.0316	0.0121	0.0113	0.0009
Scoop, BL1, BL2	0.4530	0.4396	1.0307	0.0000	0.0000	0.0000
Scoop, BL1, BL2 (60%)	0.5677	0.5415	1.0485	0.1147	0.1019	0.0178
Scoop, BL1, BL2 (80%)	0.4927	0.4744	1.0384	0.0396	0.0349	0.0077
Scoop, BL1, BL2, TB	0.4045	0.3936	1.0276	-0.0485	-0.0459	-0.0031

Table A.5: Boundary layer analysis $x = -2275$ mm and $y = 0$ mm at 100 km/h.

Mode	δ^* [mm]	θ [mm]	H	$\Delta\delta^*$[mm]	$\Delta\theta$ [mm]	ΔH
Scoop	3.5624	3.0300	1.1757	3.1839	2.6647	0.1395
Scoop (80%)	3.9816	3.3605	1.1848	3.6031	2.9952	0.1486
Scoop (80%), BL1 (60%), BL2	0.3870	0.3728	1.0380	0.0084	0.0074	0.0018
Scoop, BL1	0.9648	0.8720	1.1064	0.5862	0.5066	0.0702
Scoop, BL1 (60%)	1.1342	1.0150	1.1174	0.7556	0.6497	0.0812
Scoop, BL1 (60%), BL2	0.3732	0.3595	1.0380	-0.0054	-0.0059	0.0018
Scoop, BL1, BL2	0.3786	0.3654	1.0362	0.0000	0.0000	0.0000
Scoop, BL1, BL2 (60%)	0.4537	0.4303	1.0544	0.0751	0.0649	0.0182
Scoop, BL1, BL2 (80%)	0.4137	0.3965	1.0434	0.0351	0.0311	0.0072
Scoop, BL1, BL2, TB	0.3180	0.3073	1.0346	-0.0606	-0.0580	-0.0016

Table A.6: Boundary layer analysis $x = -2275$ mm and $y = 400$ mm at 100 km/h.

Mode	δ^* [mm]	θ [mm]	H	$\Delta\delta^*$[mm]	$\Delta\theta$ [mm]	ΔH
Scoop	4.1769	3.4617	1.2066	4.0641	3.3522	0.1765
Scoop (80%)	4.8610	4.0149	1.2107	4.7482	3.9054	0.1806
Scoop (80%), BL1 (60%), BL2	0.1336	0.1303	1.0255	0.0208	0.0208	-0.0047
Scoop, BL1	0.8612	0.7624	1.1296	0.7484	0.6529	0.0995
Scoop, BL1 (60%)	0.9730	0.8512	1.1432	0.8602	0.7417	0.1131
Scoop, BL1 (60%), BL2	0.0699	0.0666	1.0488	-0.0429	-0.0429	0.0187
Scoop, BL1, BL2	0.1128	0.1095	1.0301	0.0000	0.0000	0.0000
Scoop, BL1, BL2 (60%)	0.1328	0.1263	1.0512	0.0200	0.0168	0.0210
Scoop, BL1, BL2 (80%)	0.1209	0.1167	1.0361	0.0081	0.0072	0.0060
Scoop, BL1, BL2, TB	0.0817	0.0787	1.0379	-0.0311	-0.0308	0.0078

Table A.7: Boundary layer analysis $x = -2275$ mm and $y = 1130$ mm at 100 km/h.

Mode	δ^* [mm]	θ [mm]	H	$\Delta\delta^*$[mm]	$\Delta\theta$ [mm]	ΔH
Scoop	4.9268	3.9963	1.2328	4.7843	3.8597	0.1904
Scoop (80%)	5.4837	4.4727	1.2260	5.3412	4.3360	0.1836
Scoop (80%), BL1 (60%), BL2	0.1756	0.1696	1.0352	0.0331	0.0330	-0.0073
Scoop, BL1	0.9299	0.8097	1.1484	0.7874	0.6731	0.1059
Scoop, BL1 (60%)	1.0093	0.8711	1.1588	0.8669	0.7344	0.1163
Scoop, BL1 (60%), BL2	0.1742	0.1681	1.0358	0.0317	0.0315	-0.0066
Scoop, BL1, BL2	0.1424	0.1366	1.0425	0.0000	0.0000	0.0000
Scoop, BL1, BL2 (60%)	0.2251	0.2131	1.0563	0.0826	0.0764	0.0139
Scoop, BL1, BL2 (80%)	0.1906	0.1832	1.0405	0.0481	0.0465	-0.0020
Scoop, BL1, BL2, TB	0.2271	0.2213	1.0262	0.0847	0.0847	-0.0162

Table A.8: Boundary layer analysis $x = -2275$ mm and $y = 1530$ mm at 100 km/h.

Mode	δ^* [mm]	θ [mm]	H	$\Delta\delta^*$[mm]	$\Delta\theta$ [mm]	ΔH
Scoop	5.2123	4.2724	1.2200	5.0565	4.1192	0.2029
Scoop (80%)	6.0184	4.9841	1.2075	5.8626	4.8310	0.1904
Scoop (80%), BL1 (60%), BL2	0.1235	0.1207	1.0238	-0.0323	-0.0325	0.0067
Scoop, BL1	0.3994	0.3642	1.0969	0.2437	0.2110	0.0798
Scoop, BL1 (60%)	0.4744	0.4313	1.1001	0.3186	0.2781	0.0829
Scoop, BL1 (60%), BL2	0.1364	0.1337	1.0203	-0.0194	-0.0195	0.0032
Scoop, BL1, BL2	0.1558	0.1532	1.0171	0.0000	0.0000	0.0000
Scoop, BL1, BL2 (60%)	0.1975	0.1890	1.0448	0.0417	0.0359	0.0277
Scoop, BL1, BL2 (80%)	0.1363	0.1318	1.0340	-0.0195	-0.0214	0.0169
Scoop, BL1, BL2, TB	0.1295	0.1273	1.0172	-0.0263	-0.0259	0.0001

Table A.9: Boundary layer analysis $x = -2275$ mm and $y = 1930$ mm at 100 km/h.

Mode	δ^* [mm]	θ [mm]	H	$\Delta\delta^*$[mm]	$\Delta\theta$ [mm]	ΔH
Scoop	8.8126	7.0568	1.2488	4.3909	3.5656	-0.0177
Scoop (80%)	9.4624	7.5695	1.2501	5.0407	4.0783	-0.0165
Scoop (80%), BL1 (60%), BL2	4.4739	3.5188	1.2714	0.0522	0.0277	0.0049
Scoop, BL1	5.0992	4.0143	1.2703	0.6775	0.5231	0.0037
Scoop, BL1 (60%)	5.1857	4.0714	1.2737	0.7640	0.5802	0.0072
Scoop, BL1 (60%), BL2	4.5602	3.5967	1.2679	0.1386	0.1055	0.0014
Scoop, BL1, BL2	4.4217	3.4912	1.2665	0.0000	0.0000	0.0000
Scoop, BL1, BL2 (60%)	4.5452	3.5812	1.2692	0.1235	0.0901	0.0026
Scoop, BL1, BL2 (80%)	4.4526	3.5135	1.2673	0.0309	0.0223	0.0007
Scoop, BL1, BL2, TB	4.4017	3.4728	1.2675	-0.0200	-0.0183	0.0009

Table A.10: Boundary layer analysis $x = 0$ mm and $y = -1930$ mm at 100 km/h.

Mode	δ^* [mm]	θ [mm]	H	$\Delta\delta^*$[mm]	$\Delta\theta$ [mm]	ΔH
Scoop	8.6397	6.9374	1.2454	4.3658	3.5320	-0.0096
Scoop (80%)	9.5535	7.6504	1.2488	5.2796	4.2450	-0.0063
Scoop (80%), BL1 (60%), BL2	4.3905	3.4922	1.2572	0.1166	0.0868	0.0022
Scoop, BL1	5.1191	4.0718	1.2572	0.8452	0.6664	0.0022
Scoop, BL1 (60%)	5.3630	4.2620	1.2583	1.0891	0.8566	0.0033
Scoop, BL1 (60%), BL2	4.2831	3.4117	1.2554	0.0092	0.0063	0.0004
Scoop, BL1, BL2	4.2739	3.4054	1.2550	0.0000	0.0000	0.0000
Scoop, BL1, BL2 (60%)	4.4574	3.5466	1.2568	0.1835	0.1412	0.0018
Scoop, BL1, BL2 (80%)	4.3509	3.4643	1.2559	0.0770	0.0589	0.0009
Scoop, BL1, BL2, TB	4.2771	3.4068	1.2555	0.0032	0.0013	0.0004

Table A.11: Boundary layer analysis $x = 0$ mm and $y = -1530$ mm at 100 km/h.

Mode	δ^* [mm]	θ [mm]	H	$\Delta\delta^*$[mm]	$\Delta\theta$ [mm]	ΔH
Scoop	8.8716	7.0262	1.2626	4.2617	3.3663	0.0031
Scoop (80%)	9.3533	7.3799	1.2674	4.7435	3.7200	0.0078
Scoop (80%), BL1 (60%), BL2	4.7416	3.7488	1.2648	0.1318	0.0889	0.0053
Scoop, BL1	5.8147	4.5926	1.2661	1.2048	0.9327	0.0065
Scoop, BL1 (60%)	5.9686	4.7022	1.2693	1.3588	1.0423	0.0098
Scoop, BL1 (60%), BL2	4.6724	3.7029	1.2618	0.0625	0.0430	0.0023
Scoop, BL1, BL2	4.6098	3.6599	1.2595	0.0000	0.0000	0.0000
Scoop, BL1, BL2 (60%)	4.7607	3.7569	1.2672	0.1509	0.0969	0.0077
Scoop, BL1, BL2 (80%)	4.6618	3.6874	1.2643	0.0520	0.0274	0.0047
Scoop, BL1, BL2, TB	-0.1613	-0.4123	0.3913	-4.7712	-4.0723	-0.8683

Table A.12: Boundary layer analysis $x = 0$ mm and $y = -1130$ mm at 100 km/h.

Mode	δ^* [mm]	θ [mm]	H	$\Delta\delta^*$[mm]	$\Delta\theta$ [mm]	ΔH
Scoop	4.0212	3.7070	1.0848	3.4621	3.1585	0.0654
Scoop (80%)	4.5761	4.1840	1.0937	4.0170	3.6355	0.0744
Scoop (80%), BL1 (60%), BL2	0.5356	0.5252	1.0198	-0.0234	-0.0232	0.0005
Scoop, BL1	1.2125	1.1671	1.0389	0.6534	0.6186	0.0196
Scoop, BL1 (60%)	1.3114	1.2593	1.0414	0.7524	0.7108	0.0221
Scoop, BL1 (60%), BL2	0.5295	0.5189	1.0204	-0.0295	-0.0295	0.0011
Scoop, BL1, BL2	0.5591	0.5485	1.0193	0.0000	0.0000	0.0000
Scoop, BL1, BL2 (60%)	0.6137	0.5999	1.0229	0.0546	0.0515	0.0036
Scoop, BL1, BL2 (80%)	0.5664	0.5547	1.0212	0.0074	0.0062	0.0019
Scoop, BL1, BL2, TB	0.5222	0.5122	1.0194	-0.0369	-0.0362	0.0001

Table A.13: Boundary layer analysis $x = 0$ mm and $y = -400$ mm at 100 km/h.

Mode	δ^* [mm]	θ [mm]	H	$\Delta\delta^*$[mm]	$\Delta\theta$ [mm]	ΔH
Scoop	4.0158	3.7114	1.0820	3.5685	3.2721	0.0637
Scoop (80%)	4.5431	4.1702	1.0894	4.0957	3.7309	0.0711
Scoop (80%), BL1 (60%), BL2	0.4911	0.4825	1.0177	0.0438	0.0432	-0.0005
Scoop, BL1	1.1713	1.1275	1.0388	0.7239	0.6882	0.0205
Scoop, BL1 (60%)	1.4031	1.3444	1.0436	0.9558	0.9051	0.0254
Scoop, BL1 (60%), BL2	0.4791	0.4706	1.0180	0.0317	0.0313	-0.0003
Scoop, BL1, BL2	0.4473	0.4393	1.0183	0.0000	0.0000	0.0000
Scoop, BL1, BL2 (60%)	0.5659	0.5540	1.0215	0.1185	0.1147	0.0032
Scoop, BL1, BL2 (80%)	0.4723	0.4630	1.0200	0.0250	0.0237	0.0018
Scoop, BL1, BL2, TB	0.4040	0.3976	1.0160	-0.0433	-0.0417	-0.0022

Table A.14: Boundary layer analysis $x = 0$ mm and $y = 400$ mm at 100 km/h.

Mode	δ^* [mm]	θ [mm]	H	$\Delta\delta^*$[mm]	$\Delta\theta$ [mm]	ΔH
Scoop	9.1490	7.2407	1.2636	4.6549	3.6939	-0.0036
Scoop (80%)	9.9280	7.8346	1.2672	5.4338	4.2879	0.0001
Scoop (80%), BL1 (60%), BL2	4.6075	3.6213	1.2723	0.1133	0.0745	0.0052
Scoop, BL1	5.6211	4.4290	1.2691	1.1269	0.8823	0.0020
Scoop, BL1 (60%)	5.9303	4.6528	1.2746	1.4361	1.1061	0.0074
Scoop, BL1 (60%), BL2	4.6112	3.6313	1.2699	0.1171	0.0846	0.0027
Scoop, BL1, BL2	4.4942	3.5467	1.2671	0.0000	0.0000	0.0000
Scoop, BL1, BL2 (60%)	4.5768	3.5995	1.2715	0.0826	0.0528	0.0044
Scoop, BL1, BL2 (80%)	4.4865	3.5316	1.2704	-0.0077	-0.0151	0.0033
Scoop, BL1, BL2, TB	4.0386	3.2639	1.2374	-0.4556	-0.2828	-0.0298

Table A.15: Boundary layer analysis $x = 0$ mm and $y = 1130$ mm at 100 km/h.

Mode	δ^* [mm]	θ [mm]	H	$\Delta\delta^*$[mm]	$\Delta\theta$ [mm]	ΔH
Scoop	9.5742	7.5879	1.2618	4.7616	3.7869	-0.0044
Scoop (80%)	10.3155	8.1900	1.2595	5.5029	4.3890	-0.0066
Scoop (80%), BL1 (60%), BL2	4.8943	3.8466	1.2724	0.0816	0.0456	0.0062
Scoop, BL1	5.5699	4.3919	1.2682	0.7572	0.5909	0.0021
Scoop, BL1 (60%)	5.6979	4.4927	1.2683	0.8852	0.6917	0.0021
Scoop, BL1 (60%), BL2	4.8371	3.8138	1.2683	0.0245	0.0128	0.0022
Scoop, BL1, BL2	4.8126	3.8010	1.2661	0.0000	0.0000	0.0000
Scoop, BL1, BL2 (60%)	4.9689	3.9149	1.2692	0.1563	0.1139	0.0031
Scoop, BL1, BL2 (80%)	4.9137	3.8818	1.2658	0.1011	0.0808	-0.0003
Scoop, BL1, BL2, TB	4.7034	3.6984	1.2717	-0.1093	-0.1026	0.0056

Table A.16: Boundary layer analysis $x = 0$ mm and $y = 1530$ mm at 100 km/h.

Mode	δ^* [mm]	θ [mm]	H	$\Delta\delta^*$[mm]	$\Delta\theta$ [mm]	ΔH
Scoop	11.1030	8.7612	1.2673	6.3230	4.9921	-0.0009
Scoop (80%)	11.8313	9.3366	1.2672	7.0513	5.5676	-0.0010
Scoop (80%), BL1 (60%), BL2	4.8711	3.8204	1.2750	0.0911	0.0513	0.0068
Scoop, BL1	5.6294	4.4203	1.2735	0.8494	0.6513	0.0053
Scoop, BL1 (60%)	5.8185	4.5440	1.2805	1.0385	0.7749	0.0123
Scoop, BL1 (60%), BL2	4.7476	3.7388	1.2698	-0.0324	-0.0303	0.0016
Scoop, BL1, BL2	4.7800	3.7691	1.2682	0.0000	0.0000	0.0000
Scoop, BL1, BL2 (60%)	4.9240	3.8687	1.2728	0.1440	0.0997	0.0045
Scoop, BL1, BL2 (80%)	4.8419	3.8194	1.2677	0.0619	0.0504	-0.0005
Scoop, BL1, BL2, TB	4.7165	3.7164	1.2691	-0.0635	-0.0527	0.0009

Table A.17: Boundary layer analysis $x = 0$ mm and $y = 1930$ mm at 100 km/h.

A.1.2 140 km/h

Mode	δ^* [mm]	θ [mm]	H	$\Delta\delta^*$[mm]	$\Delta\theta$ [mm]	ΔH
Scoop	5.6821	4.6516	1.2216	5.4265	4.4038	0.1894
Scoop (80%)	5.5544	4.6534	1.1936	5.2987	4.4057	0.1615
Scoop (80%), BL1 (60%), BL2	0.2703	0.2613	1.0345	0.0146	0.0136	0.0024
Scoop, BL1	0.5645	0.5161	1.0937	0.3088	0.2684	0.0616
Scoop, BL1 (60%)	0.6457	0.5875	1.0990	0.3900	0.3398	0.0668
Scoop, BL1 (60%), BL2	0.2603	0.2514	1.0352	0.0046	0.0037	0.0031
Scoop, BL1, BL2	0.2557	0.2477	1.0321	0.0000	0.0000	0.0000
Scoop, BL1, BL2 (60%)	0.3308	0.3146	1.0516	0.0751	0.0669	0.0195
Scoop, BL1, BL2 (80%)	0.2740	0.2635	1.0401	0.0183	0.0157	0.0080

Table A.18: Boundary layer analysis $x = -2275$ mm and $y = -1930$ mm at 140 km/h.

Mode	δ^* [mm]	θ [mm]	H	$\Delta\delta^*$[mm]	$\Delta\theta$ [mm]	ΔH
Scoop	4.8542	3.9649	1.2243	4.5722	3.6895	0.2004
Scoop (80%)	4.9660	4.1120	1.2077	4.6840	3.8366	0.1838
Scoop (80%), BL1 (60%), BL2	0.2803	0.2734	1.0252	-0.0018	-0.0021	0.0013
Scoop, BL1	0.9281	0.8243	1.1259	0.6461	0.5489	0.1020
Scoop, BL1 (60%)	1.0288	0.9018	1.1408	0.7467	0.6264	0.1169
Scoop, BL1 (60%), BL2	0.2805	0.2734	1.0259	-0.0015	-0.0020	0.0020
Scoop, BL1, BL2	0.2820	0.2754	1.0239	0.0000	0.0000	0.0000
Scoop, BL1, BL2 (60%)	0.3909	0.3727	1.0488	0.1089	0.0973	0.0248
Scoop, BL1, BL2 (80%)	0.3101	0.3000	1.0337	0.0281	0.0246	0.0098

Table A.19: Boundary layer analysis $x = -2275$ mm and $y = -1530$ mm at 140 km/h.

Mode	δ^* [mm]	θ [mm]	H	$\Delta\delta^*$[mm]	$\Delta\theta$ [mm]	ΔH
Scoop	4.2958	3.5354	1.2151	4.1467	3.3870	0.2103
Scoop (80%)	4.2336	3.5106	1.2059	4.0845	3.3622	0.2012
Scoop (80%), BL1 (60%), BL2	0.1684	0.1676	1.0052	0.0193	0.0192	0.0004
Scoop, BL1	0.9223	0.8142	1.1327	0.7732	0.6658	0.1279
Scoop, BL1 (60%)	1.0395	0.9102	1.1422	0.8904	0.7618	0.1374
Scoop, BL1 (60%), BL2	0.1641	0.1633	1.0050	0.0150	0.0149	0.0003
Scoop, BL1, BL2	0.1491	0.1484	1.0048	0.0000	0.0000	0.0000
Scoop, BL1, BL2 (60%)	0.2374	0.2296	1.0340	0.0883	0.0812	0.0292
Scoop, BL1, BL2 (80%)	0.1753	0.1732	1.0119	0.0262	0.0248	0.0071

Table A.20: Boundary layer analysis $x = -2275$ mm and $y = -1130$ mm at 140 km/h.

Mode	δ^* [mm]	θ [mm]	H	$\Delta\delta^*$[mm]	$\Delta\theta$ [mm]	ΔH
Scoop	3.9793	3.4012	1.1700	3.3102	2.7555	0.1338
Scoop (80%)	4.0656	3.4660	1.1730	3.3965	2.8204	0.1367
Scoop (80%), BL1 (60%), BL2	0.6975	0.6722	1.0376	0.0284	0.0265	0.0013
Scoop, BL1	1.3794	1.2570	1.0974	0.7104	0.6113	0.0612
Scoop, BL1 (60%)	1.5474	1.3951	1.1091	0.8783	0.7494	0.0729
Scoop, BL1 (60%), BL2	0.6891	0.6645	1.0371	0.0201	0.0188	0.0009
Scoop, BL1, BL2	0.6691	0.6457	1.0362	0.0000	0.0000	0.0000
Scoop, BL1, BL2 (60%)	0.7763	0.7388	1.0507	0.1072	0.0932	0.0144
Scoop, BL1, BL2 (80%)	0.7251	0.6953	1.0428	0.0560	0.0496	0.0066

Table A.21: Boundary layer analysis $x = -2275$ mm and $y = -400$ mm at 140 km/h.

Mode	δ^* [mm]	θ [mm]	H	$\Delta\delta^*$[mm]	$\Delta\theta$ [mm]	ΔH
Scoop	4.0383	3.4583	1.1677	3.6552	3.0863	0.1375
Scoop (80%)	4.4116	3.7460	1.1777	4.0284	3.3741	0.1474
Scoop (80%), BL1 (60%), BL2	0.4073	0.3964	1.0274	0.0241	0.0245	-0.0029
Scoop, BL1	1.1880	1.0793	1.1008	0.8049	0.7074	0.0705
Scoop, BL1 (60%)	1.4744	1.3217	1.1155	1.0913	0.9498	0.0853
Scoop, BL1 (60%), BL2	0.4004	0.3896	1.0277	0.0172	0.0176	-0.0025
Scoop, BL1, BL2	0.3832	0.3719	1.0302	0.0000	0.0000	0.0000
Scoop, BL1, BL2 (60%)	0.5246	0.5013	1.0465	0.1414	0.1294	0.0163
Scoop, BL1, BL2 (80%)	0.4408	0.4248	1.0376	0.0576	0.0529	0.0074

Table A.22: Boundary layer analysis $x = -2275$ mm and $y = 0$ mm at 140 km/h.

Mode	δ^* [mm]	θ [mm]	H	$\Delta\delta^*$[mm]	$\Delta\theta$ [mm]	ΔH
Scoop	3.7127	3.1780	1.1683	3.3232	2.8010	0.1349
Scoop (80%)	3.7634	3.2150	1.1706	3.3739	2.8381	0.1372
Scoop (80%), BL1 (60%), BL2	0.4280	0.4146	1.0324	0.0385	0.0376	-0.0009
Scoop, BL1	1.0618	0.9633	1.1023	0.6723	0.5863	0.0690
Scoop, BL1 (60%)	1.2624	1.1318	1.1154	0.8729	0.7549	0.0821
Scoop, BL1 (60%), BL2	0.4213	0.4082	1.0321	0.0318	0.0313	-0.0013
Scoop, BL1, BL2	0.3895	0.3769	1.0333	0.0000	0.0000	0.0000
Scoop, BL1, BL2 (60%)	0.5152	0.4913	1.0487	0.1257	0.1144	0.0154
Scoop, BL1, BL2 (80%)	0.4565	0.4393	1.0393	0.0670	0.0623	0.0059

Table A.23: Boundary layer analysis $x = -2275$ mm and $y = 400$ mm at 140 km/h.

Mode	δ^* [mm]	θ [mm]	H	$\Delta\delta^*$[mm]	$\Delta\theta$ [mm]	ΔH
Scoop	4.0148	3.3473	1.1994	3.8982	3.2352	0.1592
Scoop (80%)	4.3600	3.6327	1.2002	4.2433	3.5206	0.1599
Scoop (80%), BL1 (60%), BL2	0.1451	0.1405	1.0325	0.0284	0.0284	-0.0077
Scoop, BL1	0.8302	0.7296	1.1379	0.7136	0.6175	0.0977
Scoop, BL1 (60%)	0.9341	0.8120	1.1503	0.8175	0.6999	0.1100
Scoop, BL1 (60%), BL2	0.1358	0.1313	1.0346	0.0192	0.0191	-0.0057
Scoop, BL1, BL2	0.1166	0.1121	1.0403	0.0000	0.0000	0.0000
Scoop, BL1, BL2 (60%)	0.1658	0.1566	1.0590	0.0492	0.0444	0.0187
Scoop, BL1, BL2 (80%)	0.1611	0.1547	1.0411	0.0445	0.0426	0.0008

Table A.24: Boundary layer analysis $x = -2275$ mm and $y = 1130$ mm at 140 km/h.

Mode	δ^* [mm]	θ [mm]	H	$\Delta\delta^*$[mm]	$\Delta\theta$ [mm]	ΔH
Scoop	4.6434	3.7897	1.2253	4.5152	3.6671	0.1804
Scoop (80%)	4.9545	4.0791	1.2146	4.8263	3.9564	0.1697
Scoop (80%), BL1 (60%), BL2	0.1615	0.1558	1.0364	0.0334	0.0332	-0.0085
Scoop, BL1	0.8357	0.7301	1.1446	0.7075	0.6075	0.0997
Scoop, BL1 (60%)	0.9444	0.8210	1.1502	0.8163	0.6984	0.1054
Scoop, BL1 (60%), BL2	0.1498	0.1442	1.0391	0.0217	0.0215	-0.0058
Scoop, BL1, BL2	0.1281	0.1226	1.0449	0.0000	0.0000	0.0000
Scoop, BL1, BL2 (60%)	0.1939	0.1839	1.0543	0.0658	0.0613	0.0094
Scoop, BL1, BL2 (80%)	0.1601	0.1532	1.0453	0.0320	0.0305	0.0004

Table A.25: Boundary layer analysis $x = -2275$ mm and $y = 1530$ mm at 140 km/h.

Mode	δ^* [mm]	θ [mm]	H	$\Delta\delta^*$[mm]	$\Delta\theta$ [mm]	ΔH
Scoop	4.8530	4.0046	1.2118	4.6649	3.8201	0.1928
Scoop (80%)	4.9410	4.1543	1.1894	4.7530	3.9697	0.1704
Scoop (80%), BL1 (60%), BL2	0.1668	0.1633	1.0212	-0.0213	-0.0213	0.0022
Scoop, BL1	0.4764	0.4372	1.0895	0.2883	0.2527	0.0705
Scoop, BL1 (60%)	0.5182	0.4722	1.0975	0.3301	0.2876	0.0785
Scoop, BL1 (60%), BL2	0.1678	0.1644	1.0205	-0.0203	-0.0202	0.0015
Scoop, BL1, BL2	0.1881	0.1846	1.0190	0.0000	0.0000	0.0000
Scoop, BL1, BL2 (60%)	0.2306	0.2200	1.0482	0.0425	0.0354	0.0292
Scoop, BL1, BL2 (80%)	0.1999	0.1940	1.0303	0.0118	0.0095	0.0113

Table A.26: Boundary layer analysis $x = -2275$ mm and $y = 1930$ mm at 140 km/h.

Mode	δ^* [mm]	θ [mm]	H	$\Delta\delta^*$[mm]	$\Delta\theta$ [mm]	ΔH
Scoop	8.8508	7.1070	1.2454	4.5106	3.6799	-0.0210
Scoop (80%)	8.5854	6.8913	1.2458	4.2452	3.4642	-0.0206
Scoop (80%), BL1 (60%), BL2	4.5316	3.5611	1.2725	0.1914	0.1340	0.0061
Scoop, BL1	4.9080	3.8670	1.2692	0.5678	0.4398	0.0028
Scoop, BL1 (60%)	5.0199	3.9446	1.2726	0.6797	0.5174	0.0062
Scoop, BL1 (60%), BL2	4.4302	3.4969	1.2669	0.0900	0.0697	0.0005
Scoop, BL1, BL2	4.3402	3.4272	1.2664	0.0000	0.0000	0.0000
Scoop, BL1, BL2 (60%)	4.4145	3.4834	1.2673	0.0743	0.0562	0.0009
Scoop, BL1, BL2 (80%)	4.3711	3.4461	1.2684	0.0309	0.0189	0.0020

Table A.27: Boundary layer analysis $x = 0$ mm and $y = -1930$ mm at 140 km/h.

Mode	δ^* [mm]	θ [mm]	H	$\Delta\delta^*$[mm]	$\Delta\theta$ [mm]	ΔH
Scoop	8.1392	6.4971	1.2527	3.8223	3.1130	-0.0229
Scoop (80%)	8.3213	6.6163	1.2577	4.0045	3.2321	-0.0179
Scoop (80%), BL1 (60%), BL2	4.3922	3.4335	1.2792	0.0754	0.0494	0.0036
Scoop, BL1	5.0418	3.9632	1.2721	0.7249	0.5790	-0.0035
Scoop, BL1 (60%)	5.1327	4.0401	1.2704	0.8158	0.6560	-0.0052
Scoop, BL1 (60%), BL2	4.3787	3.4287	1.2771	0.0618	0.0446	0.0014
Scoop, BL1, BL2	4.3169	3.3842	1.2756	0.0000	0.0000	0.0000
Scoop, BL1, BL2 (60%)	4.4656	3.4953	1.2776	0.1487	0.1111	0.0020
Scoop, BL1, BL2 (80%)	4.3336	3.3964	1.2759	0.0167	0.0122	0.0003

Table A.28: Boundary layer analysis $x = 0$ mm and $y = -1530$ mm at 140 km/h.

Mode	δ^* [mm]	θ [mm]	H	$\Delta\delta^*$[mm]	$\Delta\theta$ [mm]	ΔH
Scoop	8.2944	6.6142	1.2540	4.0307	3.2143	-0.0000
Scoop (80%)	8.4601	6.7034	1.2620	4.1964	3.3035	0.0080
Scoop (80%), BL1 (60%), BL2	4.3312	3.4431	1.2580	0.0676	0.0431	0.0039
Scoop, BL1	5.2997	4.2200	1.2558	1.0360	0.8201	0.0018
Scoop, BL1 (60%)	5.4289	4.3148	1.2582	1.1652	0.9148	0.0042
Scoop, BL1 (60%), BL2	4.2587	3.3915	1.2557	-0.0050	-0.0084	0.0017
Scoop, BL1, BL2	4.2637	3.4000	1.2540	0.0000	0.0000	0.0000
Scoop, BL1, BL2 (60%)	4.4455	3.5412	1.2554	0.1818	0.1413	0.0013
Scoop, BL1, BL2 (80%)	4.2909	3.4224	1.2538	0.0272	0.0225	-0.0003

Table A.29: Boundary layer analysis $x = 0$ mm and $y = -1130$ mm at 140 km/h.

Mode	δ^* [mm]	θ [mm]	H	$\Delta\delta^*$[mm]	$\Delta\theta$ [mm]	ΔH
Scoop	3.9045	3.6116	1.0811	3.3552	3.0728	0.0617
Scoop (80%)	4.1088	3.7852	1.0855	3.5596	3.2464	0.0661
Scoop (80%), BL1 (60%), BL2	0.5393	0.5291	1.0192	-0.0100	-0.0097	-0.0003
Scoop, BL1	1.1848	1.1413	1.0381	0.6355	0.6025	0.0186
Scoop, BL1 (60%)	1.3206	1.2674	1.0420	0.7713	0.7285	0.0226
Scoop, BL1 (60%), BL2	0.5587	0.5481	1.0194	0.0094	0.0093	-0.0000
Scoop, BL1, BL2	0.5493	0.5388	1.0194	0.0000	0.0000	0.0000
Scoop, BL1, BL2 (60%)	0.6646	0.6503	1.0220	0.1153	0.1115	0.0025
Scoop, BL1, BL2 (80%)	0.5904	0.5783	1.0209	0.0411	0.0394	0.0015

Table A.30: Boundary layer analysis $x = 0$ mm and $y = -400$ mm at 140 km/h.

Mode	δ^* [mm]	θ [mm]	H	$\Delta\delta^*$[mm]	$\Delta\theta$ [mm]	ΔH
Scoop	3.7518	3.4760	1.0793	3.3151	3.0465	0.0626
Scoop (80%)	3.9873	3.6803	1.0834	3.5507	3.2508	0.0667
Scoop (80%), BL1 (60%), BL2	0.4328	0.4254	1.0173	-0.0039	-0.0041	0.0006
Scoop, BL1	1.1218	1.0804	1.0383	0.6851	0.6509	0.0216
Scoop, BL1 (60%)	1.3577	1.3009	1.0437	0.9210	0.8714	0.0270
Scoop, BL1 (60%), BL2	0.4201	0.4128	1.0176	-0.0166	-0.0167	0.0009
Scoop, BL1, BL2	0.4367	0.4295	1.0167	0.0000	0.0000	0.0000
Scoop, BL1, BL2 (60%)	0.5250	0.5138	1.0219	0.0883	0.0843	0.0052
Scoop, BL1, BL2 (80%)	0.4690	0.4602	1.0190	0.0323	0.0307	0.0023

Table A.31: Boundary layer analysis $x = 0$ mm and $y = 400$ mm at 140 km/h.

Mode	δ^* [mm]	θ [mm]	H	$\Delta\delta^*$[mm]	$\Delta\theta$ [mm]	ΔH
Scoop	8.5154	6.7809	1.2558	4.3157	3.4682	-0.0120
Scoop (80%)	8.8533	7.0285	1.2596	4.6535	3.7159	-0.0082
Scoop (80%), BL1 (60%), BL2	4.4524	3.5030	1.2710	0.2526	0.1903	0.0032
Scoop, BL1	5.2808	4.1736	1.2653	1.0810	0.8609	-0.0025
Scoop, BL1 (60%)	5.5485	4.3720	1.2691	1.3487	1.0594	0.0013
Scoop, BL1 (60%), BL2	4.3022	3.3899	1.2691	0.1024	0.0773	0.0013
Scoop, BL1, BL2	4.1998	3.3126	1.2678	0.0000	0.0000	0.0000
Scoop, BL1, BL2 (60%)	4.2659	3.3599	1.2696	0.0661	0.0473	0.0018
Scoop, BL1, BL2 (80%)	4.2377	3.3448	1.2670	0.0379	0.0321	-0.0008

Table A.32: Boundary layer analysis $x = 0$ mm and $y = 1130$ mm at 140 km/h.

Mode	δ^* [mm]	θ [mm]	H	$\Delta\delta^*$[mm]	$\Delta\theta$ [mm]	ΔH
Scoop	9.1091	7.2090	1.2636	4.4397	3.5787	-0.0226
Scoop (80%)	9.6687	7.6120	1.2702	4.9993	3.9816	-0.0160
Scoop (80%), BL1 (60%), BL2	4.7977	3.7240	1.2883	0.1283	0.0937	0.0021
Scoop, BL1	5.3474	4.1707	1.2821	0.6780	0.5403	-0.0041
Scoop, BL1 (60%)	5.4624	4.2664	1.2803	0.7930	0.6361	-0.0059
Scoop, BL1 (60%), BL2	4.7433	3.6858	1.2869	0.0739	0.0555	0.0007
Scoop, BL1, BL2	4.6694	3.6303	1.2862	0.0000	0.0000	0.0000
Scoop, BL1, BL2 (60%)	4.8051	3.7292	1.2885	0.1357	0.0989	0.0023
Scoop, BL1, BL2 (80%)	4.6921	3.6438	1.2877	0.0227	0.0135	0.0015

Table A.33: Boundary layer analysis $x = 0$ mm and $y = 1530$ mm at 140 km/h.

Mode	δ^* [mm]	θ [mm]	H	$\Delta\delta^*$[mm]	$\Delta\theta$ [mm]	ΔH
Scoop	10.7079	8.4534	1.2667	6.1407	4.8772	-0.0104
Scoop (80%)	10.8938	8.5836	1.2691	6.3266	5.0074	-0.0080
Scoop (80%), BL1 (60%), BL2	4.6503	3.6222	1.2838	0.0831	0.0460	0.0067
Scoop, BL1	5.4007	4.2126	1.2820	0.8335	0.6363	0.0049
Scoop, BL1 (60%)	5.5799	4.3399	1.2857	1.0127	0.7637	0.0086
Scoop, BL1 (60%), BL2	4.6199	3.6089	1.2802	0.0527	0.0327	0.0031
Scoop, BL1, BL2	4.5672	3.5762	1.2771	0.0000	0.0000	0.0000
Scoop, BL1, BL2 (60%)	4.7314	3.6901	1.2822	0.1642	0.1138	0.0051
Scoop, BL1, BL2 (80%)	4.6201	3.6104	1.2797	0.0529	0.0342	0.0026

Table A.34: Boundary layer analysis $x = 0$ mm and $y = 1930$ mm at 140 km/h.

TRITA – EECS-EX 2024:0000
Stockholm, Sweden 2025

www.kth.se

€€€€ For DIVA €€€€

{
"Author1": { "Last name": "De Jourday",
"First name": "Dylan",
"Local User Id": "u100001",
"E-mail": "dylandj@kth.se",
"organisation": {"L1": "School of Engineering Sciences",
}
},
"Cycle": "2",
"Course code": "SG213X",
"Credits": "30.0",
"Degree1": {"Educational program": "Degree Programme in Vehicle Engineering"
,"programcode": "CFATE"
,"Degree": "Both Degree of Master of Science in Engineering and Master's degree"
,"subjectArea": "Fluid Mechanics"
},
"Title": {
"Main title": "An Experimental Investigation of the Boundary Layer Control System of Volvo's Slotted Wall Automotive Wind Tunnel",
"Subtitle": "Uncovering the Relationship between Boundary Layer Control, Static Pressure, and Drag",
"Language": "eng" },
"Alternative title": {
"Main title": "En Undersökning av Inverkan av Gränsskiktkontrollsystem på Aerodynamiska Mätningar i Vindtunnel för Vägfordon",
"Subtitle": "Att Avslöja Sambandet mellan Gränsskiktkontroll, Statiskt Tryck och Luftmotstånd",
"Language": "swe"
},
"Supervisor1": { "Last name": "Fransson",
"First name": "Jens H. M.",
"Local User Id": "u100003",
"E-mail": "jensfransson@kth.se",
"organisation": {"L1": "School of Engineering Sciences",
"L2": "Engineering Mechanics" }
},
"Supervisor2": { "Last name": "Sällström",
"First name": "Erik",
"E-mail": "eriksällstrom@volvocars.se",
},
"Examiner1": { "Last name": "Fransson",
"First name": "Jens H. M.",
"Local User Id": "u1d13l2c",
"E-mail": "jensfransson@kth.se",
"organisation": {"L1": "School of Engineering Sciences",
"L2": "Engineering Mechanics" }
},
"Cooperation": { "Partner_name": "Volvo Cars"},
"National Subject Categories": "20301, 20306",
"Other information": {"Year": "2025", "Number of pages": "xx,97"},
"Copyrightleft": "copyright",
"Series": { "Title of series": "TRITA – EECS-EX" , "No. in series": "2024:0000" },
"Opponents": { "Name": "A. B. Normal & A. X. E. Normalè"},
"Presentation": { "Date": "2022-03-15 13:00"
,"Language":"eng"
,"Room": "via Zoom https://kth-se.zoom.us/j/ddddddddddd"
,"Address": "Isafjordsgatan 22 (Kistagången 16)"
,"City": "Stockholm" },
"Number of lang instances": "2",
"Abstract[eng]": €€€€

This thesis investigates the impact that boundary layer control systems have on aerodynamic measurements in an automotive wind tunnel with a slotted-wall test section. The study was carried out in the Volvo Cars PVT wind tunnel at the Torslanda site in Gothenburg. Through experimentation a relationship was established between the suction rate of the boundary layer control systems, static pressure, and measured drag.

Reviewing the design and upgrade of the Volvo Cars PVT wind tunnel along with designs of other modern automobile wind tunnels and the relevant literature in the field led to the conclusion that the suction rate of the boundary layer control systems used in the tunnel was too high and excess suction provided little benefit. By reducing the suction rate of these systems by up to $40-50\%$ *in some cases, a remarkable reduction of five counts in measured drag was observed ($\Delta C_D=-0.005$), with a small increase in displacement thickness. This change is related to the flattening of the axial static pressure curve and is related to the static pressure gradient; however, the large change in C_D cannot be explained by just looking at the change in the centerline axial static pressure in the empty test section. The shape of the boundary layer profiles remained largely unchanged, with negligible influence on the shape factor seen. With further refinement of the parameters of the boundary layer suction systems, the change in C_D could be even greater. This, in combination with the turning off of the tangential blowers and the change of the wind speed determination method from nozzle to plenum led to a large reduction in C_D. The total change with all these changes was twenty counts $(\Delta C_D=-0.020)$, with the change in method reducing the measured drag by ten counts $(\Delta C_D=-0.010)$ and disabling tangential blowers reducing the measured drag by five counts $(\Delta C_D=-0.005)$.*

The insights gained in this thesis are valuable both for Volvo Cars and the automobile industry as a whole. Studies related to slotted-wall test sections in automobile wind tunnels are few in number and the effects of boundary layer control systems on the flow in the test section are not as well studied as their $3/4$ open-jet counterpart. This study helps fill that knowledge gap a little more and provides a starting point for further investigation on the topic. The ideas for future investigations are outlined in the conclusion of this thesis.

€€€€,
"Keywords[eng]": €€€€
Slotted wall wind tunnel, Automotive wind tunnels, Drag, Static pressure, Boundary layer control, Boundary layer suction, Aerodynamic measurments, Volvo Cars, Ground simulation systems, Automobile aerodynamics, Pressure coefficient, Drag coefficient, Moving ground system, Boundary layer thickness, Displacement thickness €€€€,
"Abstract[swe]": €€€€

Denna uppsats undersöker hur gränsskiktkontrollsystem påverkar aerodynamiska mätningar i en vindtunnel för passagerarfordon med en testsektion med slits-väggar. Studien genomfördes i Volvo Cars vindtunnel PVT vid Torslanda-anläggningen i Göteborg. Genom experiment upptäcktes ett samband mellan sughastigheten hos gränsskiktkontrollsystemen, statiskt tryck och uppmätt luftmotstånd.

En genomgång av designen och uppgraderingen av Volvo Cars vindtunnel PVT, tillsammans med designen av andra moderna fordonsvindtunnlar och relevant litteratur inom området, ledde till slutsatsen att sughastigheten hos de använda gränsskiktkontrollsystemen är för hög och att den förhöjda hastigheten ger liten effeckt. Genom att minska sughastigheten, med i vissa fall upp till −4050%, *observerades en anmärkningsvärd minskning med upp till fem enheter i uppmätt luftmotstånd ($\Delta C_D = -0.005$), tillsammans med en liten ökning av förträngningstjockleken. Denna förändring är relaterad till en tillplattning av den axiella statiska tryckkurvan och är kopplad till den statiska tryckgradienten. Den stora förändringen i C_D kan dock inte förklaras enbart genom att titta på förändringen i det axiella statiska trycket längs mittlinjen i en tom mätsträcka. Gränsskiktsprofilerna förblev i stort sett oförändrade, med en försumbar påverkan på formfaktorn. Vid ytterligare förfining av parametrarna för gränsskiktets sugsystem skulle förändringen av C_D kunna bli ännu större. Detta, i kombination med att de tangentiella blåsarna stängdes av och att metoden för att bestämma vindhastigheten ändrades från munstycke till plenum, ledde till en stor minskning av C_D. Den totala förändringen med alla dessa ändringan var tjugo enheter $(\Delta C_D=-0.020)$, där metodbytet minskade det uppmätta C_D-värdet med tio enheter $(\Delta C_D=-0.010)$ och avaktiveringen av de tangentiella blåsarna minskade det uppmätta C_D-värdet med fem enheter $(\Delta C_D=-0.005)$.*

De insikter som erhållits i denna uppsats är värdefulla både för Volvo Cars och för fordonsindustrin i stort. Studier relaterade till testsektioner med slitsade väggar i fordonsvindtunnlar är få till antalet, och effekterna av gränsskiktkontrollsystem på flödet i testsektionen är inte lika väl studerade som för deras 3/4s öppna jet-motsvarighet. Denna studie bidrar till att fylla denna kunskapslucka något och utgör en utgångspunkt för vidare undersökningar inom området. Förslag på framtida undersökningar beskrivs i slutsatsen av denna uppsats.

€€€€,
"Keywords[swe]": €€€€
Vindtunnel med slitsväggar, Vindtunnel för vägfordon, Luftmotstånd, Statiskt tryck, Gränsskiktkontroll, Gränsskiktsutsug, Aerodynamiska mätningar, Volvo Cars, Marksimuleringssystem, Fordonsaerodynamik, Tryckkoefficient, Luftmotståndskoefficient €€€€,
}

acronyms.tex

```
%%% Local Variables:
%%% mode: latex
%%% TeX-master: t
%%% End:
% The following command is used with glossaries-extra
\setabbreviationstyle[acronym]{long-short}
% The form of the entries in this file is \newacronym{label}{acronym}{phrase}
%                                     or \newacronym[options]{label}{acronym}{phrase}
% see "User Manual for glossaries.sty" for the  details about the options, one example is shown below
% note the specification of the long form plural in the line below
%\newacronym[longplural={Debugging Information Entities}]{DIE}{DIE}{Debugging Information Entity}
%
% The following example also uses options
%\newacronym[shortplural={OSes}, firstplural={operating systems (OSes)}]{OS}{OS}{operating system}

% note the use of a non-breaking dash in long text for the following acronym
%\newacronym{IQL}{IQL}{Independent -QLearning}

% example of putting in a trademark on first expansion
%\newacronym[first={NVIDIA OpenSHMEM Library (NVSHMEM\texttrademark)}]{NVSHMEM}{NVSHMEM}{NVIDIA OpenSHMEM Library}

\newacronym{KTH}{KTH}{KTH Royal Institute of Technology}


% note the use of a non-breaking dash in the following acronym
\newacronym[shortplural={PVT},longplural={Personvängtunnel(?)}]{PVT}{PVT}{Personvängtunnel(?)}

\newacronym[shortplural={BLRS}]{BLRS}{BLRS}{Boundary Layer Removal System}

\newacronym[shortplural={BLCS}]{BLCS}{BLCS}{Boundary Layer Control System}

\newacronym[shortplural={PIV},longplural={Particle Image Velocimetry}]{PIV}{PIV}{Particle Image Velocimetry}

\newacronym[shortplural={MGP},longplural={Moving Ground Plane}]{MGP}{MGP}{Moving Ground Plane}

\newacronym[shortplural={CFD},longplural={Computational Fluid Dynamics}]{CFD}{CFD}{Computational Fluid Dynamics}

\newacronym[shortplural={ICE},longplural={Internal Combustion Engines}]{ICE}{ICE}{Internal Combustion Engine}

\newacronym[shortplural={CATARC},longplural={China Automotive
Technology and Research Center}]{CATARC}{CATARC}{China Automotive
Technology and Research Center}

\newacronym[shortplural={TGR},longplural={Toyota Gazoo Racing}]{TGR}{TGR}{Toyota Gazoo Racing}

\newacronym[shortplural={BL}]{BL}{BL}{Boundary layer}

\newacronym[shortplural={BL1},longplural={Boundary layer pre-suction zone one}]{BL1}{BL1}{Boundary layer pre-suction zone one}

\newacronym[shortplural={BL2},longplural={Boundary layer pre-suction zone two}]{BL2}{BL2}{Boundary layer pre-suction zone two}

\newacronym[shortplural={TB}]{TB}{TB}{Tangential Blower}


\newacronym[shortplural={WDU},longplural={Wheel Drive Unit}]{WDU}{WDU}{Wheel Drive Unit}

\newacronym[shortplural={GESS},longplural={Ground Effect Simulation Systems}]{GESS}{GESS}{Ground Effect Simulation Systems}


%% my acronyms
```